NCPTT

Structural Health Monitoring of Nation's Cultural Heritage | 2011-15

Clemson University

National Park Service
U.S. Department of the Interior

National Center for Preservation Technology and Training

STRUCTURAL HEALTH MONITORING OF NATION'S CULTURAL HERITAGE

Huriye Sezer Atamturktur
Department of Civil Engineering
Clemson University
110 Lowry Hall
S Palmetto Blvd, Clemson, SC 29634
(864) 656-3003
sez@clemson.edu

prepared for

US Department of the Interior
National Park Service
National Center for Preservation Technology and Training

10th July 2011

ABSTRACT

Structural Health *Monitoring* (SHM) is a well-accepted diagnostic technique being used to evaluate modern structures. This method involves monitoring the vibration responses of structure to detect changes in the structural state of a building. The primary intention of this report is to address two practical and technical difficulties encountered in deploying SHM on historic masonry monuments: (i) the selection of suitable low dimensional vibration response features that are highly sensitive to the presence and extent of damage, while having low sensitivity to extraneous noise and (ii) the selection of optimal sensor locations for efficient system identification applied to Gothic Cathedrals. All three of the features of this report achieve reduction in the size of the raw data to be analyzed leading to reduced computational as well as monetary effort. Compression of the raw vibration response data acquired from the vibration tests on structures is vital from the standpoint of faster real time monitoring of historic structures.

This report is composed of three manuscripts. The first manuscript illustrates the concepts of feature assimilation and noise sensitivity on an arch-like structure using both numerical and experimental analysis. The second study investigates the damage indicative features extracted in the modal, frequency and time domain. Vibration measurements of a Gothic vaulted masonry monument undergoing differential support settlement are used and it is shown that vibration measurements offer a practical solution to detect vault-wall separation. The third study is focused on finding optimal sensor locations for vibration testing of Gothic Cathedrals. A modified version of the Effective Independence Method is used for this purpose. This report aims to develop a best-

practices guide for effective application of SHM for the use of professionals involved in assessing, preserving and maintaining cultural monuments.

TABLE OF CONTENTS

Page

TITLE PAGE i

ABSTRACT ii

LIST OF FIGURES vi

LIST OF TABLES xi

CHAPTER

I. INTRODUCTION 1

II. FEATURE ASSIMILATION FOR CONDITION BASED MAINTENANCE 6

Introduction 7
Case Study Application: Arch Prototype 10
Experimental Procedure 11
Extracting Vibration Response Features 13
Assimilation Vibration Response Features 20
Discussion 25
Conclusion 26
Acknowledgments 27

III. VIBRATION CHARACTERISTICS OF VAULTED MASONRY MONUMENTS UNDERGOING DIFFERENTIAL SUPPORT SETTLEMENT 28

Introduction 29
Background 34
Beverly Minster 38
Vaulted Structure under Study 40
Finite Element Simulations of the Vaults 44
Vibration Test Campaign 51
Evaluation in the Modal Domain 60
Evaluation in the Frequency Domain 64
Evaluation in the Time Domain 66
Conclusions 71
Acknowledgments 74

IV. VIBRATION TESTING OF GOTHIC CATHEDRALS: OPTIMAL SENSOR LOCATIONS BASED ON MODIFIED EFFECTIVE INDEPENDENCE METHOD 75

Introduction 76
Modified Effective Independence Method 78
The Case Study Structure 83
Development and Validation of Finite Element Model 84
Sensor Optimization 90
Discussions 94
Conclusions 99
Acknowledgments 100

CONCLUSIONS 102
REFERENCES 104

LIST OF FIGURES

Figure		Page
2.1	Sensitivity of damage indicators to varying levels of damage.....	8
2.2	Crack locations in an arch due to concentrated load at the quarter span using the inverted chain analogy, reprinted from Heyman (1997) with permission**. .....**	10
2.3	(Left) FE model of the arch with a static load at quarter span, (Right) arch experiencing maximum damage through artificial cracks.	11
2.4	(Left) Test structure used for experimental study, (Right) hammer impact locations on the test arch.	12
2.5	Percentage change in the first four natural frequencies with progressive damage.	14
2.6	Percentage change in the first four mode shape vectors with progressive damage..	15
2.7	Percentage change in mode shape curvature with progressive damage.	16
2.8	(top) Skewness and (bottom) kurtosis of FRF measurements from the experimental hammer impact test.	18
2.9	Absolute percentage change in the (Left) skewness and (Right) kurtosis for FRFs from the experimental campaign with the dashed lines signifying the noise sensitivity..	19
2.10	Singular Value Decomposition (SVD) scores for AR model parameters of the FRFs from the experimental campaign.....	20
2.11	Damage sensitivity comparison of various damage indicators with progressive damage: (Top) experimental campaign with three features, (Bottom) experimental campaign with five features..	22

List of Figures (Continued)

Figure Page

2.12 Changes in FRFs for increasing damage levels with and without ambient noise..... 24

2.13 Assimilated damage indicator with the change in skewness and kurtosis and the assimilated noise level for the two features..... 25

3.1 The interior view of the nave of the Beverley Minster displays the limestone piers that support the stone vaulting. The leaning of the columns outwards is visually observable onsite. 31

3.2 A schematic of Sabouret Cracks, by Heyman [2] (with permission). 32

3.3 The movement of the walls is not uniform along the length of the nave; as such the Minster now has ten vaults with varying damage states. Two vaults representing the most damaged and undamaged states are selected for the study. 33

3.4 The cross section of the vault displays how the stone walls and buttresses horizontally support the nave vaults. The settlement of the buttresses pulls the walls outward, causing separation between the walls and vaults. 38

3.5 The interface between the nave walls and vaults of (left) damaged and (right) undamaged vaults. The gap between the walls and vaults of the undamaged vault is filled with plastic sheets. 39

3.6 The originally concave down curvature of the vaults is flattened: (top) undamaged and (bottom) damaged vault. The formation of the 6‘‘ wide Sabouret cracks results in an 8’’ sagging of the crown of the vaults..... 41

List of Figures (Continued)

Figure Page

3.7 The impact echo measurements are used to estimate the standard deviation of the homogenized material properties of the mortar and masonry assembly 43

3.8 The dimensions of the masonry vaults of the Beverley Minster. 45

3.9 FE model of Beverley Minster used to simulate the changes in the vibration response of the vaults due to the variability in geometry and material properties present in the Minster. 47

3.10 The FRFs are simulated for the four scenarios: (1) the undamaged vault, (2) the damaged vault, (3) the undamaged vault with variation in geometry and (4) the undamaged vault with variation in material..... 49

3.11 The uni-axial accelerometers are placed on the curved vault surface with the help of adjustable mounting cases such that their axes remain vertical..... 53

3.12 A total of 39 measurement points are selected according to the mode shape predictions of the preliminary model. The excitation points are #20, #18, #12 and #11. 54

3.13 The hammer operator exciting the pre-determined excitation points with the sledgehammer. Maintaining a relatively consistent excitation level is one of the keys for the success of hammer excitation. 55

3.14 Examples of measured signals: (top) hammer impact force in the time domain and (bottom) the response of the vaults due to the hammer impact. 57

3.15 A representative FRF and coherence function obtained from the undamaged vaults. 58

3.16 The frequency response function of the damaged vault tends to have higher amplitudes compared to the undamaged vault, especially at higher frequencies... 58

List of Figures (Continued)

Figure Page

3.17 The reciprocity check completed between measurement point 18 and 20 for the damaged vault. 59

3.18 The first mode shape of (a) undamaged vault, (b) damaged vault. 63

3.19 The imaginary component of the FRF conveys the relative deformations of the measurement points, which are observed to be comparable for the damaged (red dashed) and undamaged (blue solid) vault for frequencies below 7Hz. Frequencies higher than 7Hz have significantly higher amplitudes for the damaged vaults. 65

3.20 The coherence plot indicates the linear relationship between the input force and output response. The damaged vault coherence plot shows a reduction in this linear relationship.. 66

3.21 Comparison of AR-SVM fit to normalized transient impact data in (top) undamaged and (bottom) damaged cases. Average absolute residuals for this sensor in the undamaged and damaged cases are 0.0412 and 0.1308 respectively, indicating significantly improved model fit to the undamaged case. 69

3.22 Average absolute values of lack-of-fit residuals of AR-SVM predictions at 46 sensor locations for the undamaged and damaged cases. 71

4.1 (a) The west front of the Cathedral Church of St. John the. Divine, New York, (b) sectional elevation drawing of the nave. 83

4.2 (a) Photo of the nave vaults, (b) FE model of the vaults.. 86

4.3 The 3-D meshed FE model of the bay. 88

4.4 Cracks at the rose opening (highlighted) corresponding to high tensile stress regions in the FE model. 89

List of Figures (Continued)

Figure Page

4.5 Cracks at the walkways (highlighted) between the buttress and the nave corresponding to the high tensile stress regions in the FE model..... 90

4.6 (a) The accessible locations on the structure highlighted; (b) the candidate sensor locations shown as dots. 91

4.7 Nine target mode shapes desired to be extracted during the *in-situ* modal analysis..... 92

4.8 Fisher information matrix determinant updated with sensors eliminated iteratively. 92

4.9 Effective independence values of the sensors with respect to the iteratively updated mode shape matrix; (inset) zoomed in to 80 optimal sensors.. 93

4.10 Optimal sensor locations for triaxial sensors on the full bay (a) without DBC, (b) with DBC of 3 meters. 94

4.11 Behavior of the Fisher information matrix determinant for different DBC. 95

4.12 Optimal sensor locations after 5% reduction in the Elastic modulus of each of five materials without a DBC. 96

4.13 The optimal sensor locations for the 6 models with DBC of (a) 0m (or no DBC); (b) 1m; (c) 1.5m; (d) 2m; (e) 2.5m; (f) 3m. 97

4.14 Optimum sensor locations in the six FE models using a DBC of 1.5m and applying the error theory. 98

LIST OF TABLES

Table		Page
3.1	Prior knowledge on the material properties of structural components	46
3.2	Absolute Average Residuals of AR-SVM Fit Under Several Scenarios	50
3.3	The modal parameters identified from damaged and undamaged vaults.	62
4.1	Comparison of experimental and analytical modal analysis results of the vaults of St John the Divine.	87
4.2	Element type and material properties used in the FE model for different parts of the structure	88

CHAPTER ONE

INTRODUCTION

There are a large number of monumental masonry buildings currently in service that have been built using medieval construction techniques. The U.S. National Register of Historic Places (National Park Service 2009) for instance, lists over 2,000 historic buildings in the continental U.S. built in the 'Gothic' style alone. These historic masonry monuments experience the degrading effects of aging and accumulated damage over their lifetime. If the structural integrity of these monuments is not proactively maintained, these monuments may experience sudden failure without warning. In the past few decades, numerous historic structures have failed suddenly; some of the more notable examples include the Civic Tower of Pavia, Italy (Binda et al. 1992); the bell tower of St. Magdalena in Goch, Germany (Gantert Engineering Studio 1993); Cathedral of Noto, Italy (Binda et al. 1999); the bell tower of the St. Willibrordus Church in Meldert, Belgium (Ignoul and Van Gemert 2006); “Maagdentoren” in Zichem, Belgium (Ignoul and Van Gemert 2007); Church of Kerksken, Belgium (Verstrynge et al. 2011). These incidents have increased the relevance and awareness of safeguarding culturally significant masonry structures through periodic evaluation and assessment. This is currently done using localized techniques (such as endoscopes, thermographs, sonic tomography, ultrasonic, acoustics, radiographs, and the impact-echo method) that are limited in effectiveness when the vicinity of damage is unknown or inaccessible. Also, localized methods are labor intensive and require highly trained personnel. Structural Health Monitoring (SHM) has the potential to be a fully automated, long-term diagnostic approach for use in the continuous monitoring of structural behaviors (for a review of the method, see Carden and Fanning 2004 and Doebling et al. 1996).

SHM techniques based on global vibration measurements are particularly advantageous when structural problems occur internally, making visual identification of impending failure difficult. Through early diagnosis, sudden collapse of the structure can be avoided and, thus, the costs of reconstruction can be reduced significantly in addition to the life-safety of the occupants. It is unlikely that one can perform destructive testing on historic monuments owing to its historic and cultural significance.

The basic concept in SHM is that the vibration response of a structure is dependent upon physical properties such as mass, stiffness, and damping. A change in the structural state of a building will change these properties, which in turn alters in the vibration response. With the assumption that changes in vibration response, as measured through *in situ* measurements, can be related to the structural state of a building, vibration testing is typically accomplished by exciting a structure using controlled vibrations (e.g. impact hammers, shakers) and capturing the response of the system over time. These time history responses are transformed into the frequency domain through fast Fourier transform. Estimates of the vibration parameters of the structure i.e. the natural frequencies, mode shapes, and damping ratios are obtained by applying various signal processing techniques.

By taking advantage of frequency response characteristics, SHM has been successively applied to modern structures. However, the application of this new technology to existing historic masonry monuments is still considered to be an unsolved issue (De Stefano and Ceravolo 2007). The greatest obstacle to the successful application of SHM in existing monumental structures is the lack of guidance in making *suitable* decisions about the following two aspects:

1. Selection of suitable vibration response features (damage indicator) for symptom-based diagnosis of damage, such as peak response, FRF amplitude, natural frequencies, mode shapes, mode shape curvature, etc. (Farrar et al. 2007).

2. Placement of sensors in optimum locations so that vibration response is sensitive to damage;

This report aims at addressing these two major issues: The first manuscript introduces the concept of feature assimilation with an intention of early detection of damage in the structure and increased confidence in presence of extraneous noise that corrupts the data. It is emphasized that observing multiple low dimensional features together is more advantageous than focusing on a single feature. This concept is illustrated on an arch, a common structural component of historic masonry construction. The second manuscript illustrates the extraction of damage indicators in the time, frequency and modal domains from vibration measurements from the Beverly Minster, a Gothic church in UK. The objective is to detect the damage in the vaults of the church caused due to the long term support settlements. The third manuscript presents an elaborate methodology applied for finding optimal sensor locations for deploying SHM on Gothic style Cathedrals. Ultimately, a best practice guide is developed to be used by engineers for testing Gothic style masonry Cathedrals. Although, demonstrated on a Gothic architecture building, the methodology applied is deemed suitable for any structure.

With proper guidance, the techniques of SHM can be extended beyond modern buildings to existing historic masonry monuments. It is the intention of this report to make such guidance available to professionals involved in assessing, preserving and maintaining historic structures.

CHAPTER TWO
FEATURE ASSIMILATION FOR CONDITION BASED MAINTENANCE

ABSTRACT

Structural health monitoring (SHM) technology for the early detection and mitigation of adverse structural effects, such as degradation or damage, is useful in enhancing the proactive maintenance of civil infrastructure. SHM techniques are advantageous since they eliminate the need for both *a priori* knowledge of the location of damage and access to the damaged portion of the structure. The underlying principle behind SHM involves measuring changes in a system's vibration response, which ultimately indicates changes in physical properties due to structural damage. A challenge to the successful application of SHM to civil infrastructure is the selection of suitable vibration response features that are highly sensitive to the presence and extent of damage, while having low sensitivity to extraneous noise. This study reveals that both damage and noise sensitivity of vibration response features vary for different states of structural health; therefore, the selection of optimum features is dependent on the damage severity, which is not known *a priori*. This study illustrates that assimilating multiple low-dimensional features lessens this dependency and improves the sensitivity of the damage indicators for SHM diagnosis.

KEYWORDS: Vibration Testing, Experimental Modal Analysis, Damage Detection, System Identification, Feature Extraction, Masonry Arches.

1 INTRODUCTION

Structural Health Monitoring (SHM) based on vibration measurements, has emerged as a global monitoring technique to diagnose damage in a system prior to the structural condition reaching a critical stage. The underlying principle of SHM is straightforward: the onset of damage in a built system modifies the structural properties, such as mass, stiffness and damping, which in turn alters the vibration response of the system. Focusing on this indirect relationship between the structural damage and changes in the measured vibration response, SHM aims to detect the onset of damage as well as determine damage characteristics (Doebling et al. 1996). In an ideal situation, the changes in the measured vibration response are directly correlated with the desired damage characteristics, such as the severity, type and location of damage (Rytter 1993). However, attempts to correlate the changes in the measured raw time domain vibration response to damage characteristics are hindered by two factors: (i) the difficulty in monitoring the trends in the oversized measurement data and (ii) the high sensitivity of the time domain measurements to extraneous factors caused by the natural variations in the operational and environmental conditions. Thus, low-dimensional vibration response features are extracted from the raw time domain measurements through data processing and interrogation (Ruotolo and Surace 1997). While the most common vibration response features include natural frequencies, mode shapes, and basic properties of the time history response, such as peak acceleration, many other forms of vibration response features can be extracted from the raw time domain vibration measurements. Ideally, the extracted vibration response features should be sensitive to damage, but insensitive to extraneous noise factors (Farrar and Worden 2007). For practical applications of SHM on civil structures, there has been much debate over whether vibration response features can be sufficiently sensitive to damage, while remaining insensitive to noise (Maeck 2003, Garaygordóbil 2003, Carden and Fanning 2004, Chang et al. 2003). For instance, while some

studies (Begg et al. 1976, Duggan et al. 1980, Fox 1992, Farrar et al. 1994) found vibration response to be insensitive to damage; other studies (Ju and Mimovich 1986, Rizos et al. 1990, Dong et al. 1994, Meneghetti and Maggiore 1994, Fritzen at al. 1995) observed vibration features to be reliable damage indicators.

Figure 1 schematically illustrates the difference between a damage-sensitive and -insensitive vibration response feature. In Figure 1, the unitless *damage indicator* represents the measured change in a vibration response feature corresponding to the unitless *damage index*. The *damage index*, which quantitatively represents the extent of damage, ranges from a value of zero, representing an undamaged structure, to a value that represents the most severe damage condition of interest. The slope of the plot, denoted by α, defines the damage sensitivity of a given feature. A steeper slope, α, of the plot means a more sensitive feature. Hypothetically, in a worst case scenario, as the damage sensitivity of a feature approaches zero, the feature has insignificant sensitivity; and in a best case scenario, as the damage sensitivity approaches infinity, the feature has significant sensitivity to damage.

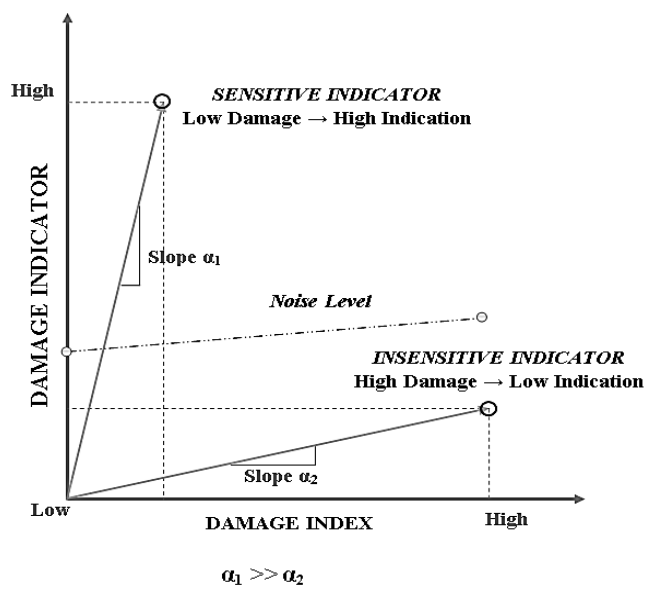

Figure 1: Sensitivity of damage indicators to varying levels of damage.

The presence of extraneous noise during vibration testing decreases the ability of vibration features to indicate changes due to damage. Therefore, the damage sensitivity must be considered in light of the noise sensitivity of the feature, which also varies for varying structural states. The schematic illustration in Figure 1 represents the noise sensitivity level gradually increasing for increasing stages of damage. As Figure 1 illustrates, insensitive damage indicators may remain below their noise level even for very high damage indices. On the other hand, sensitive indicators are those that yield values significantly above noise levels at early stages of damage. The schematic illustration of Figure 1 is, of course, an idealized approximation. In practice, both damage and noise sensitivity of vibration response features may vary nonlinearly for different states of structural health; therefore, the selection of optimum features may become dependent upon the damage severity. Moreover, the difficulty in selection of optimum features is compounded with the fact that the feature sensitivity may also change for different damage types. Of course, neither the damage type nor the severity is known *a priori*; therefore, it becomes necessary to use *multiple* vibration response features to account for the non-uniform relationship of a feature's sensitivity to varying damage type and severity.

The objective of this study is to investigate if damage sensitivity of SHM diagnostics can be improved by assimilating multiple low dimensional vibration response features instead of focusing on a single feature. An experimental study is completed on a scaled semi-circular arch. Section 2 introduces the case study structure and Section 3 overviews the design and execution of the experimental campaign. Section 4 investigates discusses the damage sensitivity of commonly used features. Section 5 overviews the practical application of the assimilation concept and presents the noise sensitivity of selected features. Finally in Section 6, overview of the main findings, discussions on the underlying premises and suggestions for future directions are given.

2 CASE STUDY APPLICATION: ARCH PROTOTYPE

The present study investigates the vibration response of an idealized arch model, a common structural form found in masonry construction, and mimics a typical failure mechanism of masonry arches. If a masonry arch is loaded beyond its capacity, cracks incrementally develop within the arch assembly. A crack propagating through the entire depth of the arch forms a hinge. According to mechanism analysis, the development of four hinges is needed to ensure the failure of an arch with a fixed support (Heyman 1997) (Figure 2), while the location of these four hinges depends upon the loading condition. Herein, a numerical model is used to determine the precise locations of the cracks under a static concentrated load applied at quarter span (Figure 3). Four distinct locations with the highest von Mises stress are approximated as the locations of the four hinges, which agree well with those obtained through a nonlinear FE analysis by Ramos (2007) (Figure 3).

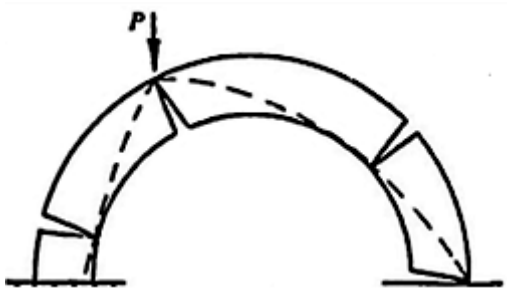

Figure 2: Crack locations in an arch due to concentrated load at the quarter span using the inverted chain analogy, reprinted from Heyman (1997) with permission.

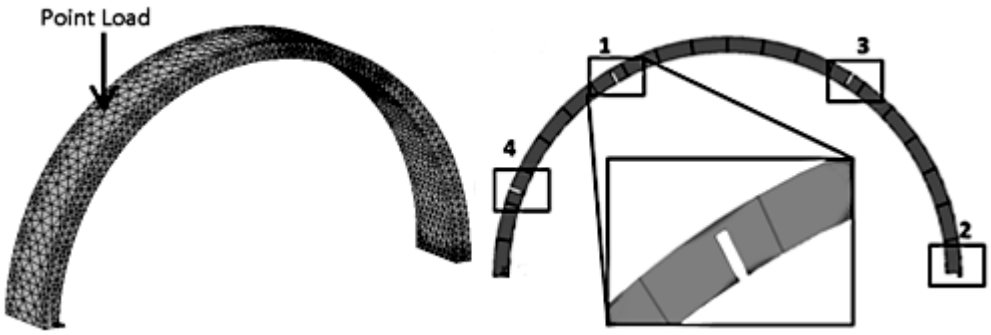

Figure 3: (Left) FE model of the arch with a static load at quarter span, (Right) arch experiencing maximum damage through artificial cracks.

For the experimental campaign, a PVC arch with a.31.8cm radius, 64cm depth and 2.5cm thickness is used (Figure 4). The arch is damaged to four levels in succession, with a 2cm deep crack at each of the four hinge locations as shown in Figure 3a. A total of four damage states are obtained with varying levels of structural damage.

3 EXPERIMENTAL PROCEDURE

The response is measured at 33 equidistant measurement points with three across the width of the arch and 11 on the perimeter. Hammer impact tests are performed exciting two points (points 21 and 23) on the arch, allowing the excitation of both bending and torsional modes (Figure 4). Point 23, located through the centerline of the arch, primarily excites the bending modes, while Point 21, located at the edge, primarily excites the torsional modes. Piezoelectric IEPE accelerometers with a sensitivity of 500 mV/g are used to measure the vibrations, while an impact hammer with a sensitivity of 2.27 mV/N and a maximum force capacity of 2200 N is used to excite the structure. The impact hammer is used with the softest plastic tip available.

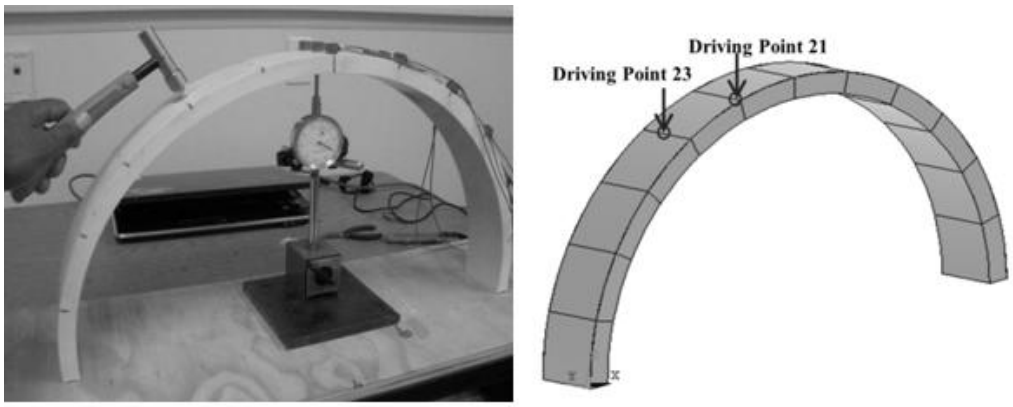

Figure 4: (Left) Test structure used for experimental study, (Right) hammer impact locations on the test arch.

Impact hammer tests are performed with a frequency range of 0 to 1.6 kHz. The frequency resolution is set to 1 Hz and the time resolution is set at 244 μsec. The acceleration response is measured for 1 second, within which the response of the arch is attenuated; therefore, no windowing function is applied. To reduce the degrading effects of noise and to increase statistical reliability, a total of five averages are obtained. Anti-aliasing filters are used to prevent higher frequencies from contaminating the measurements.

Using the Rational Fraction Polynomial algorithm, Frequency Response Functions (FRFs) collected for each damage state, are analyzed to identify the natural frequency and mode shapes of the arch. The modes are selected using both the Summation and Multivariate Mode Indicator Functions (MMIF) (Williams st al. 1985). These functions make the resonance peaks in the FRFs more evident. The first four modes of the model arch are identified. Next, the tests are repeated in the presence of artificial, random noise to investigate the effect of damage levels on the noise sensitivity of FRFs.

4 EXTRACTING VIBRATION RESPONSE FEATURES

Rarely, multiple vibration response features are objectively and quantitatively compared in their ability to indicate damage (Garaygordóbil 2003). In this study, an extensive list of vibration response features is evaluated, including Frequency Response Assurance Criterion (FRAC) (Heylen and Lammens 1996), Root-Mean-Square (RMS) Time Domain Response (Lawler 1979), Modal Assurance Criterion (MAC) (Allemang 1980), and Coordinate Modal Assurance Criterion (COMAC) (Lieven and Ewins 1988). For brevity only a select few of the most common of these features are reported in detail, while a brief summary of the results for the rest are provided in Section 6.

4.1 NATURAL FREQUENCY CHANGES

Natural frequencies (also known as resonant frequencies) supply convenient, low-dimensional and physically meaningful vibration response features (Carden and Fanning 2004), Atamturktur et al. 2009, Aoki et al. 2005, Gentile and Saisi 2007). In earlier SHM related studies, higher order natural frequencies are reported to be more sensitive to damage than lower order natural frequencies (Alampalli et al 1997, Doebling et al. 1998). For instance in a recent study, the first three natural frequencies are observed to be identical for a damaged and undamaged masonry vault of Beverley Minster, a masonry cathedral located in the U.K. (Atamturktur et al. 2010). In contrast with earlier studies, for the arch studied herein, the natural frequencies are noted to exhibit sensitivity to the propagation of cracks (Figure 5).

The measured changes in the first, third and fourth natural frequencies reach approximately 18% for the most severe damage state. The experiments identify the frequency of the second mode as the least sensitive feature. The first, third and fourth natural frequencies exhibit a monotonic increase for increasing levels of damage; while the second natural frequency exhibits false-negatives since the % change in the frequency is reduced from the second damage state to

the third. In such a situation, the monitored structure may appear to be at the same (or better) structural health level, while in fact the damage is propagating, i.e. the structure exhibits a false negative.

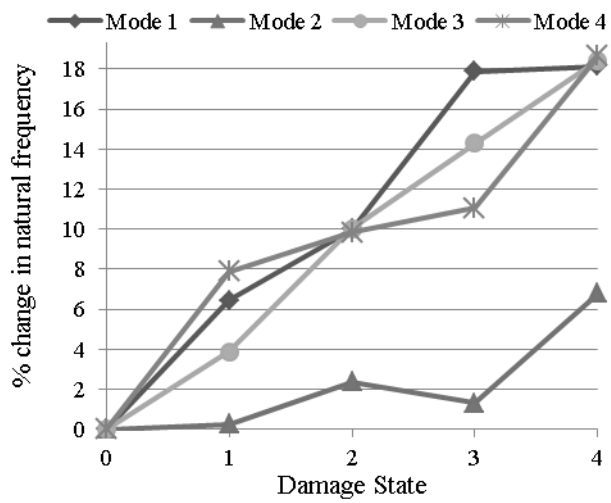

Figure 5: Percentage change in the first four natural frequencies with progressive damage.

4.2 MODE SHAPE DISTORTIONS

The onset of damage in a structural system tends to distort the mode shapes (Bayraktar et al. 2011). For SHM purposes, the mode shape distortions can be exploited in a variety of forms, such as MAC correlation or percentage change, as reviewed by Ewins and Ho (2000). In this study, when determining mode shape distortion, the mode shape vectors are first normalized between 0 and 1, and then the percentage change in mode shape difference is calculated according to Equation (1):

$$\frac{\sum_{i=1}^{N}|x_{di}-x_{ui}|}{\sum x_{ui}} * 100 \qquad (1)$$

where:

x_d = the modal displacement of damaged structure

x_u = the modal displacement of undamaged structure

N = the number of measurement points.

This percentage change is reported for the 33 measurement points of the experimental arch model in Figure 6.

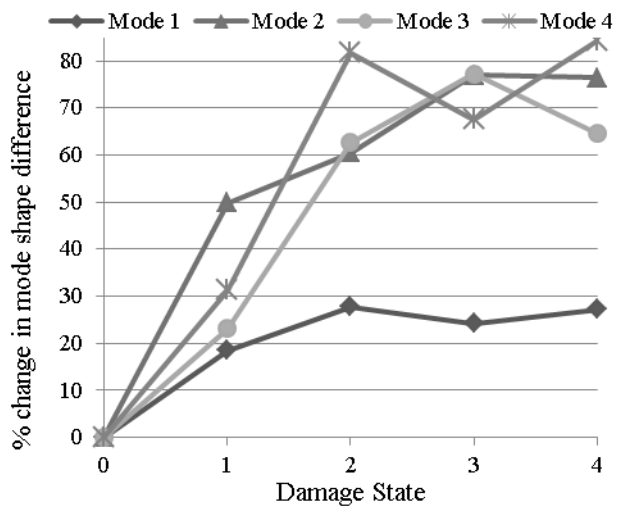

Figure 6: Percentage change in the first four mode shape vectors with progressive damage.

Compared to the natural frequencies, the sensitivity of the mode shape distortion is observed to be significantly higher. The second, third and fourth mode shapes exhibit an approximately 65-85% distortion for the most severe damage state; this value is only 30% for the first mode shape. The experimental findings presented in Figure 6 reveal a nonlinear and non-monotonic relationship between the mode shape distortions and the extent of damage. The sensitivity of mode shape distortion as a damage-indicating feature is observed to decrease at certain damage levels resulting in false-negatives.

4.3 MODE SHAPE CURVATURE

Mode shape curvature is a localized vibration feature that is inversely related to the stiffness at the location it is calculated (Pandey et al. 1991). Since the presence of a crack or separation abruptly decreases the stiffness in the vicinity of damage, the mode shape curvature also abruptly

changes near the location of the damage. The mode shape curvature at node *i* is calculated according to Equation (2).

$$MSC_i = \frac{\emptyset_{i+1} - 2\emptyset_i - \emptyset_{i-1}}{h^2} \quad (2)$$

where:

Φ_i = Modal displacement at degree of freedom *i*

h = distance between degree of freedom *i+1* and *i-1*

Figure 7 represents the summation of the mode shape curvature changes for the first four modes summed for all 33 measurement points. The sensitivity of mode shape curvature is noted to be slightly lower than that of the mode shape distortions varying between 55-80% for the most severe damage state. The experimental campaign indicates that the second mode shape curvature is the most sensitive to damage and the first mode shape curvature the least sensitive.

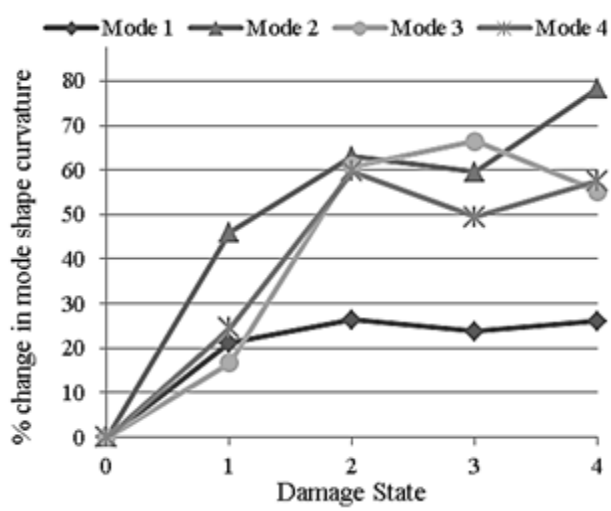

Figure 7: Percentage change in mode shape curvature with progressive damage.

4.4 STATISTICAL MOMENTS

Statistical moments, such as mean, standard deviation, skewness and kurtosis, can be used to effectively compress and characterize raw vibration response measurements, x_t. The first statistical moment is the *mean* of the vibration response measurements given in Equation 3

(Statistics Toolbox Users Guide 2003), which describes the central tendency of the data. The second statistical moment is the *standard deviation*, which measures the dispersion of the data from the mean. The standard deviation of the dataset is given in Equation 4. The third statistical moment is *skewness*, which measures the asymmetry of the probability density function (PDF). The skewness of a time series is given by Equation 5. A zero skewness value means that the values are evenly distributed on both sides of the mean. The fourth statistical moment is the *kurtosis*, which is a measure of the weight of the tails, i.e. the relative amount of data within the tails of a time series. The kurtosis is calculated according to Equation 6. A higher kurtosis indicates a distribution, where a majority of the variance is caused by a few severe deviations from the mean rather than more frequent modest deviations.

$$\mu = \frac{\sum_{t=1}^{N} x_t}{N} = E(x_t) \tag{3}$$

$$\sigma_x = \sqrt{\frac{\sum_{t=1}^{N}(x_t-\mu_x)^2}{N}} = \frac{E(x_t-\mu_x)}{\sqrt{N}} \tag{4}$$

$$S = \frac{E(x_t-\mu_x)^3}{\sigma_x^3} \tag{5}$$

$$k = \frac{E(x_t-\mu_x)^4}{\sigma_x^4} \tag{6}$$

where:

x_t = vibration response data

N = the number of data points

E= expectation operator, calculates the mean of a random quantity

The first four statistical moments are calculated considering all the FRFs for 33 measurement locations on the test arch. The first two statistical moments are observed to be insensitive to damage and thus left out of further discussion. The third (skewness) and the fourth (kurtosis) statistical moments, plotted in Figure 8 are observed to exhibit high sensitivity to damage. The

percentage changes in these two features are plotted for the experimental data in Figure 9. The skewness feature yields a 90% total change for all sensor locations due to damage for the most severe damage state. The kurtosis feature is more than 3 times as sensitive as the skewness and yields a 300% change for the same damage level.

The damage sensitivity of the skewness and kurtosis are significantly higher compared to the natural frequencies and mode shape derivatives. However, as it will be discussed in Section 4.3, one must bear in mind that skewness and kurtosis are also sensitive to environmental noise.

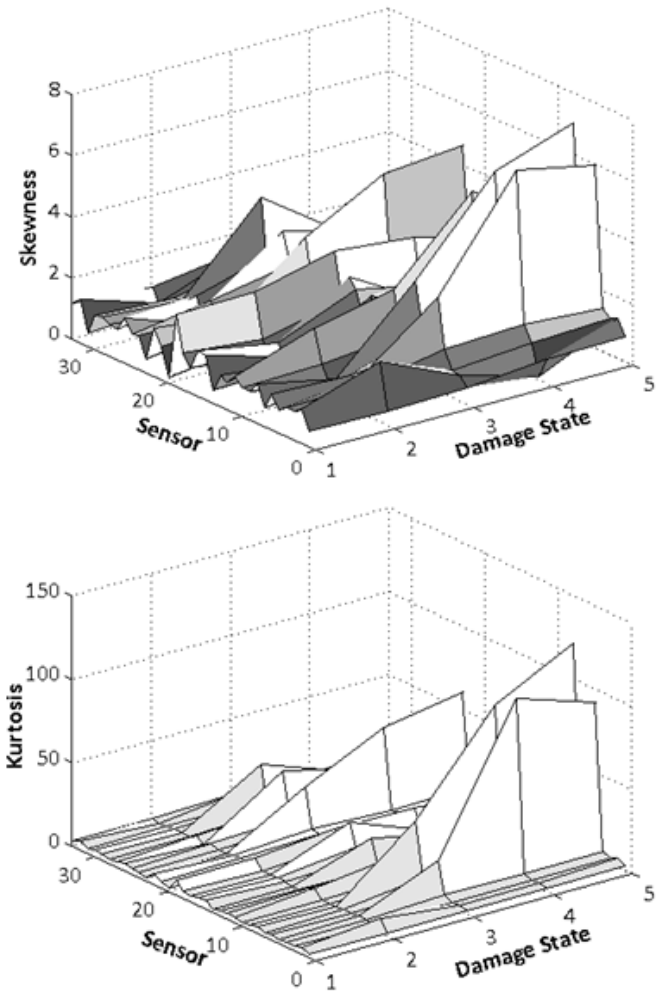

Figure 8: (Top) Skewness and (Bottom) Kurtosis of FRF measurements from the experimental hammer impact test.

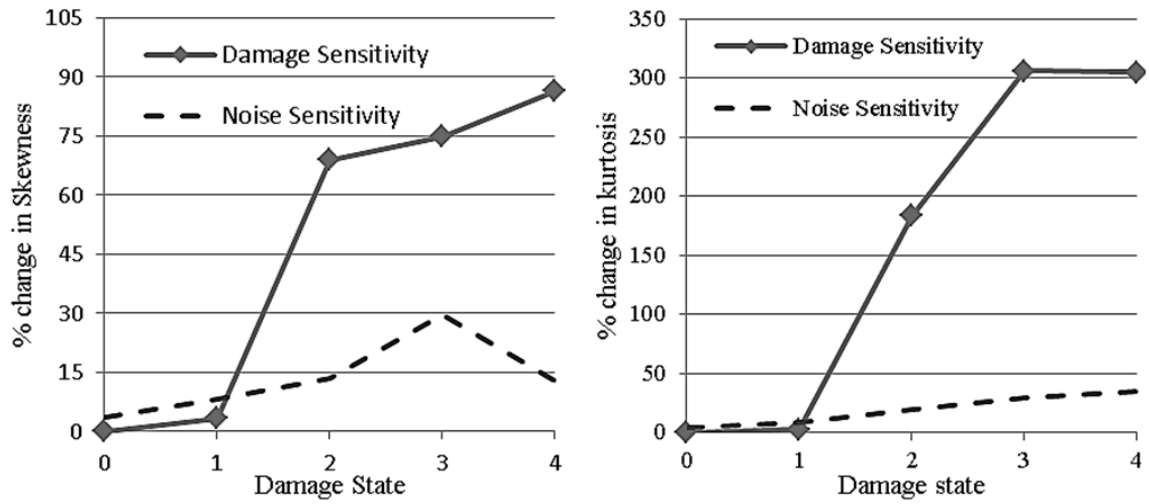

Figure 9: Absolute percentage change in the (Left) skewness and (Right) kurtosis for FRFs from the experimental campaign with the dashed lines signifying the noise sensitivity.

4.5 REGRESSION ANALYSIS

Time domain regression analysis aims to train models to fit auto-correlated time-series data. The coefficients of the fitted model, the residuals between the model and the time domain data, or as in our case, the singular values of the fitted model can be used as features. Perhaps, the most common regression analysis is the Autoregressive (AR) model, which is given for an order *p* in Equation 7 (Akaike 1969). Herein, the Root Mean Square Error measure is implemented to find the optimal AR order. Root Mean Square Error is a measure of the total difference between values estimated by the AR model and actual measured values. A maximum order of 22 and a minimum order of 2 are obtained for the FRFs from the experiments. Therefore, to avoid any loss of information and reduce the residuals, a model order of 22 is used for future analyses.

$$x_t = \sum_{i=1}^{p} \emptyset_i x(t-i) + e_t \qquad (7)$$

where:

x_t =the time or frequency domain response under investigation,

e_t = the residual term

φ_i = the AR parameters

Herein, an AR model is trained using the least squares estimation of the undamaged arch. The magnitude of the singular values of these trained models act as features, while the changes in the features are calculated based on Euclidean norm of residuals between the undamaged and damaged singular values. The changes in features are normalized and summed for all 33 measurement points to obtain the damage indicator (Figure 10).

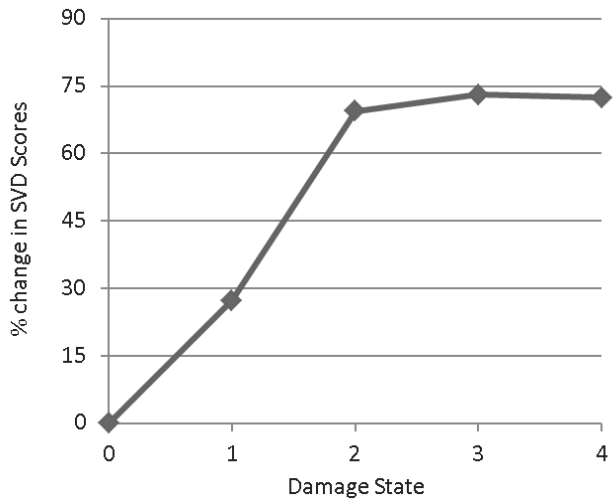

Figure10: Singular Value Decomposition (SVD) scores for AR model parameters of the FRFs from the experimental campaign.

5 ASSIMILATING VIBRATION RESPONSE FEATURES

The vibration response features described in the previous section are advantageous, since they are low-dimensional and thus make trends in the vibration response readily observable. Moreover, the mathematical model-fitting during feature extraction acts as a filter and to a certain extent, removes the extraneous effects of noise factors from these low-dimensional features. However, while operating with such low dimensional features, there is the danger of excessively reducing the measurement data, which may result in the loss of important information about the

structural damage. This section illustrates an approach to remedy this problem by assimilating multiple low dimensional vibration features.

5.1 DAMAGE SENSITIVITY OF ASSIMILATED FEATURES

Earlier in the paper, Figure 1 introduced the concept of determining the damage sensitivity of a vibration feature based on the slope, α, between the damage indicator and damage index. Recall that the damage indicator is a unitless entity and thus, can be directly compared against each other. Therefore, once all the damage indicators are normalized and made dimensionless, they can be added together to increase the sensitivity to damage. This approach can be extended to all possible combinations of vibration features, as long as the damage indicators derived from the changes in the vibration features are treated as normalized values.

Figure 11 illustrates the assimilated damage indicators obtained through the experimental campaigns considering only the frequency, mode shape distortion and mode shape curvature. Here, the damage sensitive indicators of the vibration response features are summed together to obtain a more sensitive damage indicator. As seen, assimilation of various vibration features greatly increases the slope, α, of the damage indicator with respect to the damage index. By adding new features through assimilation, this slope, α, can be further improved up to an asymptote of infinity. For instance, see the bottom figure in Figure 11, where features obtained from statistical moments and regression analysis are added to those in the top figure in Figure 11 to reach an even more sensitive damage indicator. As seen, the slope, α, of the plot increases approximately from seven to 13 by the addition of two new features.

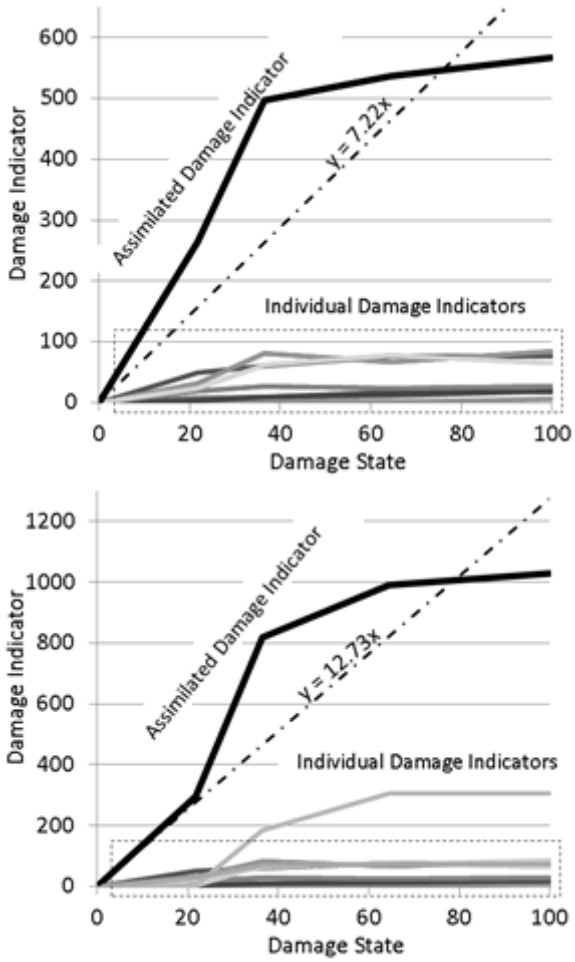

Figure11: Damage sensitivity comparison of various damage indicators with progressive damage: (Top) experimental campaign with three features, (Bottom) experimental campaign with five features.

Section 4 revealed that the sensitivity of features may vary for different damage levels and exhibit decreasing trends. However, as seen in Figures 11, the assimilation of multiple low-dimensional features yields a monotonic, non-decreasing trend and reduces the risk of false negatives, i.e. interpreting the data as if the structure is maintaining its state, while the damage is in fact propagating.

5.2 NOISE SENSITIVITY

The selection of vibration response features must go beyond damage sensitivity and consider the effects of noise on features. In this study, the vibration response features are identified under controlled excitation forces (i.e., impact excitation); therefore herein noise constitutes the effects of ambient noise in the system on identified features.

This section investigates the degrading effects of random noise by applying an artificial white noise signal with amplitude of 0.25Vrms and a frequency range of 0 to 1.6KHz to the scaled arch structure using electrodynamic shakers. Figure 12 presents the FRFs for the five damage levels obtained with and without artificial noise. As evidenced in Figure 12, the effect of noise on FRFs is not constant for all damage levels. In fact, the noise sensitivity of FRFs increases as the damage level increases. Therefore, as damage progresses, system identification of modal parameters and extraction of other low dimensional features form FRFs become increasingly difficult and the parameters extracted become increasingly uncertain. This implies that in Figure 1 the noise sensitivity of features should in fact be represented as a non-constant variable.

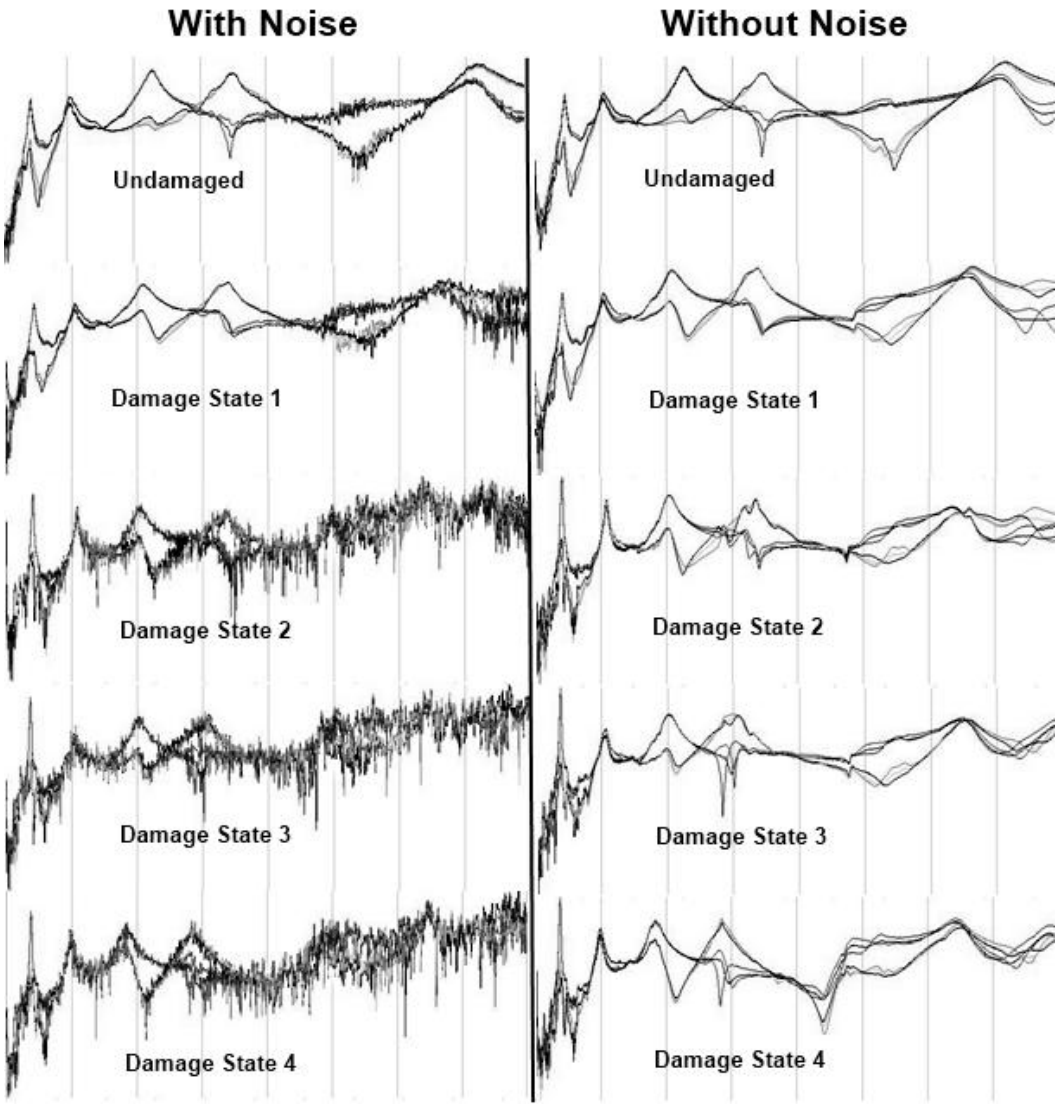

Figure 12: Changes in FRFs for increasing damage levels with and without ambient noise.

In Figure 9, the dash-lines display the percentage change in the skewness and the kurtosis, respectively, between the FRFs with and without the applied noise for all experimental damage states. The change in noise sensitivity of skewness remains below 30% and exhibits a non-monotonic trend as the damage increases. On the other hand, for increasing levels of damage, the absolute change in kurtosis, i.e. the peakedness of the FRF, remains below 35%. As seen in

Figure 12, the FRFs become noisier as damage a level increase, which makes it more difficult to identify features in the FRFs (Balanda and MacGillivray 1988).

In Figure 13, the assimilation of both damage and noise sensitivity plots considering the skewness and kurtosis features is demonstrated. Here, for the most severe damage state, the assimilated damage indicator reaches as high as 400%, while the assimilated noise effects remain as low as 50%, yielding a signal-to-noise ratio of eight to one. However, from Figure 13, it is also evident that the first damage state with a single crack is not diagnosable when skewness and kurtosis features are used. The changes in the selected vibration response features are approximately 6%, which fall below the noise levels of 17%.

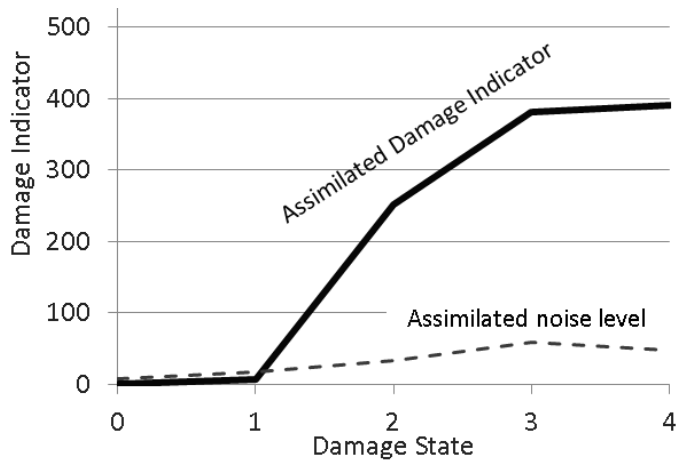

Figure 13: Assimilated damage indicator with the change in skewness and kurtosis and the assimilated noise level for the two features.

6 DISCUSSION

Through the case study structure evaluated herein, it is observed that the noise sensitivity of a structure increases as the damage level increases. Therefore, for varying levels of damage severity, there is a need to determine optimum features, which concurrently exhibit high damage sensitivity and low noise sensitivity, and thus yield high signal-to-noise ratios. A variety of vibration response based features are experimentally evaluated for the semi-circular arch

considering the propagation of cracks due to a hypothetical, gradually increasing concentrated load. The development of four distinct hinges is approximated as cut-outs from the cross-section. Experimentally obtained natural frequencies, mode shape distortions, mode shape curvature, as well as features obtained from statistical moments and regression analysis exhibit monotonic, non-decreasing trends as the damage level increases. For higher order modes, difficulties are observed when calculating the MAC and COMAC features due to the modes swapping order, appearing and disappearing as damage propagates. Owing to the abrupt changes in the sequence of modes, the FRAC are observed to yield significantly high changes. However, it must be emphasized that the noise sensitivity of the FRFs is observed to increases with the increase in damage; therefore, for practical applications a change in FRAC may overestimate the presence of damage. The maximum vibration response of the structure is found to be increasing in a linear relationship to an increase in the damage index, due to the increased flexibility of the structure. However, the RMS vibration response feature is observed to have a highly nonlinear relationship to the severity of damage.

7 CONCLUSION

SHM is a global diagnostic technique for condition-based maintenance of civil infrastructure. In the past, the research community involved in SHM has used a variety of vibration based features. Largely based on the convenience and ease in their identification from measurements, natural frequencies and mode shapes as well as their derivatives have received the most attention in published work. An overview of pertinent literature reveals that optimum damage indicating features vary based on the varied user end requirements of SHM, i.e. the specifics of the structure and damage types to be diagnosed. Therefore, it becomes challenging to select a single, best feature, while maintaining the general applicability of the diagnostic procedure. Our contribution

to the state-of-the-art is the concept of assimilating normalized unitless damage indicators. By first normalizing the damage indicators, one can obtain unitless quantities which cannot only be objectively compared in their damage and noise sensitivity, but also be added together to become better indicators of damage.

The experimental campaign is configured to mimic an impact hammer test, which is a type of test where controlled excitation sources are used. However, the experimental findings of ambient vibration testing can easily be incorporated into the proposed framework. This study presumes the availability of measurements from the undamaged state of the structure of interest and this assumption, in real life applications, may reduce the practicality of the proposed method.

Although the vibration response features are observed to be successful in indicating damage in general, the results presented herein may vary for different structure types and damage scenarios. Therefore, similar studies must be completed for other common forms of masonry structures, such as domes, vaults, buttresses, etc.

ACKNOWLEDGMENTS

This work is performed under the auspices of the PTT Grants program of National Center for Preservation Technology and Training (NCPTT) of Department of Interior: the Grant Agreement Number MT-2210-10-NC-01.

CHAPTER THREE
VIBRATION CHARACTERISTICS OF VAULTED MASONRY MONUMENTS UNDERGOING DIFFERENTIAL SUPPORT SETTLEMENT

ABSTRACT:

This paper assesses the feasibility of vibration testing to detect structural damage caused by the settlement of buttresses in the Beverley Minster, a Gothic church located in the UK. Over the last eight centuries, the accumulated support settlements of the buttresses of Beverley Minster have pulled the main nave walls outward, causing severe separation along the edges of the masonry vaults. Bays closer to the main crossing tower have remained intact; however, at the west end of the Minster, the crack width between the walls and vaults has reached about 150 mm, leading to approximately 200 mm of sag at the crown of the vaults. Due to uneven settlement of buttresses along the nave of the church, the Minster now has ten nominally identical vaults at different damage states. In this work, two of these vaults representing the two extremes, the most damaged and undamaged structural states, are subjected to vibration testing with impact hammer excitation. From these vibration measurements, damage indicators are extracted in the modal, frequency, and time domains. In the modal domain, the differences between modal parameters are observed to be comparable to measurement uncertainty and hence insufficient to reach conclusions about the presence of vault damage. However, the amplitudes of frequency response functions in the frequency domain are observed to indicate a clear difference between the damaged and undamaged states of the structure. A time domain autoregressive model, support vector machine regression, is also found to be successful at indicating the differences between the two structural states of the vaults. We conclude that vibration measurements offer a practical

solution to detect wall-vault separation in historic masonry monuments, provided that multiple damage indicators are evaluated.

1 INTRODUCTION

Masonry is a common building material in many historic monuments and has unique intrinsic properties that make it particularly susceptible to differential support settlements. Support settlement is a more frequent problem among masonry buildings because masonry structural systems tend to be significantly heavier than those of reinforced concrete or steel buildings. When the demand for large bearing capacities from supporting foundations are not met due to deteriorating soil conditions, the supports of a masonry building incrementally settle and induce tensile forces in the structure. However, unreinforced masonry buildings are primarily designed to be loaded in compression; as such, they are characterized by stiff units separated by relatively soft mortar joints. As a result, tensile forces induced by differential support settlement easily lead to geometric deformation and structural discontinuity, which alters the mass, stiffness and energy dissipation properties of the structure. Because the vibration response is intimately dependent on these properties, the change in the structural behavior due to damage may be detectable by vibration measurements. This hypothesis is the focal point of this manuscript.

The success of vibration testing-based structural health monitoring (SHM) depends not only on the structural characteristics of the building and the type and severity of damage, but also the response ***features*** used to characterize the vibration properties. In an ideal situation, a measured vibration response feature is directly correlated to the presence and extent of damage. However, in practice the response of a structure is typically measured in terms of time-dependent

acceleration. Any attempt to directly correlate these raw time domain acceleration measurements to structural damage is hindered by the sensitivity of the time domain response to many factors, such as environmental conditions and ambient vibrations that are unrelated to the presence or extent of damage. Therefore, data processing and/or coordinate transformation become necessary to extract low-dimensional diagnostic features from the raw time-domain measurements. The clear requirement for these features is that they must be sensitive to damage and insensitive to noise factors, such as changes in environmental conditions and ambient vibrations. This requirement makes feature selection challenging since both the damage-sensitivity and noise-sensitivity of vibration features are application-specific. Therefore, the most suitable feature for a structure with a particular type of damage may be unsuitable for another structure or even for a different type of damage within the same structure. As a result, the damage-sensitivity of vibration features for a given structural system must be individually evaluated for a given damage scenario. In this manuscript, we evaluate the damage-sensitivity of various vibration response features to the separation between walls and vaults, a common structural problem in Gothic churches.

Figure 1: The interior view of the nave of the Beverley Minster displays the limestone piers that support the stone vaulting. The leaning of the columns outwards is visually observable onsite.

This evaluation can be performed most effectively by separately testing damaged and undamaged states of the same structure. However, one can hardly imagine damaging an existing historic structure for such evaluations. In fact, engineers involved in SHM applications rarely have the opportunity to test an existing structure in its damaged and undamaged states. Considering this difficulty, Beverley Minster presents a unique opportunity by allowing the investigation of ten masonry vaults, which are substantially similar in their geometry, boundary conditions, construction materials, erection technique and workmanship, varying only in the extent of structural damage they have endured [Figure 1]. Structural damage in Beverley Minster's vaults manifests itself primarily as Sabouret cracks (Heyman 1966) and has been primarily caused by settlement of nave buttress foundations [Figure 2]. Section 3 discusses the

details of the damage in Beverley Minster's vaults and briefly overviews the history of the structure.

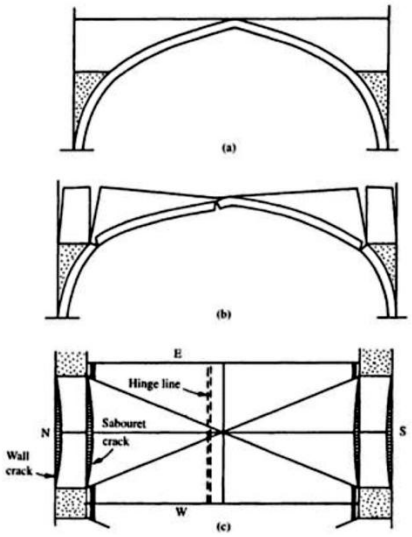

Figure 2: A schematic of Sabouret Cracks, by Heyman [2] (with permission).

In the present study, two vaults, one that exhibits the most severe wall-vault separation and the other visually no wall-vault separation, were selected and subjected to vibration testing. Hereafter, these two vaults are referred to as the damaged and undamaged vault prototypes [Figure 3]. These two prototypes provide the opportunity to obtain vibration measurements from two different structural states of otherwise similar vaults of Beverley Minster. With this statement comes a caveat; these two prototypes are assumed to be different only in their damage states, while their initial geometry, boundary conditions, construction materials, erection techniques and workmanship are accepted to be sufficiently similar. Actions taken to justify this assumption include (1) performing full-size geometrical surveys to determine geometric variability, (2) conducting local non-destructive tests to estimate material variability and finally (3) simulating

the effect that estimated geometric and material variability have on the vibration response of the structure through finite element models. Section 4 discusses the actions taken to quantify the vault-to-vault variability and Section 5 discusses the finite element model simulations. The finite element model simulations illustrate that the vault-to-vault variations have an insignificant effect relative to the effect of the structural damage on the vibration response.

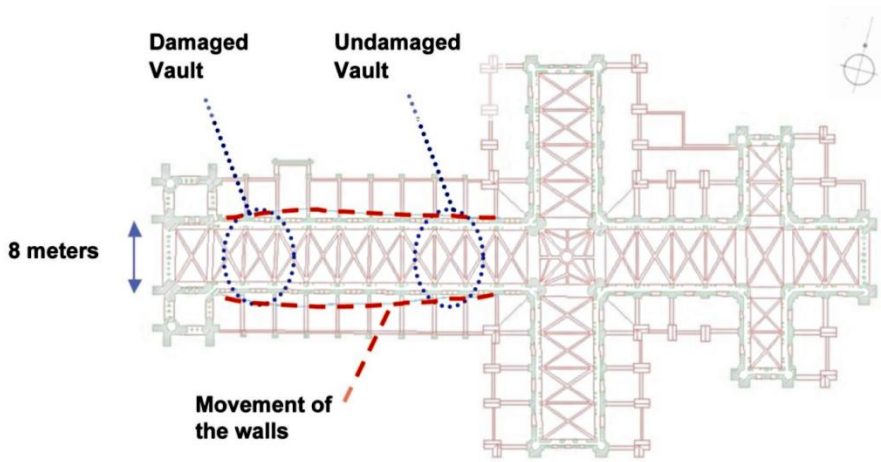

Figure 3: The movement of the walls is not uniform along the length of the nave; as such the Minster now has ten vaults with varying damage states. Two vaults representing the most damaged and undamaged states are selected for the study.

The remainder of this paper consists of discussing the adopted testing campaign, namely, vibration testing with impact hammer in Section 6 and evaluating the collected vibration measurements. In Section 7, this evaluation is completed in the modal domain. Section 7 includes the finding that certain modal features, such as natural frequencies and mode shapes of the first three modes, fail to indicate the differences in the structural states of the two prototype vaults. Further evaluations are completed in the frequency and time domains in Sections 8 and 9,

respectively. In the frequency domain, the amplitudes of frequency response functions (FRF) acquired from the damaged vault are noticeably higher than that of the undamaged vault, providing a clear indication of the structural differences between the two vaults. In the time domain, the time domain autoregressive methodology implemented herein also exhibits sensitivity to the damage present in the vaults and provides clear indication of the structural differences between the two vaults.

2 BACKGROUND

Although the majority of vibration-based damage detection studies in civil engineering literature focuses on reinforced concrete and steel structures, , a number of key studies on historic masonry monuments have been reported over the last three decades. In this section, we organize these relevant studies into three categories: scaled laboratory models, existing damaged structures, and structures with retrofit.

Scaled Laboratory Models**:** One of the earlier studies on vibration-based damage detection was applied by Armstrong, et al. (1995a) to investigate spandrel wall separation. The authors measured the vibration response of two scaled masonry arch bridge models under impact hammer excitation, one of which featured damage due to wall separation. The authors had success in relating the deviations in modal parameters obtained from the two scaled arch bridge models to their structural condition. Armstrong, et al. (1995b) obtained consistent results when a similar study was performed on the scaled arch bridge models that focused on the dynamic stiffness instead of modal parameters. These two successful studies suggest that vibration measurements are a viable monitoring tool for detecting spandrel wall separation in existing masonry arch bridges. However, the authors stressed the necessity to investigate the damage-sensitivity of arch

bridge vibration characteristics to a wider range of structural defects. This call to evaluate the damage-sensitivity of vibration characteristics for a wider range of damage scenarios is reflected in the attempt of the present study to investigate the feasibility of vibration testing to detect damage induced by support settlement.

Bensalem et al. (1995 and 1997) also investigated the vibration response of scaled brick arch models. By observing the difference in the peak amplitude frequency response functions, Bensalem et al. (1999) detected void presence and size in the arch bridge backfill. This finding is consistent with the observations of the present study, see Section 8.

SHM tools have also been applied to scaled masonry building models. Vestroni et al. (1996) tested a 1/5th scale masonry building under shaker excitation. Vestroni et al. successively increased the excitation force and incrementally induced structural damage. As damage was induced, a reduction in the dynamic stiffness was observed. Ramos (2005) also had success in observing a consistent decrease in natural frequencies as the cracks in a full-scale rubble stone building successively increased. Ramos (2007) conducted a similar study on scaled arch and wall models built with clay bricks of low compressive strength and mortar with poor mechanical properties, such that the models were representative of historic construction. Controlled static forces were applied to the scaled models to progressively induce cracks. By monitoring the modal parameters of the scaled models, a clear loss of stiffness was observed after the first crack. Modal parameters provided evidence consistent with damage in the system—with increasing levels of damage, frequencies were reduced while damping coefficients were increased. In contrast with the natural frequencies, Ramos (2007) noted that the mode shapes of the test structure generally remained unchanged.

Existing Damaged Structures: Studies conducted under controlled laboratory conditions are largely immune from complications caused by support settlements, environmental loads, material deterioration, prior damage, and operational conditions. That is why laboratory experiments on scaled masonry models typically yield higher quality measurements compared to the tests conducted on existing masonry structures. Moreover, laboratory experiments often overlook the practical difficulties of performing in-situ vibration tests, thus providing a poor reflection of the difficulties involved in SHM. Therefore, studies completed on existing structures are of great value for SHM literature.

Gentile and Saisi (2006) completed a damage detection study on a historic masonry tower based on finite element model calibration. The tower was partially damaged with extensive vertical cracks as a result of excessive compressive forces. The modal parameters of the tower were identified by ambient vibration testing. The finite element model was built with six distinct regions each representing a different damage severity. After calibration, the finite element model yielded relatively low Young's modulus values in the damaged regions, illustrating the potential of simulation-based methods to deliver useful information about the state and location of damage in a masonry structure. A unique vibration-based damage detection study was completed on 534 stone pinnacles in the Palace of Westminster in London (Ellis 1998). The natural frequencies of the pinnacles were obtained by using impact excitation for smaller pinnacles and exploiting wind excitation for larger pinnacles. The natural frequencies of the pinnacles were compared against each other and the outliers were detected. The five pinnacles with outlier natural frequencies were successfully identified as damaged pinnacles.

As seen when investigating an existing structure, the analysts can typically collect only a restricted number of measurements from either one of the undamaged or damaged states. This restriction has received significant attention in technical literature. Some researchers attempted to simulate the damage scenarios with numerical models (Yang and Lee 1999), while others focus on scaled experimental specimens at undamaged vs. damaged states (Rytter and Kirkegaard 1997). The former approach is hindered by errors and uncertainty inherent in the numerical simulations, while the latter fails to represent the challenges present in real life applications. Methods successful in detecting damage, in the absence of *a priori* data from the undamaged structure, focus on outliers and novelty analysis to detect the onset of future damage. These methods have recently been deployed on historic masonry monuments (Safak 2003; Durukal, Cimilli and Erdik 2003). Implicit in this approach is the assumption that damage will manifest itself as observable changes in the vibration measurements (Sohn, et al. 2004). One contribution of the present manuscript is to demonstrate that this assumption is not always applicable.

Structures with Retrofit: An alternative approach to gain information about the various states of a structural system is the assessment of structural improvements after retrofit or strengthening campaigns. In their ambient vibration analysis, which compared identified modal parameters before and after retrofit, Turek, et al. (2002) found an increase in the dynamic structural stiffness of a recently repaired historic church. Increased dynamic stiffness after retrofit was also observed in a similar study on a historic basilica by Antonacci, et al. (2001) and on a historic masonry tower by Ramos (2007).

The previously successful studies, whether focusing on scaled laboratory models or existing structures, predominantly use differences in modal parameters or their derivatives as damage

indicators. In earlier studies, other response features, such as frequency domain or time domain features, have seldom been incorporated. Furthermore, there is a need to investigate the damage-sensitivity of vibration response features for a variety of masonry structures, i.e. arch bridges, towers and churches, under all plausible damage scenarios. Another contribution of this work is to take a step in this direction by proposing response features that may be better indicators of wall-vault separation in Gothic churches.

3 BEVERLEY MINSTER

Beverley Minster is typical of Gothic churches. The vaulted ceilings of the Minster are supported vertically by stone arches and piers and horizontally by flying buttresses, which transfer horizontal thrust to aisle vaults on each side. The church is predominantly constructed with limestone blocks of varying strengths and brickwork, which forms the vaults (Horrox 2001) [Figure 4].

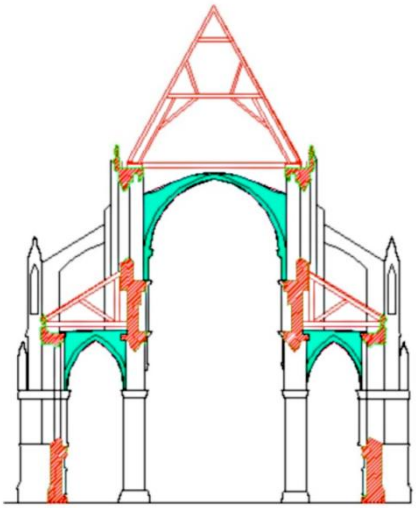

Figure 4: The cross section of the vault displays how the stone walls and buttresses horizontally support the nave vaults. The settlement of the buttresses pulls the walls outward, causing separation between the walls and vaults.

According to historical documents, the movement of the nave walls has been a concern since its construction in the early thirteenth century. Ever since the nave walls were erected, they have increasingly leaned out due to the foundation settlement of the buttresses (Barnwell 2007). In the eighteenth century, ties were added at roof level to prevent further separation of the walls. According to historical documents, the outward movement progressed and a century later wood beams spanning the width of the nave were fixed to the nave walls with steel ties in the hope of mitigating further deformation. Although this intervention was partially effective, it did not completely eliminate movement in the nave walls (Price & Meyers Consulting Engineers 2004).

The settlement of the buttresses has pulled the nave walls outward, detaching the walls from the masonry vaults. With this separation, vaults have been unable to transfer horizontal thrust to the walls, resulting in the flattening of the nave vaults. The movement of walls, however, has not been uniform along the length of the nave. Assessment reports, completed by Price & Meyers Consulting Engineers in 2004, document the magnitude and patterns of wall movement. According to the site survey, maximum separation between the walls and vaults of 135 mm (5.3”) occurs at the west side of the nave [Figure 5]. The vaults at the east end of the nave, however, appear restrained by the tower and the walls and buttresses of the transepts, thus remaining intact. As a result, Beverley Minster, in its current state, has ten vaults with different damage states (Price & Meyers Consulting Engineers, 2004).

Figure 5: The interface between the nave walls and vaults of (left) damaged and (right) undamaged vaults. The gap between the walls and vaults of the undamaged vault is filled with plastic sheets.

As seen in Figure 5, while there is a gap between the walls and vaults for the damaged vaults, the brick webbing of the undamaged vault rests intact on the stonewalls. However, the degree of lateral restraint provided to the undamaged vaults by the nave walls is difficult to determine. During the finite element simulations, discussed in Section 5, this difference in the two vaults is represented as free lateral movement and restrained lateral movement.

4 VAULTED STRUCTURE UNDER STUDY

The two prototype vaults investigated in this study have two significant differences due to damage: the Sabouret cracks and consequent geometric distortion [Figure 6]. Aside from these two aspects, the two prototype vaults are expected to exhibit minor variations in their geometric and material properties. The present study relies on the important premise that these minor differences between the two prototype vaults have negligible effect on the vibration response.

This premise will later be verified through FE simulations in Section 5. In the present section, however, we discuss two campaigns implemented to quantify (1) variations in the vault geometry and (2) the natural variations in the construction material. The findings of these two campaigns are then entered into the finite element models to quantify the effect that geometric and material variability have on the vault vibration response.

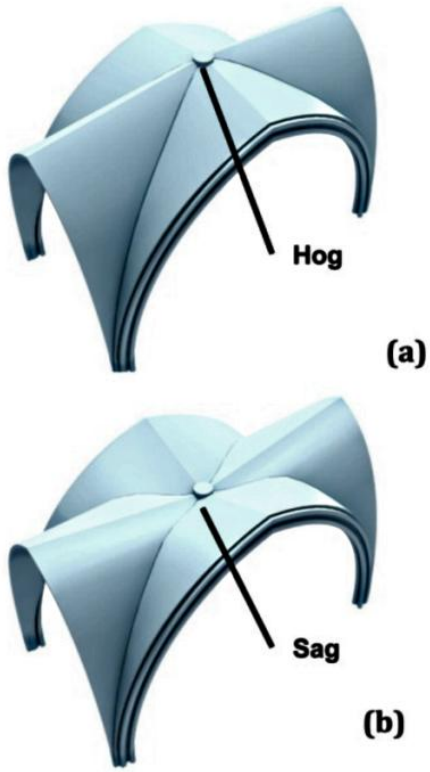

Figure 6: The originally concave down curvature of the vaults is flattened: (top) undamaged and (bottom) damaged vault. The formation of the 6‘‘ wide Sabouret cracks results in an 8’’ sagging of the crown of the vaults.

Vault-to-Vault Geometric Variability due to Construction Imperfections

The vault-to-vault geometric variability discussed herein is the variability due to inconsistencies associated with the medieval construction techniques of erecting masonry vaults. These inconsistencies are expected to result in slight geometric deviation among the ten vaults, even before settlement of buttresses occurs. To estimate the degree of this geometric imperfection, a three-dimensional survey of both the vaults are completed using a Leica TPS800 series survey instrument. The upper surface (extrados) and the lower surface (intrados) of the vaults are surveyed. The survey points are taken primarily at the crowns, along the ribs, around the surcharge, and along the edge of the nave walls.

Comparison of the three-dimensional geometry of undamaged and damaged vaults should yield the geometric variability due to the combined effects of imperfect construction and structural damage. However, because the intention herein is to estimate the inherent geometric variability in construction prior to the occurrence of damage, the symmetric design of the vaults is exploited. By calculating the deviations between the four quarters of the undamaged vault, the maximum geometric variability in one dimension is estimated at 6%. The geometric variability is estimated to be predominant along the longitudinal direction of the nave. In Section 5, this variability will be represented by increasing the longitudinal dimension of the vaults in the FE model by 6%.

Vault-to-Vault Variability due to Materials

The Impact Echo (IE) method is conceptually based on the fact that the waves propagating through the thickness of a material are reflected when they encounter a change in medium (Sansalone 1997). Due to the larger wavelengths (typically greater than 10 cm) required for the IE method, wave diffusion through aggregates, cracks, and pores has less degrading effects than in

ultrasonic testing (Schubert, Wiggenhauser and Lausch 2004; Colla and Lausch 2002). Therefore, IE provides a viable solution for nondestructive testing of masonry assemblies.

In this study, IE tests are conducted to estimate the natural variability of brick units and mortar assembly. A total of 30 tests are conducted at various locations on the vaults. During the tests, the vault webbing is impacted by a hardened steel ball and the localized, high frequency vibrations caused by this impact are measured through a displacement transducer. The main resonant frequency of stress wave reflections between the internal and external boundaries of the masonry vault webbing is captured. Figure 7 illustrates a select few of these measurements. From the dominant frequency, the overall time required for a single cycle is obtained. Assuming that the vault thickness remains constant, the material properties of the vaults are mathematically related to the velocity of stress waves. The variation in the ratio of Young's modulus over density of the masonry assembly is estimated to be roughly 10%.

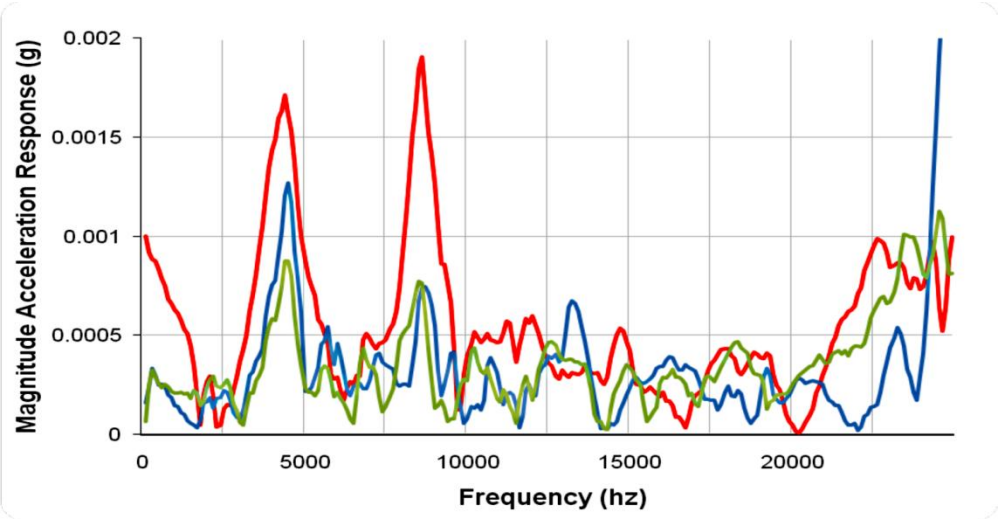

Figure.7: The impact echo measurements are used to estimate the standard deviation of the homogenized material properties of the mortar and masonry assembly.

5 FINITE ELEMENT SIMULATIONS OF THE VAULTS

In the previous section, uncontrolled variations in the geometric and material properties of the nave vaults were approximated through geometric surveying and impact-echo testing. In this section, the effects of these variations on the vibration response are investigated. This is necessary to verify that the change in the selected features due to damage is differentiable from that due to vault-to-vault variability. First, the development of the FE model is discussed, and then the methods used to estimate the variability in geometric and material properties are introduced. Finally, the post-processing of the time domain simulations is addressed.

Development of the Finite Element Model

The primary purpose of the finite element model is not to make predictions about the structural behavior of the vaults at Beverley Minster, nor to reproduce the experimental measurements. Instead, it is used to investigate the noise-sensitivity of the vibration response features, which is the sensitivity to variations in geometric and material properties.

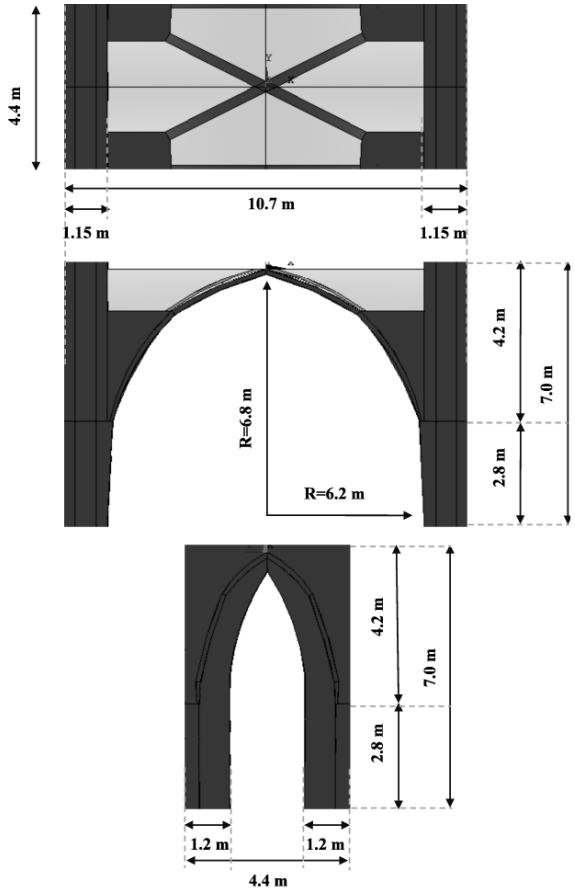

Figure.8: The dimensions of the masonry vaults of the Beverley Minster.

The initial steps in the development of a three-dimensional finite element model are the reproduction and simplification of the three-dimensional geometry. During this step, both the drawings by Price & Meyers Consulting Engineers and the measurements from the *onsite* three-dimensional survey are used [Figure 8]. The next step consists of creating a solid model utilizing the commercially available software ANSYS v. 10. Solid modeling is followed by mimicking the material properties and boundary conditions of Beverley Minster in the model [Figure 9]. The material behavior of masonry is simulated using a linear-elastic constitutive law. The material properties, such as the Young's modulus and density, are selected according to a review of

pertinent literature [Table 1]. These parameters are calibrated by comparing the ANSYS simulation results with experimental measurements (Atamturktur 2009). The finite element model is conceived to simulate the undamped vibrations of the vaults, and thus damping factors are not defined.

Table 1: Prior knowledge on the material properties of structural components.

Component	**Material Type**	**Modulus of Elasticity (E)**		**Density (d)**
		Low	**High**	**Nominal**
Walls, Columns, Vault ribs	Indiana limestone and Type O mortar	6 GPa	28 GPa	2100 kg/m^3
Vault webbing	Brick	1 GPa	6 GPa	2100 kg/m^3
Fill	Rubble and earth	0.5 GPa	5 GPa	2100kg/m^3

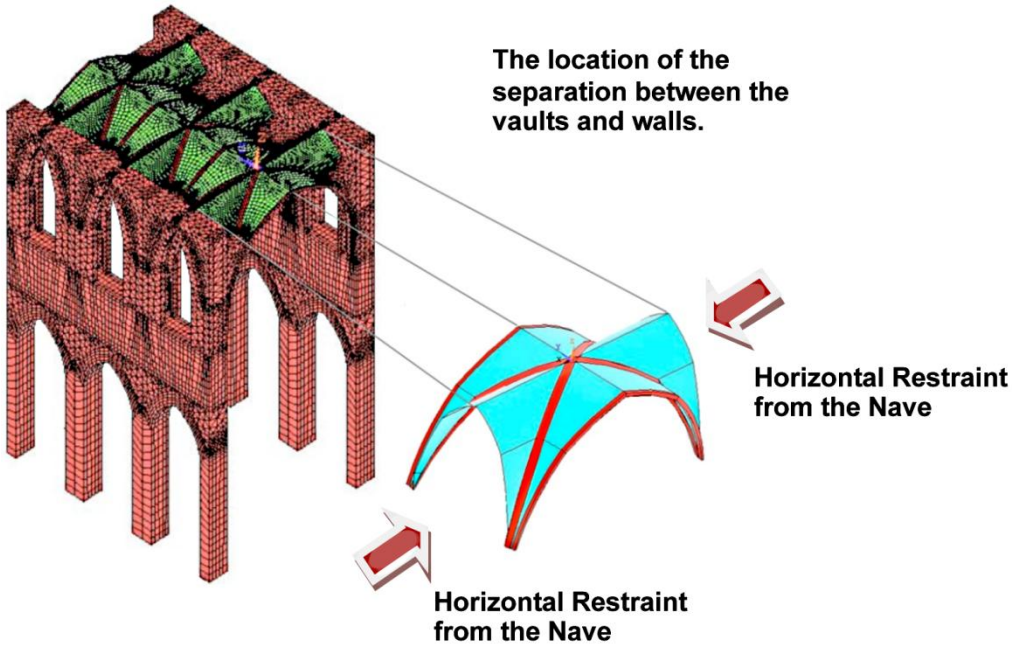

Figure.9: FE model of Beverley Minster used to simulate the changes in the vibration response of the vaults due to the variability in geometry and material properties present in the Minster.

The finite element model, to be useful, only needs to represent the primary contributors to the structural behavior of the vaults. Since the ribbed vaults absorb the majority of the energy induced by the impact hammer strike, the adjacent walls and surcharge are not modeled explicitly, but rather replaced with appropriate boundary conditions. The simplified version of the finite element model, which is used to generate transient vibration response, can be seen in Figure 9.

The developed finite element model relies on many simplifying assumptions, such as the mesh discretization and selection of constitutive models. It is important to assess whether these modeling choices are appropriate for the purpose of this study. The finite element model developed for this study underwent a thorough Verification and Validation (V&V) process.

Results of this extensive V&V study are documented by Atamturktur (2009), who quantifies the prediction accuracy relative to vibration response measurements and demonstrates the appropriateness of the aforementioned assumptions. The V&V process employed in this study is similar to the one applied to the Washington National Cathedral by Atamturktur, et al. (2010). An overview of finite element model calibration and validation studies, as applied to large scale historic masonry monuments, has been written by Atamturktur and Laman (2010).

To investigate the changes in the vibration response, four different finite element models are developed to represent (1) the undamaged vault, (2) the damaged vault, (3) the undamaged vault with variation in geometry and (4) the undamaged vault with variation in material. The finite element model of the *undamaged* vault is built with horizontal restraints from the nave walls, while the finite element model of the *damaged* vault is left free to translate horizontally at the peripheries of the walls [Figure 9]. Next, the material properties and geometry of the undamaged model are altered according to their estimated natural variability.

Finite Element Simulations

The finite element model is executed to mimic the experimental set-up as closely as possible and the vibration response of the vault is simulated for the four aforementioned scenarios: (1) the undamaged vault, (2) the damaged vault, (3) the undamaged vault with variation in geometry and (4) the undamaged vault with variation in material. The vibration response of interest is the transient response of 39 selected nodes due to an impact force applied at four separate excitation locations.

First, we look at the changes in the frequency response functions (FRF) of the vaults. Simulated frequency response functions estimate the vibration response of the structure due to a

given force within the frequency domain. The FRF can be conveniently constructed from the simulated transient response of the vaults by taking the ratio of the Fast Fourier Transform (FFT) of the measured acceleration response and forcing functions. Figure 10 compares the driving point FRFs measured at the crown of the vault. Looking at the amplitudes of these FRFs, while the change in the FRF amplitudes between the damaged and undamaged vault is about three to four fold, the change in the FRF amplitudes due to the 6% variation in geometry and 10% variation in material properties is consistently less than 20%.

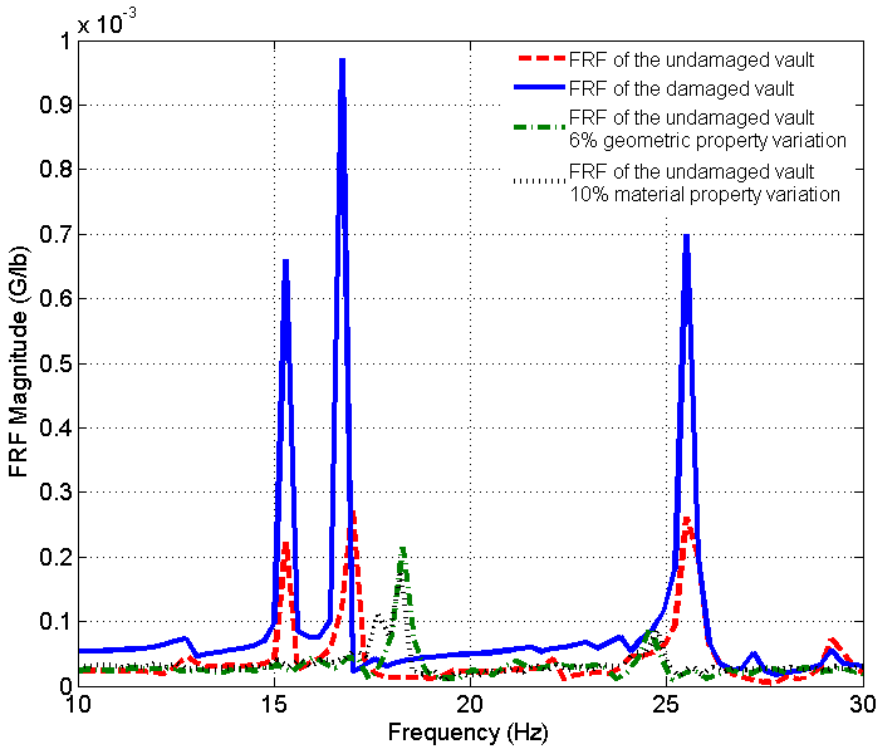

Figure.10: The FRFs are simulated for the four scenarios: (1) the undamaged vault, (2) the damaged vault, (3) the undamaged vault with variation in geometry and (4) the undamaged vault with variation in material.

Next, the autoregressive support vector machine (AR–SVM) approach is applied to these simulated vibration responses. Theoretical background of the AR-SVM approach will be provided later in Section 9. The absolute average residual errors of the AR-SVM model fit (Bornn, et al. 2009) is calculated for each scenario [Table 2]. Table 2 shows that the geometric variation case is restricted to two sensors, since the geometric distortion requires a change of sensor locations in the model. Table 2 also includes the average absolute difference between each scenario and the undamaged case. From these simulations it is obvious that the AR-SVM model best fits the material and geometric cases. Although the AR-SVM model fits for the material and geometric cases are not perfect, they are far superior to the AR-SVM model fit for the damaged case.

Table 2: Absolute Average Residuals of AR-SVM Fit Under Several Scenarios

Sensor	Undamaged	Damage	Materials	Geometry
22	0.0463	0.8221	0.1317	N/A
18	0.0478	0.7950	0.1279	N/A
4	0.0974	1.1113	0.0769	0.0795
35	0.0930	0.8115	0.1032	0.0805
Average Diff.	N/A	0.8138	0.0491	0.0152

From this comparison, we can determine that separation between the nave walls and vaults is the most significant contributor to changes in AR-SVM damage indicators. With this determination comes a caveat. The contribution of each source of uncertainty to the lack of model fit is not necessarily linear, and hence combinations of scenarios may not lead to an additive

change in model goodness-of-fit. However, the sources of uncertainty used in the simulations are representative of the most extreme cases for the material and geometric as indicated by our site surveys and field testing.

6 VIBRATION TEST CAMPAIGN

Unlike modern civil structures, historic masonry structures pose unique challenges due to the behavior of their distinct structural systems. In a masonry system, the rigidity of a connection between two structural elements is affected by several factors, such as the contact pressure, surface friction, elastic behavior of each stone unit and mortar joint and existing cracks and hinges. Compared to contemporary reinforced concrete and steel structures, the inter-element connectivity is often more flexible in masonry systems. As a result, local vibration modes tend to be more pronounced than global modes. This makes the vibration response dependent upon the location of the excitation force. Also, the amplitude of the excitation alters the behavior of connections between structural elements and thus alters the response of the system. Compounding these difficulties is the presence of high dissipative forces inherent in masonry assemblies that complicate the identification of low amplitude global modes in the spectra.

These issues common to masonry systems are only a few of the hindrances to successful vibration testing of historic structures. Practical issues of testing a large-scale vaulted church, such as Beverley Minster, affect the outcome as well. Practical issues may include, but are not limited to, limited access to the site and attaching testing devices to the curved geometry of vaulted systems. A comprehensive discussion of the particulars and practicalities of *in situ* vibration testing procedures for complex vaulted masonry structures can be found in Atamturktur, et al. (2009).

In the following sections, specifications of the vibration test are discussed, then a brief summary of quality checks implemented to verify the linearity and reciprocity of measurements is provided.

Specifications of the Vibration Test: The test is conducted in four phases, during which 16 accelerometers are moved to cover the measurement grid. The distribution of measurement points is determined according to preliminary finite element simulations of the vaults. The preliminary finite element model predicts modes as primarily composed of symmetric movements of the diagonal and orthogonal axes, as well as the crown. Based on this observation, a total of 39 measurement points are located at every quarter length on the main axis of the quadripartite vaults. To observe the interaction between the adjacent vaults, an additional eight measurement points are located on the two adjacent vaults.

The transducers used in this study are Q-Flex QA 750 model force balance accelerometers, manufactured by Honeywell Inc. The accelerometers have a nominal sensitivity of 1.5 mA/g, which results in a voltage sensitivity of 7.5 V/g, when dropped over a 5 kΩ resistor. They maintain a frequency range of 0–300 Hz and an amplitude range of ±30 g. Due to the steep, curved surfaces of the vaults, mounting cases with adjustable screws are used to achieve precise alignment. The unidirectional accelerometers are mounted on the vault surface, such that they achieve a vertical axis of alignment [Figure 11].

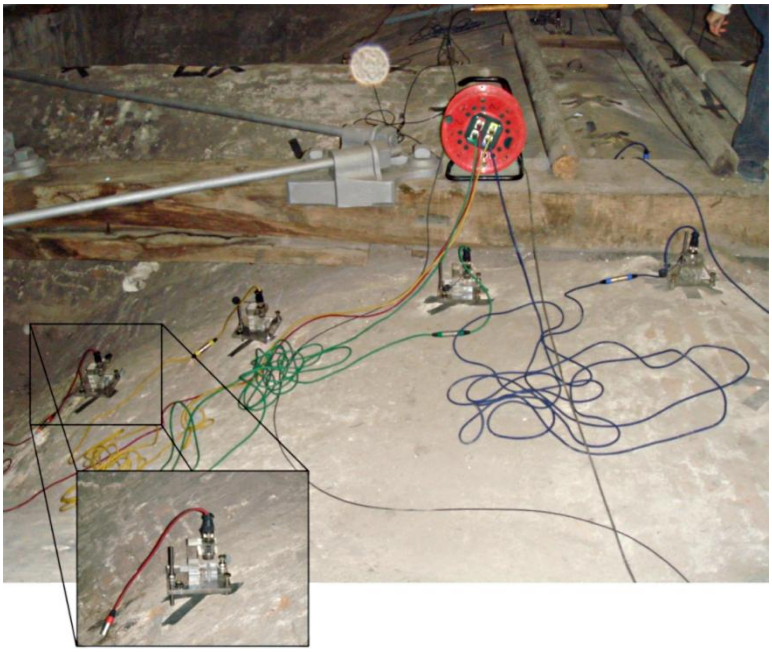

Figure 11: The uni-axial accelerometers are placed on the curved vault surface with the help of adjustable mounting cases such that their axes remain vertical.

Impact hammers, shakers, and heel-drops are common controlled excitation devices used for traditional modal analysis. Among these excitation devices, the portability of impact hammers makes them preferable for this study. The mass of the hammer and stiffness of its tip define the frequency content of the excitation. The vaults are excited through the impact of a 5803A model sledge-hammer (12 lb head), manufactured by Dytran Instruments, Inc. To broaden the impact duration and induce low-frequency vibration, the softest hammer tip is preferred.

Although the acceleration response of the vault is measured solely in the vertical direction, the hammer excitation is applied perpendicularly to the vault surface; thus, modes with predominantly horizontal movement and less dominant vertical movement are also excited. As

long as the accelerometers can detect the vertical acceleration of the vault, then the vertical components of these modes are also identifiable. *A priori* finite element model simulations and past experience gained from the testing of similar structures reveal that the first few modes involve deformation shapes that concentrate on the crown and the midpoints of the orthogonal and diagonal axes. As the resonant frequencies increase, the vault webs become more involved in the deformation and the mode shapes become complicated. To excite the majority of lower modes with detectable amplitudes, the use of four excitation points, situated at the centers of the main axis and crown, is most effective [Figure 12].

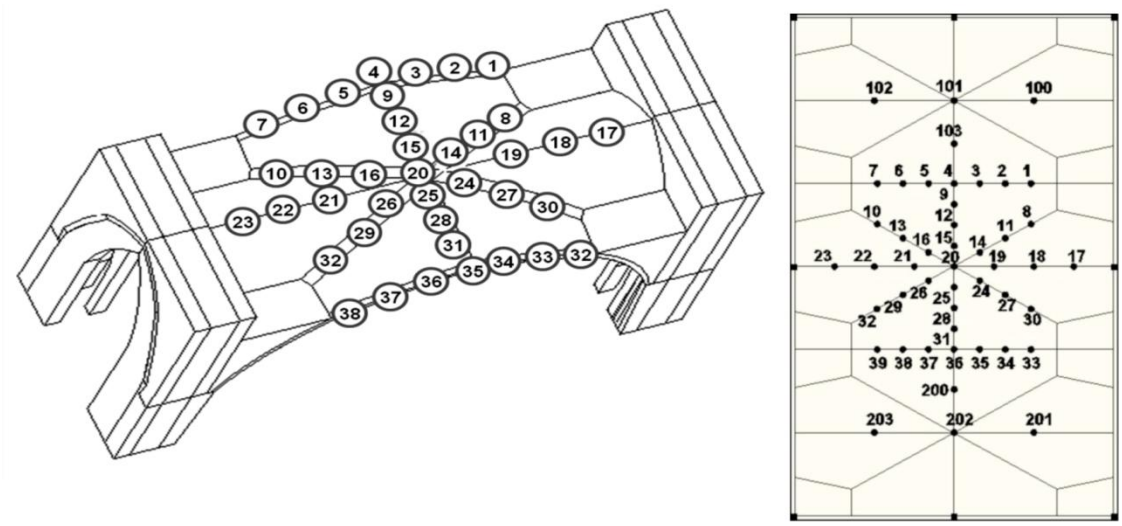

Figure 12: A total of 39 measurement points are selected according to the mode shape predictions of the preliminary model. The excitation points are #20, #18, #12 and #11.

A significant drawback of hammer excitation is the inability to replicate the impacts with consistent excitation force [Figure 13]. Although the hammer operator swung the hammer as consistently as possible, the excitation force during the experiments varied between 1800 N and

2200N throughout the tests. To reduce the degrading effects from this uncontrolled variation of impact force, as well as from ambient noise, five impacts are performed and the responses are averaged for each excitation location.

Figure 13: The hammer operator exciting the pre-determined excitation points with the sledgehammer. Maintaining a relatively consistent excitation level is one of the keys for the success of hammer excitation.

Data acquisition is conducted using a 24 channel, 24 bit Data Physics Mobilyzer II spectrum analyzer. The upper frequency limit is 100 Hz and the data capture time is 16 seconds. This data configuration yields a 0.0625 Hz frequency resolution and 0.005 second time resolution. As the amplitude of the response diminishes within the data capture time frame, a rectangular window function is used for both impact and response signals.

Since masonry systems have inherently high damping compared to steel or reinforced concrete structures, artificial damping introduced by an exponential window can result in lower amplitude global modes being overpowered by adjacent, higher amplitude local modes. For this reason, the exponential window is avoided during data acquisition. However, during the modal

extraction stage, a low order exponential window is used to clean the degrading effects of extraneous excitation.

A typical time history measurement of the hammer impulse and of the associated vault response is shown in Figure 14. These time domain measurements are readily converted into the frequency domain by the spectrum analyzer. In the frequency domain, measured vault response is normalized with respect to the corresponding hammer impulse. This normalization process yields the experimental counterpart of the previously introduced frequency response function (FRF). Moreover, the coherence functions are obtained from the five repeated measurements. Coherence functions assess the extent to which the input and output signals maintain a linear relationship and thus conveniently determine the quality of measurements. Representative FRF and coherence plots are provided in Figure 15. Given the aforementioned difficulties in performing vibration tests on large-scale historic masonry monuments, the measured coherences are deemed to be sufficiently high to verify that the structure responds within the linear regime.

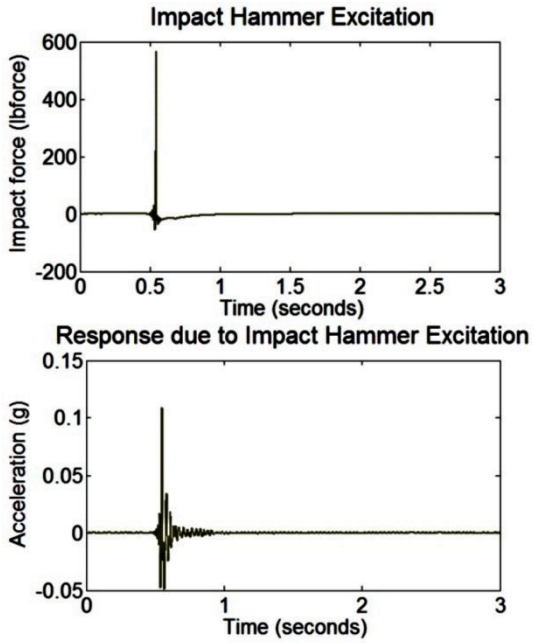

Figure 14: Examples of measured signals: (top) hammer impact force in the time domain and (bottom) the response of the vaults due to the hammer impact.

From the coherence functions, the uncertainty in magnitude and phase FRFs can be computed using Bendat and Piersol's (1980) formulation. This approach assumes that FRF variability is random and follows a Gaussian distribution. The variability of FRFs with one standard deviation is shown in Figure 15. Figure 15 was developed using driving point measurements—the excitation and measurement of the same point. The standard deviation is derived using two driving point FRFs collected from points 12 and 20. Figure 15 illustrates that while the standard deviation of the FRFs obtained from undamaged and damaged vaults are comparable, the FRF amplitudes are generally higher for the damaged vault than they are for the undamaged vault. It is plausible that the damage introduced high amplitude, local modes at a frequency higher than 100 Hz. From Figure 16, it is evident that such a high amplitude local mode is not present for the undamaged case.

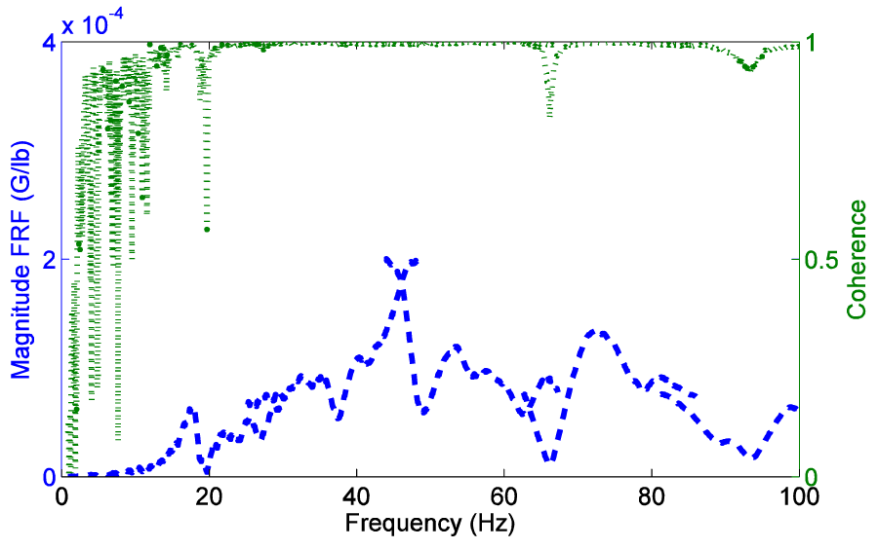

Figure 15: A representative FRF and coherence function obtained from the undamaged vaults.

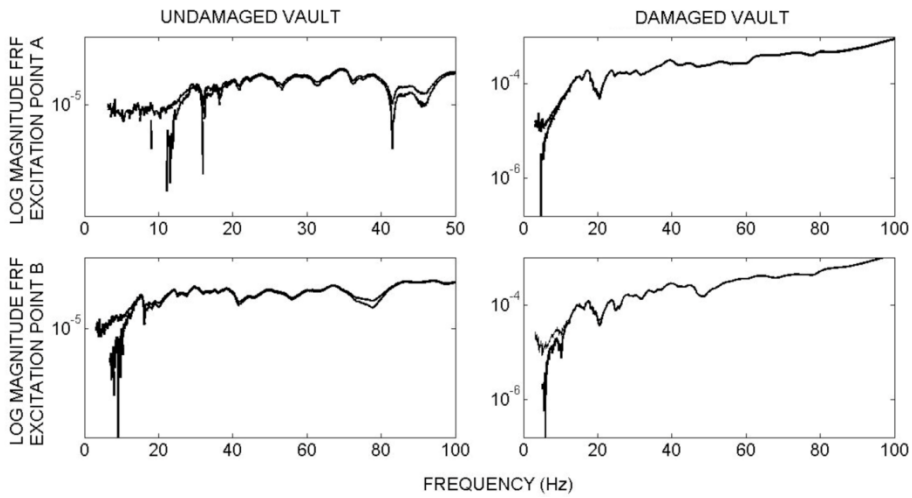

Figure 16: The frequency response function of the damaged vault tends to have higher amplitudes compared to the undamaged vault, especially at higher frequencies.

Quality Checks: Standard experimental modal analysis applications assume that the test specimen exhibits linearity and reciprocity. Reynolds and Pavic (2000) provide a discussion of quality assurance of test data obtained from civil engineering systems. As part of the quality assurance procedure, reciprocity checks are completed to confirm the linear behavior of the vaults under the excitation forces [Figure 17]. However, the judgment of the analyst is necessary for determining the acceptability of the deviations in the reciprocity check. Once again, considering the inherent variations in both the testing procedure and the tested structure, the correlation obtained between FRF(18,20) and FRF(20,18) of Figure 16 is deemed acceptable. Also, because the peaks of these two FRFs remain nearly unchanged, the identification of modal parameters is minimally affected by the presence of the deviations.

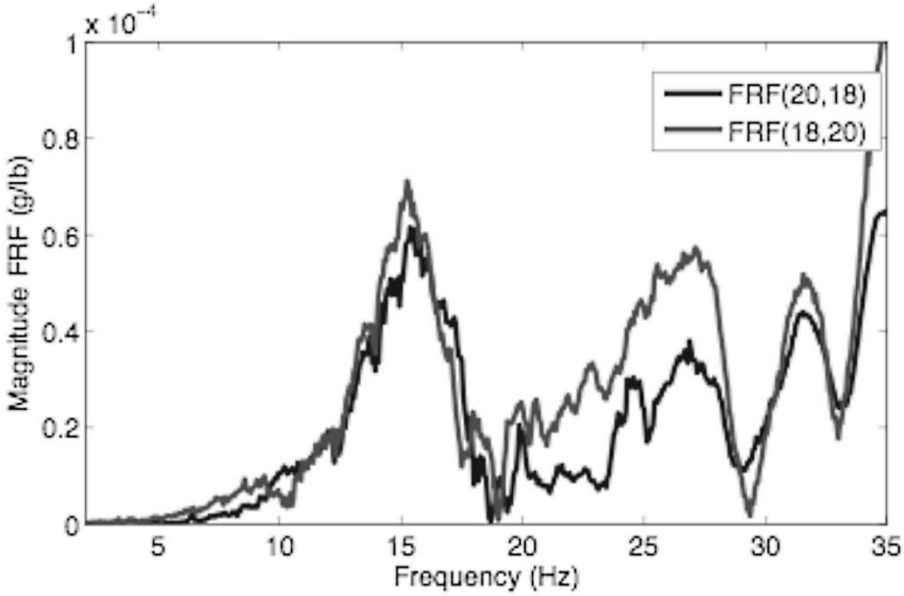

Figure 17: The reciprocity check completed between measurement point 18 and 20 for the damaged vault.

7 EVALUATION IN THE MODAL DOMAIN

In Section 5, the effect of geometric and material variability on the vibration response was quantified, through numerical simulation, to show that inherent vault-to-vault variability changes the vibration response of the vaults to a lesser extent than structural damage. Because our modeling assumptions are conservative and the FE models have undergone rigorous V&V, we conclude that analyzing measurements collected on different vaults is not detrimental to answering the main question: can the presence of damage be inferred from the vibration response? An answer is first attempted in the modal domain. Sections 8 and 9 then discuss evaluations performed in the frequency and time domains, respectively.

The complex geometry of the vaults, along with the particularities of masonry construction, often yields an abundance of complex, closely spaced modes. As evidenced by the FRF given in Figure 15, approximately twenty modes of significant amplitude are present between 0 Hz and 20 Hz. However, extracting reliable modal parameters from these high modal density measurements is a difficult endeavor, especially for modes with low participation factors. Moreover, the unique challenges of hammer testing, such as poor signal-to-noise ratio and high crest factor, further challenge the accurate extraction of higher order modal parameters. Thus, the number of modes that can be used during the comparison of undamaged and damaged vaults is typically limited. On the other hand, operating on a limited number of modes is not a significant drawback. As the mode order increases, the mode shapes become more and more dominated by local response and highly sensitive to the excitation location. Thus, higher order modes typically do not contain information regarding the global damage. In the present study, the comparisons of the undamaged and damaged vaults through modal parameters are limited to the first ten natural frequencies and mode shapes. The estimation of damping ratios is known to be significantly less accurate, when

compared to the natural frequencies and mode shapes, so the damping ratios are not to be incorporated in the comparison.

In the present study, modal extraction is conducted using the ME'scope Version 4.0 software, developed by Vibrant Technology, Inc., with a multiple-reference, global curve-fitting algorithm that combines FRF measurement data from multiple excitation locations. Once the modal parameters for damaged and undamaged states are identified from the FRF measurements, the differences between natural frequencies and mode shapes are quantified.

Table 3 presents the differences in natural frequencies of the undamaged and damaged vault. To be statistically significant, a change in natural frequency due to damage should exceed, by a factor of two or more, the level of experimental variability. This is not observed in Table 3, since the natural frequencies are shifted by a maximum of 0.14 Hz. This magnitude of frequency shift is similar to the experimental variability obtained by replicating the measurements on a similar Gothic church, Washington National Cathedral (Atamturktur 2009). The frequency variations can potentially be attributed to the perturbation introduced by the presence of a hammer operator. In contrast with earlier, successful studies that correlated damage with reduction in natural frequencies, the modal properties associated with lower-frequency global modes of the Minster vaults are observed to be insensitive to the existence of wall-vault separation.

Table 3: The modal parameters identified from damaged and undamaged vaults.

	Undamaged Vault	**Damaged Vault**		**Mode Shape Correlation**
Mode #	**Frequency (Hz)**	**Frequency (Hz)**	**Δf (Hz)**	**MAC (Unitless)**
1	3.38	3.38	0	0.936
2	3.87	3.87	0	0.813
3	4.85	4.92	0.07	0.927
4	5.62	5.72	0.04	0.493
5	6.36	6.34	0.02	0.371
6	7.77	7.63	0.14	0.464
7	8.59	8.58	0.01	0.245
8	8.99	9.00	0.01	0.742
9	9.39	9.41	0.02	0.509
10	9.96	10.0	0.04	0.658

Table 3 also includes a correlation metric used to compare the mode shapes of the two prototype vaults. In this study, the mode shape vectors include the motion of twenty-seven measurement points relative to each other and thus have a higher dimensionality than natural frequencies. Therefore, the Modal Assurance Criterion (MAC) is used to obtain a lower dimensional metric to compare the mode shapes obtained from the damaged and undamaged

vaults. A MAC value of 1.0 represents a perfect correlation between two mode shape vectors, while 0.0 indicates two orthogonal mode shape vectors, i.e. uncorrelated mode shapes. Due to the complexity of *in situ* experiments, MAC values of 80% or higher are considered satisfactory for the purposes of this study. Figure 18 provides a visual comparison of the first modes of the two prototype vaults, which yield a MAC of higher than 90%. In Table 3, mode shape vectors are shown to yield good correlation for the first three modes, while higher-order modes exhibit less correlation. This observation is in agreement with an earlier study by Ramos (2007), which demonstrated the insensitivity of mode shapes to structural damage. However, the higher order, uncorrelated mode shapes are possible indicators of differences between two structural conditions, i.e. wall-vault separations. This statement assumes that the system identification is completed with sufficient accuracy.

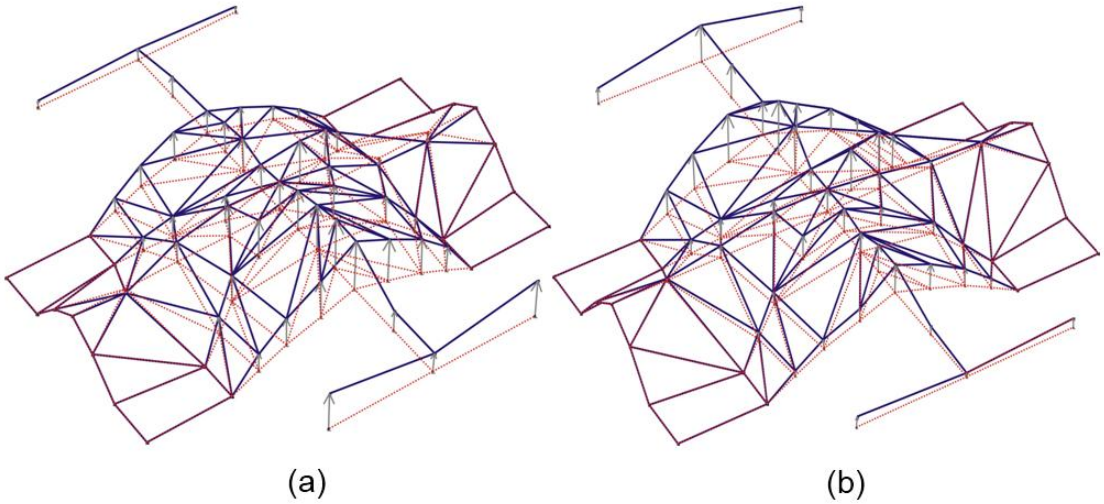

Figure 18: The first mode shape of (a) undamaged vault, (b) damaged vault.

Our initial hypothesis was that structural damage manifests itself as a change in the natural frequency of the low order resonances. However, as seen in Table 3, the first three modal parameters remain unchanged irrespective of the damage state of the vaults. The similarities in the first three global modes in the two test structures supports our assumption that these two vaults indeed have comparable structural properties, such as boundary conditions and material properties.

8 EVALUATION IN THE FREQUENCY DOMAIN

Modal parameters provide physically meaningful and convenient features for the comparison of two datasets. However, when using modal parameters the comparative analysis may suffer from (1) low feature dimensionality and (2) incomplete measurements. In this section, the direct comparison of FRFs is used as a convenient, higher dimension alternative to comparing modal parameters. Also, the use of FRFs eliminates the use of curve-fitting algorithms to extract modal parameters.

Overlaying FRFs obtained from the damaged and undamaged vaults gives a visual indication of change between the structures. As Figure 19 shows, the FRFs obtained from the two vaults agree relatively well up to 7 Hz. For higher frequencies, the FRF obtained from the undamaged vault has significantly lower amplitudes than the FRF obtained from damaged vault. The same trend is observed consistently in all FRFs [Figure 19] and is in agreement with the simulated response of the vaults as given in Figure 10. Through this visual assessment, the FRFs yield a clear indication that a change between the two structural systems has occurred.

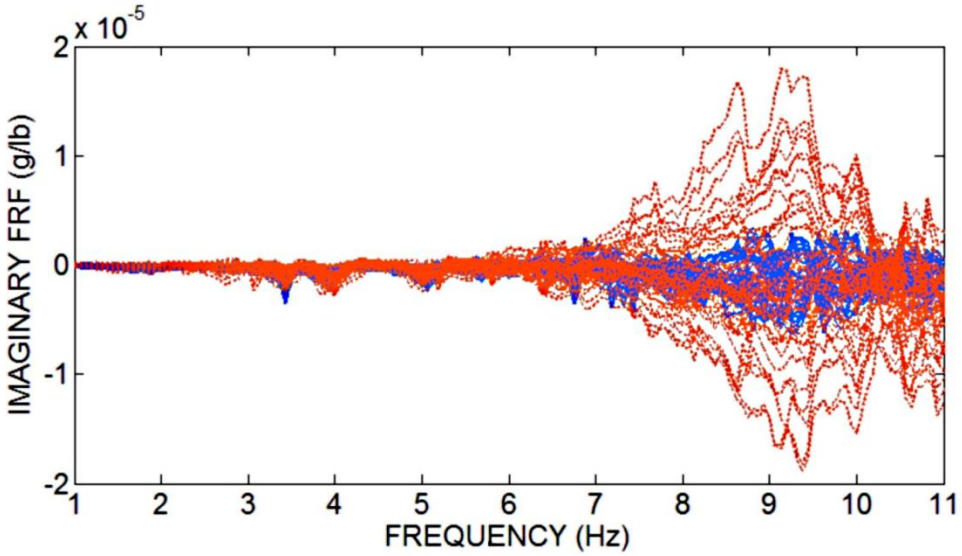

Figure 19: The imaginary component of the FRF conveys the relative deformations of the measurement points, which are observed to be comparable for the damaged (red dashed) and undamaged (blue solid) vault for frequencies below 7Hz. Frequencies higher than 7Hz have significantly higher amplitudes for the damaged vaults.

If the onset of damage introduces nonlinearity to a predominantly linear system, then coherence functions can be used as damage indicators. A typical coherence function, corresponding to the driving point measurement at the crown of the undamaged vault, can be seen in Figure 20. The coherence functions of the damaged vaults are observed to be lower than those of the undamaged vaults, possibly due to system damage amplifying the non-linearity of the vibration response. Using the coherence functions in addition to FRFs may provide a diagnostic that, while being insensitive to environmental and testing variability, correlates well with the presence of structural damage.

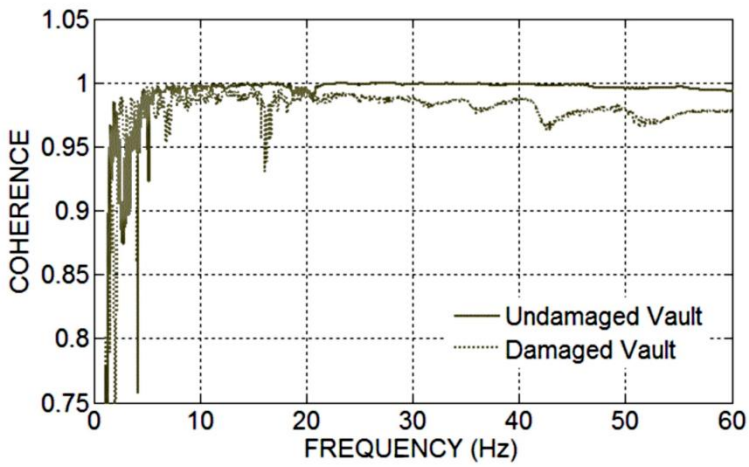

Figure 20: The coherence plot indicates the linear relationship between the input force and output response. The damaged vault coherence plot shows a reduction in this linear relationship.

9 EVALUATION IN THE TIME DOMAIN

Comparisons of FRFs are useful as they filter out the undesired noise from the measurements and provide smoothened information about system behavior over a wide frequency range. However, like modal parameters, obtaining a FRF is based on the assumption of linearity. This assumption may become a problem, since damage may introduce nonlinear effects into the system that cannot be captured adequately by a linear model (Farrar et al, 2007). Given a nonlinear response, a FRF provides a smeared representation of the nonlinear effects. Time domain methods, however, may offer higher fidelity in representing nonlinearities and may have better success in detecting structural damage.

Regression models are applied in the time domain with model residuals acting as the damage indicators. In addition to providing a smoothing effect to the raw measurements, this procedure

offers the advantage of defining scalar-valued features that lower the dimensionality of the time series. Specifically, an autoregressive (AR) model is best-fitted to a time-domain signal known (or assumed) to be collected on a damage-free structure. The degree of goodness-of-fit of the AR representation is used as the damage-sensitive indicator. Model residuals, defined as the difference between predictions of the AR model and the experimental data, are monitored for statistically significant changes assumed to be caused by damage. An AR model of the kth sensor with p autoregressive terms, AR(p), is expressed as:

$$x_t^k = \sum_{j=1}^{p} \beta_j^k \cdot x_{t-j}^k + \varepsilon_t^k \tag{1}$$

where x_t^k is the measured signal from sensor k at discrete time t, β_j^k are the AR coefficients or model parameters, and ε_t^k is an unobservable noise term.

It can be observed in equation (1) that an AR model best-fits each sample of the time-domain signal with a linear combination of the previous p samples. While autoregressive models work particularly well when modeling the response of linear, time-invariant systems, systems exhibiting nonlinearity in their initial state or time-varying responses (such as those from hammer-excitation experiments) can result in mediocre goodness-of-fit. Such poor model fit could, in turn, feature low sensitivity to the onset of damage. To address this concern, and because it is well known that AR models do not always represent transient data well, we turn to support vector regression methods (Bornn et al. 2009).

For autoregressive support vector machines (AR-SVM), the model takes the form

$$x_t^k = \sum_{j=p+1}^{t_0} \beta_j f(\mathbf{x}_{j-p:j-1}^k, \mathbf{x}_{t-p:t-1}^k) + \varepsilon_t^k. \tag{2}$$

where the vector $\{x_{t-p}^k, \ldots, x_{t-1}^k\}$ is denoted as $x^k_{t-p:t-1}$ for sensor *k*. Also, *f* is a kernel function capable of modeling nonlinear relationships and t_0 is the length of the undamaged time-domain signal used to train the model. With the appropriate choice of parameters, including the kernel function *f*, its associated parameters, and the training set length, an AR-SVM model is able to represent any nonlinear relationship between the current time point, x_t^k, and the *p* previous time points, $x^k_{t-p:t-1}$. Highly adaptable and generalizable, it has been established that this approach performs well in high-dimensional spaces and outperforms conventional AR models when applied to transient signals. Even though they can be seen as being similar to neural networks proposed for SHM (Rytter and Kirkegaard, 1997), AR-SVM models only require a simple quadratic optimization for training. Despite their simplicity relative to neural networks, these models achieve equivalent, if not superior, prediction accuracy as demonstrated by Schölkopf et al. (1997).

To ensure that signals from both damaged and undamaged vaults are comparable, they are first normalized by the impact level of the hammer strike. Further, to simplify the choice of model parameters, signals to be compared are scaled by the standard deviation of the undamaged signal (Bornn et al. 2009). An exponential smoothing window is applied to attenuate any noise artifacts. The procedure implemented to compare the vibration responses of damaged and undamaged vaults follows the steps outlined next. AR-SVM models are first trained on time series collected for the undamaged vault and one model is developed for each sensor location. Next, the trained models are used to predict signals for both undamaged and damaged vaults. To ensure that the method is insensitive to vault-to-vault, experimental, and environmental variability, the symmetry

of the vault and roving sensor placement are exploited. Each AR-SVM model is trained and tested on two separate, but related, undamaged signals opposite from each other with respect to the excitation location as shown in Figure 12. For example, the AR-SVM model developed for sensor 203 of the undamaged vault is subsequently tested on sensor 102 of both the undamaged and damaged vault. Testing predictions of the AR-SVM models with time series, other than those used to train the models, guards against over-fitting. It also helps to develop diagnostics of structural damage that, because they are based on statistics of lack-of-fit residual errors, account for the environmental variability.

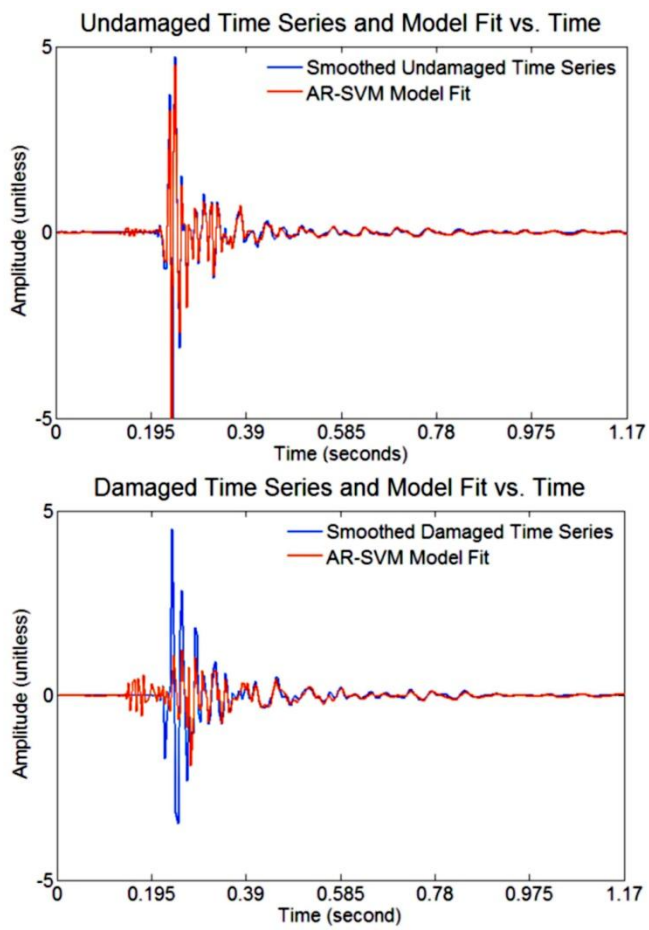

Figure 21: Comparison of AR-SVM fit to normalized transient impact data in (top) undamaged and (bottom) damaged cases. Average absolute residuals for this sensor in the undamaged and damaged cases are 0.0412 and 0.1308 respectively, indicating significantly improved model fit to the undamaged case.

This procedure is repeated for all 46 sensor locations, excluding the crown for which a complementary sensor location does not exist. Examples of time series and AR-SVM model fits for both the undamaged and damaged vault are shown in Figure 21. It can be observed that the model fit to the undamaged vault data, although not perfect, is far superior to the model fit to the data from the damaged vault. Examining the lack-of-fit residuals of AR-SVM predictions for all sensor locations reveals that the undamaged case has a significantly stronger goodness-of-fit. This can be quantified using, for example, statistics from the lack-of-fit residuals. The average absolute value of residual error is plotted for each sensor location in Figure 22, sorted according to values of the damaged vault. A *t*-test statistic, which tests for equal means between two normally distributed samples, indicates a systematic difference between the two datasets with a *p*-value below 10^{-15}. Generally *p*-values below 0.01 are considered to correlate with strong evidence. Therefore, we conclude from both graphical observation and statistical testing that the AR-SVM models provide a significantly better fit to the undamaged vault. Because the training of AR-SVM models included a cross-validation step to prevent over-fitting and to improve prediction under various sources of variability, we conclude that the systematic lack-of-fit observed when applied to signals collected on the damaged vault come from structural damage.

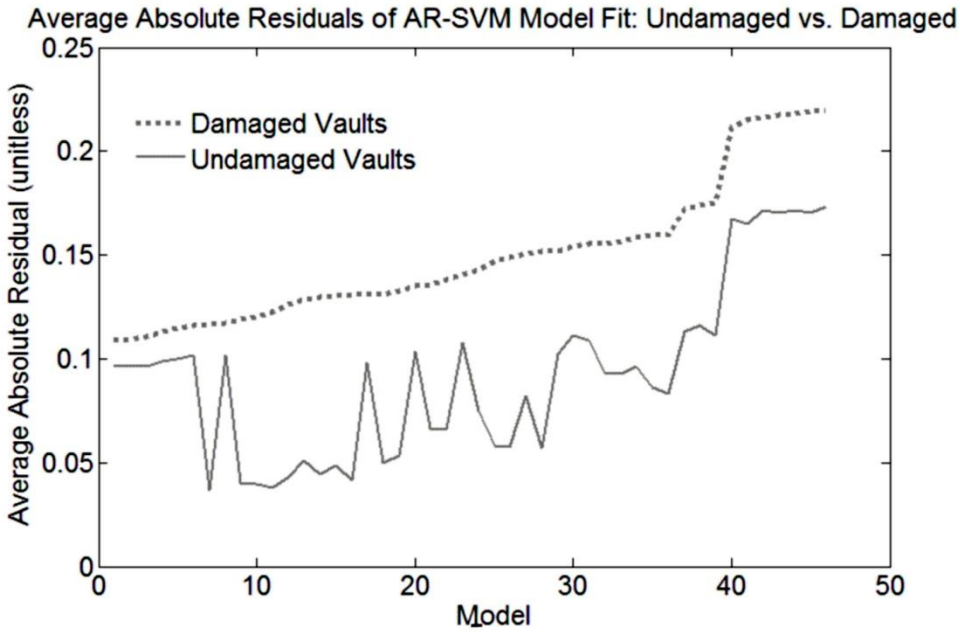

Figure 22: Average absolute values of lack-of-fit residuals of AR-SVM predictions at 46 sensor locations for the undamaged and damaged cases.

10 CONCLUSIONS

The nave walls supporting the vaults of Beverley Minster have been steadily moving for eight centuries. Due to this movement, the ten originally equivalent masonry vaults have undergone a non-uniform damage pattern. This has led to two outcomes: (1) severe separation of the vaults from the wall and (2) geometric distortions of the vaults. Both of these outcomes caused a reduction in structural strength of the vaults.

When damage occurs internally, as in the case of Beverley Minster vaults, visual identification of impending failure becomes difficult. This difficulty is often the case for tensile problems in masonry monuments. In these situations, damage detection techniques based on

vibration characteristics provide a particularly advantageous monitoring and assessment tool. If internal damage in a masonry structure is ignored completely, the load-carrying capability of the structure may be compromised, which may lead to a collapse that occurs without warning. Aside from the obvious economic and life-safety implications, the cultural and historical value of historic monuments adds significance to the development of quantifiable methods capable of assessing the adverse effects of support settlements. By implementing early diagnosis, the direct cost of repair can be reduced significantly.

The datasets analyzed in the present study are force and acceleration time series collected through modal tests performed on damaged and undamaged vaults. Given the specificities of the Beverley Minster, the hammer impact technique was deemed the most appropriate excitation. Because the raw datasets collected are transient time series, analysis can potentially take place in the time, frequency, or modal domain. Analysis in the time domain offers the advantage of processing the most general-purpose signals, but requires efforts to reduce dimensionality and eliminate potential artifacts that contaminate measurements and could mistakenly be interpreted as a manifestation of structural damage. On the other extreme, analysis in the modal domain offers the advantage of averaging, smoothing, and data compression, at the expense of relying on strong assumptions, such as stationary, reciprocal, and linear behavior.

First starting with raw measurements, Auto-Regressive Support Vector Machine (AR-SVM) models show great success in detecting the difference between the two vault conditions. In particular, AR-SVM models trained with signals from the undamaged vault are able to accurately fit measurements from the adjacent, undamaged vault, but are incapable of correctly modeling signals from the damaged state. The second option investigated is to analyze measurements in the

frequency domain. The imaginary parts of Frequency Response Functions (FRFs) indicate that local modes of the damaged vault provide significantly higher amplitudes that those of the undamaged vault. This observation is consistent with the hypothesis that the excitation causes the damaged vault to deflect more than the undamaged one, a clear indication of loss of dynamic stiffness. The direct comparison of FRF amplitudes and coherence functions may define a convenient and damage-sensitive tool for future, in-situ monitoring of historic masonry structures.

Proceeding to the most processed form of data analysis, modal frequencies and mode shapes are estimated next. Contrary to expectation, the first three natural frequencies of the damaged vault are found to be substantially similar to those of the undamaged vault. Likewise, the first three mode shape vectors are mostly unchanged even though some of the higher-order modes are difficult to correlate. This analysis is inconclusive and sheds doubt on the effectiveness of modal-based techniques when applied to realistic datasets.

Contrary to the prevalent use of modal-based methods for structural health monitoring, our overall conclusion is that time-domain analysis may provide a reliable diagnosis, as long as steps are taken to ensure that the effects of structural damage can be separated from those of environmental variability. Finite element simulations demonstrate that our AR-SVM methodology, while able to detect the difference in vibration response due to the presence of damage, can be made insensitive to various sources of uncontrolled, geometric, and material variability. Though these results point to a clear potential of time-domain methods for damage detection applied to historic masonry monuments, their effectiveness when dealing with less severe levels of damage remains to be investigated.

ACKNOWLEDGEMENTS

Part of this work is performed under the auspices of the PTTGrants program of the National Center for Preservation Technology and Training (NCPTT) of the Department of Interior: the Grant Agreement Number MT-2210-10-NC-01.The authors wish to thank Minster personnel, Steve Everett and Steve Riall, for their support and welcoming attitude during site visits. The first author wishes to thank Price and Meyers for sharing their drawings and reports; Chris Middleton, Stefanie Terentiuk and Eunice Lawton for their help during the field test; and Prasenjit Mohanty and Donald Nyawako for their help during the preparation phase of the test. The first author also gratefully acknowledges the work of Sally Gimbert in completing the geometric survey, Prof. Thomas E. Boothby for initiating the project and Paul Reynolds and Alex Pavic for supporting this research program. The first two authors wish to express their gratitude to Charles Farrar, Dave Higdon, and Todd Graves from the Los Alamos National Laboratory for their support and mentoring. The first author also wishes to convey her warmest appreciation to Godfrey Kimball of Clemson University for his editorial assistance.

CHAPTER FOUR
VIBRATION TESTING OF GOTHIC CATHEDRALS: OPTIMAL SENSOR LOCATIONS BASED ON MODIFIED EFFECTIVE INFORMATION METHOD

ABSTRACT

This manuscript supplies guidance regarding the optimal regions for placing vibration measurement sensors to properly extract the dynamic characteristics of Gothic style masonry churches based on a study completed on the Cathedral of St. John the Divine. Placing sensors at optimal locations can not only reduce the cost and time related demands of vibration testing but also lower the amount of measurement data to be post-processed. In this study, first, an accurate finite element model of the Church is built and correlated against *in-situ* measurement and inspection data. Using this correlated finite element model, optimal sensor locations are determined through a modified version of the Effective Independence Method, in which the goal is to both maximize the relative independence of mode shape vectors of interest and effectively explore the geometry of the structure. A tradeoff between information gain and the visual observability of mode shapes is noted. The relationship between the number of desired modes and the required number of sensors is investigated. The robustness of the method to modeling errors and thus, the validity of the guidelines presented herein are demonstrated. Although focus has been given to large scale testing of Gothic Cathedrals, the methodology and concepts presented herein can be applied to many forms of structural systems.

Keywords: Experimental Modal Analysis, Vibration Testing, Optimal Sensor Placement, Structural Health Monitoring.

1. INTRODUCTION

Safeguarding heritage structures requires accurate numerical models for structural assessment as well as reliable continuous monitoring systems for damage diagnosis. In both applications, *in situ* experimental measurements become necessary. In this regard, modal analysis that supplies the natural frequencies and mode shapes of the structure has gained popularity as a monitoring and assessment tool (Atamturktur et al. 2009). Modal analysis can serve two specific purposes (i) experimental evidence to calibrate and validate the numerical models of historic monuments and (ii) non-destructive testing and evaluation method for periodic monitoring of historic monuments.

Implementing modal analysis as experimental evidence for the calibration and validation of numerical models of historic masonry structures falls under the aegis of the concept known as experiment-based validation. The primary concern of experiment-based validation is to ensure that the boundary conditions and material properties of the block and mortar assembly are defined properly. Successful applications of validation include masonry arches (Ramos et al. 2010); domes (Atamturktur and Boothby 2007, Erdogmus 2008, Atamturktur and Sevim 2011); towers (Bayraktar et al. 2009); buildings (Antonacci et al. 2001, De Sortis, Antonacci and Vestroni 2005, Ramos, Laurenco and Costa. 2005); amphitheaters (Zonta 2000); and churches (Turek et al. 2002, Boothby et al. 2006, De Stefano 2007, Erdogmus et al. 2007, Atamturktur and Boothby 2010). Implementation of modal analysis as a non-destructive monitoring tool falls under the aegis of the broader concept of Structural Health Monitoring (SHM) (Farrar and Worden 2007). The basic idea behind vibration based SHM is that a change in a structure's physical properties, such as stiffness or mass, causes a change in the vibration response of the structure, which can be measured using a variety of vibration measurement techniques. The concept of vibration response

based monitoring of historic structures has gained increased popularity in the past two decades (Armstrong et al. 1995, Ellis 1998, Gentile and Saisi 2007).

For the two applications of modal analysis discussed above, performing full scale testing on a large scale historic masonry monument poses both technical difficulties and practical challenges (Atamturktur et al. 2010 and Atamturktur and Laman 2010). One of the challenges comes from the large size of these monuments. It is of course uneconomical, and more importantly unnecessary, to envelop the entire structure with closely spaced sensors. By finding optimal sensor locations from the perspective of information gain and thus, limiting the necessary number of sensors, it is not only possible to reduce the demands on experimental resources (such as time and budget), but also to reduce the volume of data that must be processed. Moreover, the success of SHM techniques for diagnosing damage has been reported to be dependent upon the proper selection of the sensor locations (Hemez and Farhat 1994); therefore, the optimal sensor placement is crucial to the success of vibration based SHM.

In the earlier published work that involves vibration testing of historic masonry monuments, the sensor locations are selected invariably based upon qualitative engineering judgment and intuition (Atamturktur et al. 2009). The focus of this paper is to supply guidance regarding the optimal sensor locations for Gothic style masonry churches based on quantitative, information gain based criteria. The procedure implemented herein, the modified Effective Independence Method (EIM), selects the optimal sensor locations such that the dynamic characteristics of the structure are properly identified.

This manuscript begins with a detailed explanation of the EIM and the modification introduced to EIM to improve the effective distribution of sensors across the structure. A discussion focused on the details of the case study structure, the Cathedral of Saint John the Divine, follows. The next section provides an overview of the development of the FE model and its correlation with the structure's dynamic and static response. We then demonstrate the relationship between the desired mode shapes and the number of necessary sensor locations. Following the discussion on the robustness of the sensor locations, the optimal sensor locations obtained through EIM are provided. Finally, we conclude with guidelines for practicing engineers and preservationists on efficiently conducting modal testing experiments on large scale Gothic Cathedrals.

2 MODIFIED EFFECTIVE INDEPENDENCE METHOD

In this section, we first overview the EIM as originally introduced by Kammer (1991). Next, to ensure that the sensor locations effectively explore the structure, we modify the EIM by adding a distance based criterion. It is shown that EIM may exhibit sensitivity to modeling errors. Finally, to remedy this sensitivity and obtain more consistent sensor locations, we implement the error theory proposed by Kammer (1992).

2.1 EFFECTIVE INDEPENDENCE METHOD:

The goal of EIM is to retain maximum information about the dynamic behavior of the structural system with a reduced number of sensors through the maximization of the Fisher information matrix (Kammer 1991). It is a relatively simple and rapid method compared to exhaustive processes like those involving neural networks and genetic algorithms; therefore, EIM is ideal for large structures with a high number of possible sensor locations (Kammer 1991).

Successful applications of EIM have been well documented in published literature; see for instance Glassburn (1994), Heo et al. (1997), Meo and Zumpano (2005), and Kammer (1996).

Let us assume a scenario in which the number of candidate sensors is s, but due to the resources available for testing it is only possible to use $m << s$ sensors. The problem then becomes the optimal placement of m sensors in s possible locations. The EIM iteratively eliminates the sensors that contribute least to the independence of the modal vectors. First, a large enough set of candidate sensors that can clearly identify the desired modes must be selected. EIM initially assumes that the mode shape matrices, obtained from the FE model with the entire set of candidate sensor locations, are linearly independent. Next, EIM chooses m optimum sensors from the s candidate sensors, while maintaining as much linear independence and orthogonality of mode shapes vectors as possible.

Conceptually, the response at any point in an elastic structure can be represented, in the time or frequency domain, as a linear combination of mode shapes (Ewins 2000). The vector of the measured vibration response y_s can be estimated as a combination of n mode shapes and a noise term through the expression:

$$y_s = q\Phi + w \tag{1}$$

Φ is the mode shape matrix with n mode shape vectors;

q is the coefficient response vector, a function of time or the natural frequency;

w is the stationary Gaussian white noise with a zero mean value;

To obtain the best estimate of a mode shape, the covariance matrix of the estimate errors must be minimized (see Equation 2). As explained by Udwadia (1994), the covariance matrix of the estimate errors is bound by the Cramer-Rao lower bound.

$$E[(q-\hat{q})(q-\hat{q})^T] \geq Q^{-1} \quad (2)$$

Udwadia (1994) explains that for unbiased and efficient estimators, the inequality in Equation 2 becomes an equality. The right hand side of Equation 2 then yields the inverse of the Fisher information matrix, Q. Alternatively, we can derive the Fisher information matrix as given in Equation 3. Accordingly, by maximizing the Fisher information matrix in Equation 3, we can obtain the best estimates of the coefficients of the response vector in Equation 2.

$$Q = \left[\left(\frac{\partial y_s}{\partial q}\right)^T \frac{1}{\Psi^2}\left(\frac{\partial y_s}{\partial q}\right)\right] \quad (3)$$

where,

Ψ^2 is the Gaussian white noise variance and

$\hat{q}$ is the efficient unbiased estimator of q

Next, by substituting Equation 1 into Equation 3, we can obtain the Fisher information matrix in the following form:

$$Q = [\Phi^T \frac{1}{\Psi^2} \Phi] \quad (4)$$

Considering the noise as uncorrelated and having identical statistical properties at all locations, the effective independence values (EIV) of the each of the sensors, *i*, can thus be calculated as:

$$\text{EIV} = \phi_i . Q . \phi_i^T \qquad i=1,2,...k \quad (5)$$

where ϕ_i is the vector of the target modal co-ordinates of the ith sensor, and k is the remaining number of sensors considered in that particular iteration. The EIV of a sensor location lies between 0 and 1, where a value of 0 implies that the target modes are not observable from the sensor location (or that the corresponding row in the mode shape matrix is null). On the other hand, an EIV of 1 implies that the sensor location is vital for maintaining independence of the mode shape matrix and for identifying the target modes. EIM, in an iterative manner, eliminates

the sensor with the minimum EIV from the list of candidate sensors. Both the mode shape and Fisher information matrices are updated after each iteration until the pre-defined number of sensors remain to serve as the optimal set of sensor locations. Because of the iterative nature of the algorithm, the final sensor configuration can be *suboptimal*; however, Kammer (1991) states that the mode shape estimates from this configuration are close approximations of the actual optimal configuration.

2.2 DISTANCE BASED CRITERION:

One major drawback of the EIM, which is especially evident for symmetric structures, is that it can select measurement locations nearly adjacent to each other. This problem occurs when there are several sensors with approximately the same value of effective independence. The closely spaced sensors measure similar (or near-similar) response and supply an incomplete spatial representation of the mode shape of the structure. Therefore, it is of value to maximize the minimum distance between the sensor locations to assure that sensors effectively explore the geometry of the structure. This way, a better visualization of the mode shapes can be obtained, which is particularly relevant when visually correlating analytical and experimental mode shapes. Therefore, we modify the EIM, originally proposed by Kammer (1991), by introducing a distance based criterion (DBC) to the optimal sensor selection as follows:

$$d^{j}{}_{i} = \sqrt{(x-\hat{x}_j)^2 + (y-\hat{y}_j)^2 + (z-\hat{z}_j)^2} \qquad i=1,2,\ldots m; \qquad j=1,2,\ldots s \qquad (6)$$

where, x, y and z are the co-ordinates of the ith *optimal sensor* chosen by the EIM and $\hat{x}_j$, $\hat{y}_j$ and $\hat{z}_j$ are the co-ordinates of the jth sensor locations. If $d^{j}{}_{i}$ < DBC, the sensor location j is eliminated. This criterion assures that the sensors are not clustered in certain regions.

2.3 ROBUSTNESS TO MODEL ERROR:

The sensor locations chosen by the EIM may be sensitive to the errors in the numerical model predictions. Such errors may be caused by imprecisions in the material properties and boundary conditions. Therefore, it is crucial to correlate the FE model predictions against experimental evidence to ensure the input values of the FE model are realistic. However, even after elaborate and successful test-analysis correlation, a level of uncertainty in model predictions may remain. To remedy the sensitivity of EIM to the uncertainty in model predictions and to obtain more consistent sensor locations, Kammer (1992) suggested the use of the error theory, where the error between the mode shapes of the FE model and those obtained by slightly inaccurate model is calculated as:

$$\delta_s = \Phi_{fs} - \Phi_{rs} \tag{7}$$

where, Φ_{fs} is the mode shape matrix obtained by the FE model with uncertain input parameters and Φ_{rs} is the reference mode shape matrix.

The net information matrix I_n is then calculated as:

$$I_n = A_r - D \tag{8}$$

where, $A_r = \Phi_{rs}^T \Phi_{rs}$ and $D = \delta_s^T \delta_s$. The information matrix, A_r, corresponds to the reference mode shapes and D is the information matrix of the mode shape errors. If the matrix I_n is positive definite (Bhatia 2007) for a particular sensor configuration, then A_r is greater than D, which means that there is more information in the reference modes than in the mode shape errors. The positive definiteness of I_n is a sufficient condition for the positive definiteness of the reference mode shape information matrix A_r (Kammer 1992). In the course of the EIM, I_n is calculated at every iteration and if it is determined to be positive definite, then the sensor eliminated by the EIM at that iteration is not vital to the independence of the reference modes.

3 THE CASE STUDY STRUCTURE

The structure considered for this study is the Cathedral Church of St. John the Divine (SJD) (Figure 1a). Located in the heart of New York City, this Cathedral of Gothic Revival design is currently the fourth largest in the world (Hall 1920). The construction of the Church began in December 1892 and is still under completion. This study focuses on one of the bays along the nave of the Cathedral (Figure 1b). The 37.8m high and 75.6m long nave consists of four bays each 44.5m wide (Wickersham 1998).

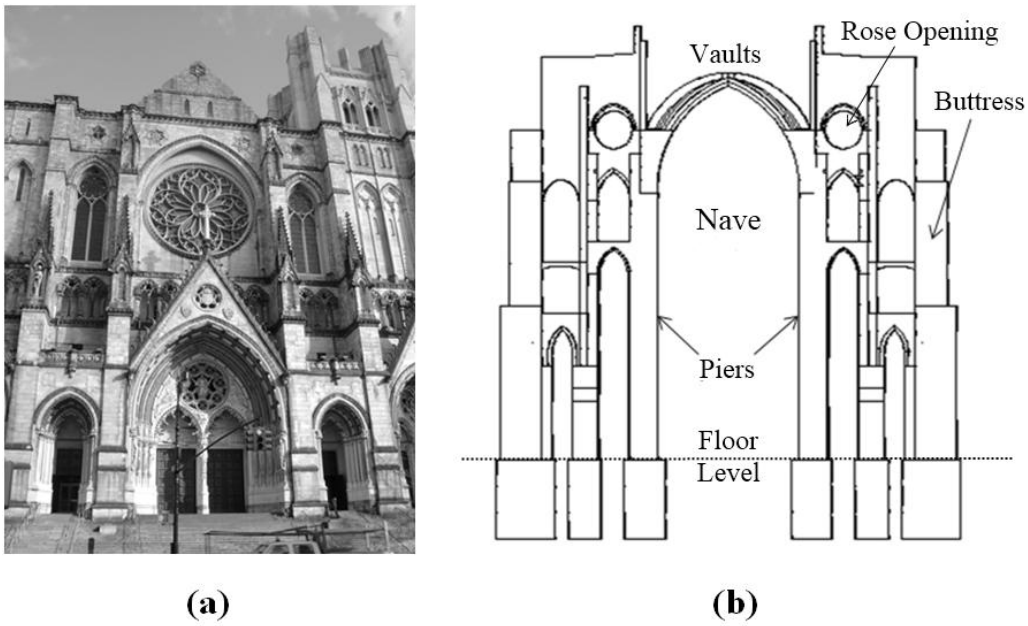

Figure 3: (a) The west front of the Cathedral Church of St. John the Divine, New York, (b) sectional elevation drawing of the nave.

The main walls of SJD are made of Maine granite with Mohegan golden granite facing on the outside and Frontenac stone facing on the inside, while the piers and buttresses are in-filled with concrete (Hall 1920). The webbing of the vaults is composed of Guastavino tile (Rossell 1995) and the vault ribs are made of cut schist (Hall 1920).

In a reconnaissance survey of the church building, all possible sensor locations are scouted for (see highlighted regions in Figure 6a). The walkways between the buttress and the nave, as well as mezzanines inside the nave, allow the placement of sensors at intermediate levels on the piers, walls and buttresses on the inside and outside of the church. The entire nave vault is accessible from the top. The availability of power sources and the length of sensor cables are also considered while selecting the candidate sensor locations.

4 DEVELOPMENT AND VALIDATION OF THE FINITE ELEMENT MODEL

A linear elastic FE model of SJD is built in two systematic phases using the FE software package ANSYS. In the first phase, a substructure consisting of the vaulted section of the naves is built and correlated with experimentally obtained dynamical characteristics of the vaults. In the second phase, the entirety of a single bay is modeled by adding the piers, buttresses and the walls.

4.1 FIRST PHASE: VAULTS OF THE NAVE

Model development: According to available construction drawings, the geometry of the Cathedral is first simplified and idealized preserving the structural properties, such as cross sectional area and the moment of inertia. The vault ribs and the vault webbing are modeled using 20-node SOLID95 brick elements and 8-node SHELL93 shell elements, respectively (ANSYS 2005). Since the stresses in the surcharge are less important, this material is modeled using lower order, 10-node SOLID92 elements. The entire model of one nave bay consists of 47194 elements.

The initial material property values for the elastic modulus, density and Poisson's ratio are determined according to historic documentation and engineering judgment (Theodossopoulos 2004, Özen 2006). The vault webbing is built out of Guastavino tile with the thickness varying from 15 cm to 20 cm. The elastic modulus and density of the Guastavino tile is reported by Saliklis, Kurtz and Furnbach (2003). Atamturktur and Sevim (2011) have conducted laboratory experiments on Guastavino tile and mortar specimens and obtained the homogenized material properties for a tile-mortar assembly. The surcharge volume behind the vaults is composed of masonry rubble for which the material properties are determined according to Erdogmus et al. (2007). The initial material properties for the ribs and arches are assigned based upon available documentation on cut schist (URL-1). The element type and material property assignments for different structural components are summarized in Table 2.

The initial boundary conditions are applied according to a combination of visual observations of support conditions, engineering judgment and the recommendations of Erdogmus (2004). These initial material properties and boundary conditions are then adjusted according to the experimentally measured natural frequencies and mode shapes, respectively. The single bay model is then reflected to obtain a three-vault model as shown in Figure 2.

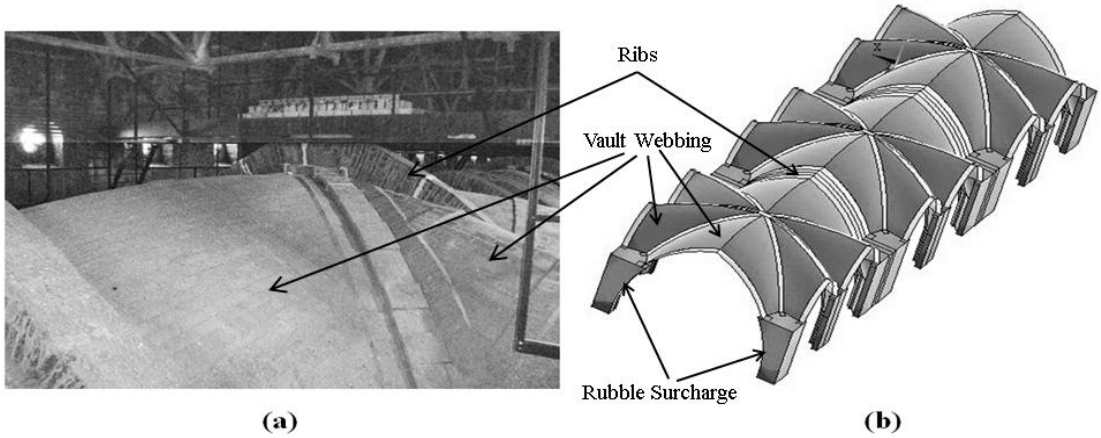

Figure 2: (a) Photo of the nave vaults, (b) FE model of the vaults.

Test-Analysis Correlation: Since only the vaulted section of SJD is modeled in the first phase, the structural effects of the unmodeled sections of the nave, such as the nave walls, aisles and buttresses are represented as boundary conditions. The initial boundary conditions in the FE model are tuned iteratively by systematically comparing the analytically obtained mode shapes and mode shape sequence with those obtained experimentally (see Table 1). The final boundary conditions consist of the following: (i) displacement and rotational restraint applied in all directions at the base of the vault springing, (ii) longitudinal horizontal restraint to represent the unmodeled adjacent vaults, and (iii) transverse horizontal restrain along the length of the piers where buttresses rest. The initial material properties of the Cathedral are fine-tuned according to the natural frequency agreement. The final values obtained for material properties are given in the first three rows of Table 2 (Boothby, Atamturktur and Hanagan 2006).

The fine-tuning of the material properties and boundary conditions are uncoupled, where the boundary conditions are adjusted according to the mode shape agreement and material properties are fine-tuned according to the natural frequency agreement. Atamturktur and Laman (2011) cautions such uncoupling since the relative ratio of material properties may also have an effect on

the mode shape vectors as well as their sequence. In this study, by perturbing the ratio of different material properties, it is verified that the mode shapes are not altered.

Table 1: Comparison of experimental and analytical modal analysis results of the vaults of St John the Divine.

Mode Shape	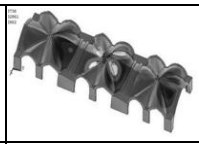		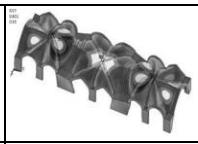		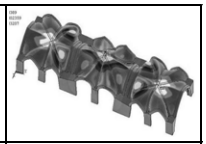
Experimental	**13.61 Hz**	**15.84 Hz**	**16.27 Hz**	**17.70 Hz**	**20.24 Hz**
Analytical	**12.31 Hz**	**15.71 Hz**	**16.68 Hz**	**17.13 Hz**	**20.51 Hz**

4.2 SECOND PHASE: ENTIRETY OF THE NAVE

Model development: In the second phase, the model of the first phase is extended to represent an entire bay, including full length piers, the buttresses and aisle vaults. The element types as well as the material properties are kept consistent with those used in the first phase. A new material is added to represent the granite walls and piers. For the elastic modulus of granite, a range of 30-55 GPa is suggested by Özen (2006) and 40-100 GPa in Gere and Timoshenko (1997). In this study, we use 50 GPa for the granite piers and walls. The densities used for the piers and walls are based on historic correspondences obtained from the SJD archives (Adamson 1917). When adding the aisle vaults, BEAM188 elements are used for the ribs. The entire model of one nave bay consists of 125,920 elements.

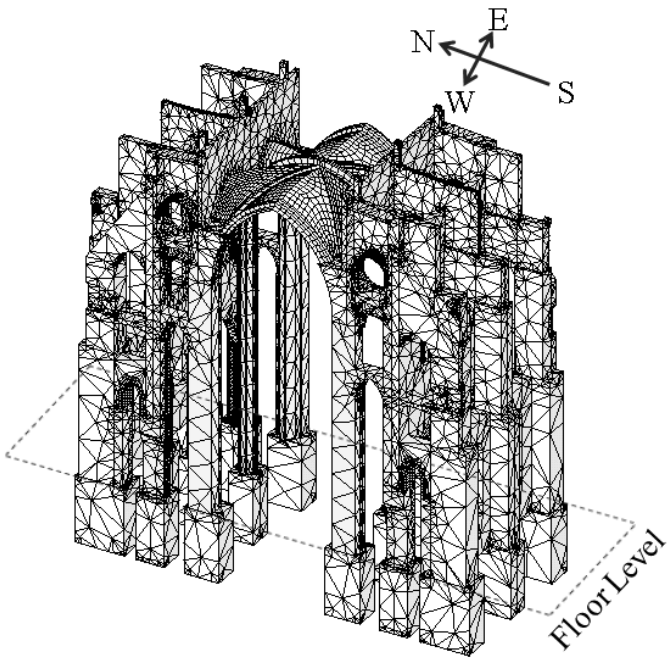

Figure 3: The 3-D meshed FE model of the bay.

A fully rigid boundary condition, which prevents translation and rotation in all three directions, is applied to the base of each foundation. At the floor level, piers and buttresses are restrained horizontally to mimic the restraining effect of floor slabs. Symmetry boundary conditions are applied to both the east and west face of the bay to simulate the existence of adjacent bays in the nave.

Table 2: Element type and material properties used in the FE model for different parts of the structure.

Structural Member	ANSYS Element	Density (kg/m^3)	E (GPa)	Poisson's Ratio
Ribs/Arches	SOLID95	2100	12	0.2
Vault Webbing	SHELL93	1600	6.5	0.15
Rubble Surcharge	SOLID92	1000	4.5	0.1
Piers	SOLID95	2640	50	0.2
Walls	SOLID92	2700	50	0.2

Inspection-Analysis Correlation: During the reconnaissance survey, the structure is closely inspected for cracking and hinging of the masonry structure. Cracks are consistently observed at the rose openings (see Figure 4) and in the walkways between the buttress and nave (see Figure 5). It is important to note that these cracks are symmetric on both sides of the nave in each of the four nave bays. If the FE model is an accurate representation of reality, then the FE model simulations under the self-weight of the structure should yield high stress concentrations at the locations of these existing cracks (Mark and Hutchinson 1986 and Ricart-Nouel 1991). However, one must take care to ensure that the cracks and hinges are indeed caused by the self-weight of the structure, and not by the differential support settlements. Therefore, during the reconnaissance survey, the entirety of the nave is inspected to determine if there are any signs of support settlement. However, no significant geometric distortions are observed in the structure. Therefore, the cracks are concluded to be caused primarily by gravitational forces, such as the self-weight of the structure; and thus the test-analysis correlation of crack locations is deemed appropriate.

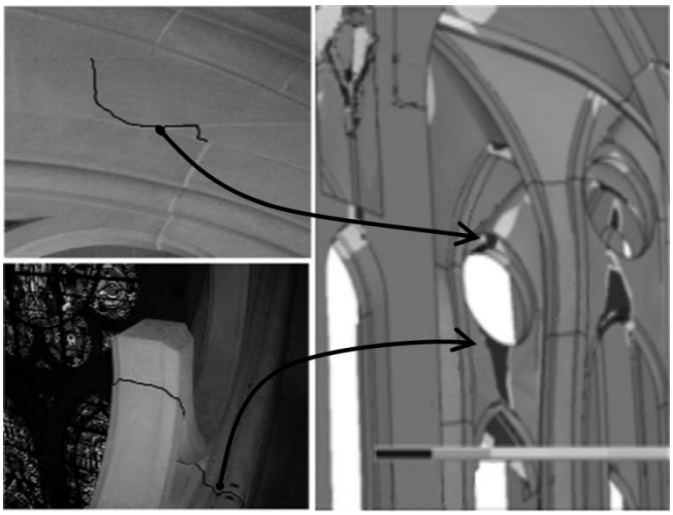

Figure 4: Cracks at the rose opening (highlighted) corresponding to high tensile stress regions in the FE model.

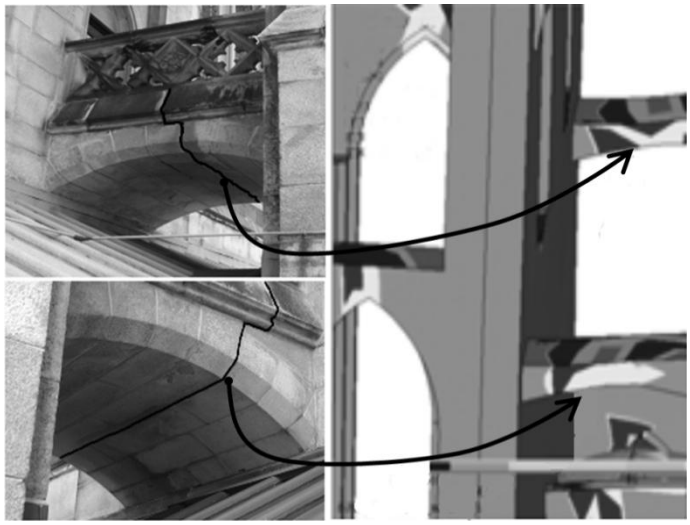

Figure 5: Cracks at the walkways (highlighted) between the buttress and the nave corresponding to the high tensile stress regions in the FE model.

The FE model is executed to analyze the behavior of SJD under its own self-weight and the regions with high tensile stresses are marked as shown in Figures 4 and 5. A close match is observed between the high tensile stress regions in the FE model and the existing crack locations in the structure. As evidenced by Figure 4 and Figure 5, the cracks near the rose openings and in the outer walkways are well predicted by the FE solution. Therefore, the FE model of the Cathedral is deemed to be an accurate representation of SJD.

5 SENSOR OPTIMIZATION

A sufficient number of candidate sensor locations need to be chosen to ensure that the target modes are well-defined. Accordingly, 205 locations are selected on the vault and additional 576 locations are selected on the rest of the structure (Figure 6). The optimal sensor locations for triaxial accelerometers are determined, with the subsequent mode shape matrix formed with 781

candidate sensor locations considering the resultant of the X, Y and Z modal displacements. If triaxial sensors are unavailable at the time of the test, then uniaxial sensors can be revolved three times at each location to obtain measurements in all three directions. Similarly, to identify modes in only one or two directions, the mode shape matrix can be modified to include only the modal displacements in those respective directions.

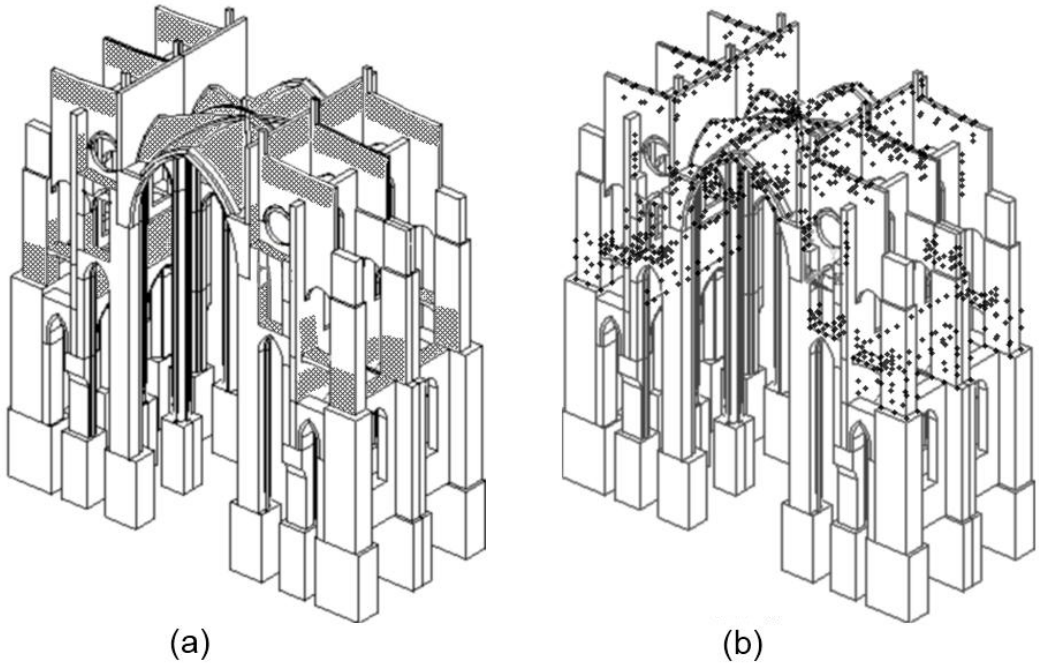

Figure 6: (a) The accessible locations on the structure highlighted; (b) the candidate sensor locations shown as dots.

Eleven of the first twenty analytical modes are observed to be local, where the motion is focused on a single structural member (typically the piers). Therefore, nine of the first 20 modes are identified as ‘target’ global modes (Figure 7). These nine global modes form the initial mode shape matrix with the 781 candidate degrees of freedom. To assure equal participation from all nine modes, the mode shapes are normalized between 0 and 1. The degrees of freedom are then iteratively reduced from 781 down to the predefined number of sensor locations (in our case, 80)

by eliminating one location in succession according to their contributions to the independence of the mode shape matrix.

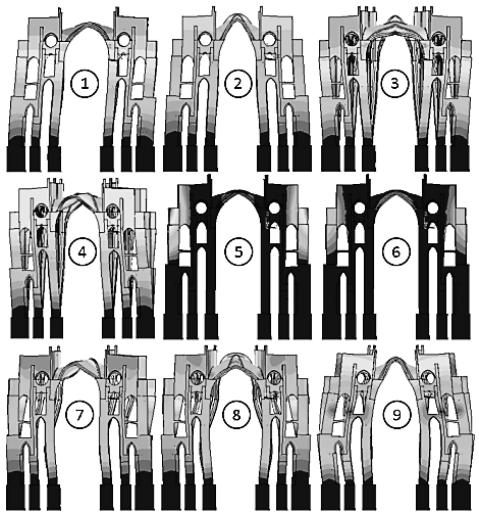

Figure 7: Nine target mode shapes desired to be extracted during the *in-situ* modal analysis.

The percentage loss in information as the sensor locations are eliminated can be calculated as the determinant of the Fisher information matrix. As shown in Figure 8, the Fisher information matrix determinant is sensitive to both the number of target modes and number of candidate locations with the number of required sensors increasing with the number of modes to be identified.

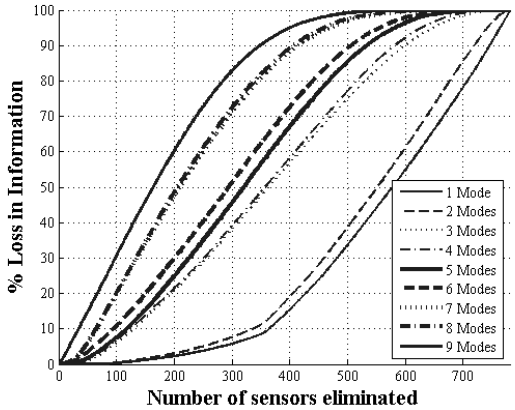

Figure 8: Fisher information matrix determinant updated with sensors eliminated iteratively.

Figure 9 shows the EIV of the eliminated sensors with respect to the iteratively updated mode shape matrix, i.e. the mode shape matrix with only the remaining candidate locations. To identify nine modes with each sensor having an EIV of more than 0.1, it is possible to eliminate 701 sensors and use only 80 sensors. As indicated in Figure 9, the number of candidate locations and number of target modes dictates the information content of the mode shape matrix.

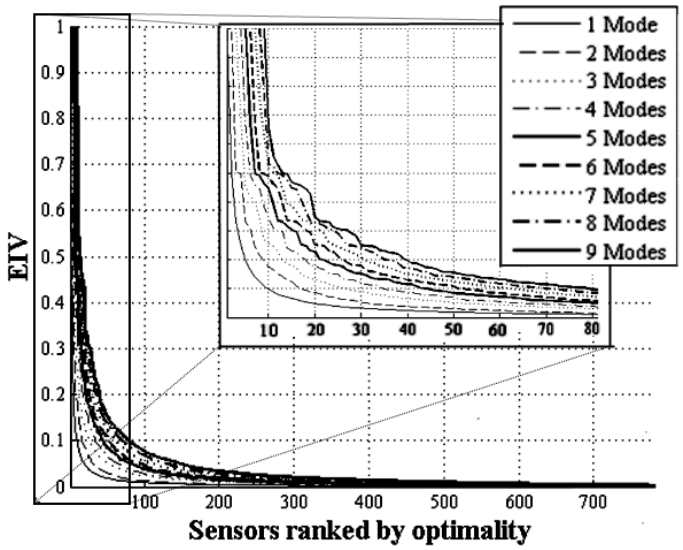

Figure 9: Effective independence values of the sensors with respect to the iteratively updated mode shape matrix; (inset) zoomed in to 80 optimal sensors.

For this study, a total of 80 optimal sensor locations for triaxial sensors are sought for the entire bay. Figure 10a and 10b show the optimal locations computed by the EIM before and after applying the DBC. Without the minimum distance specified, the EIM picks closely spaced sensors at locations that yield an incomplete visual representation of the mode shapes. However, in Figure 10b, each of the 80 triaxial sensors is placed at least three meters apart in all directions. The sensors are thoroughly distributed on the structure, which is ideal for visualizing the target modes of interest. Note that the sensor locations computed without the DBC contain more

information. Therefore, one must accommodate for the tradeoff between mode independence and visual observability, depending upon the application.

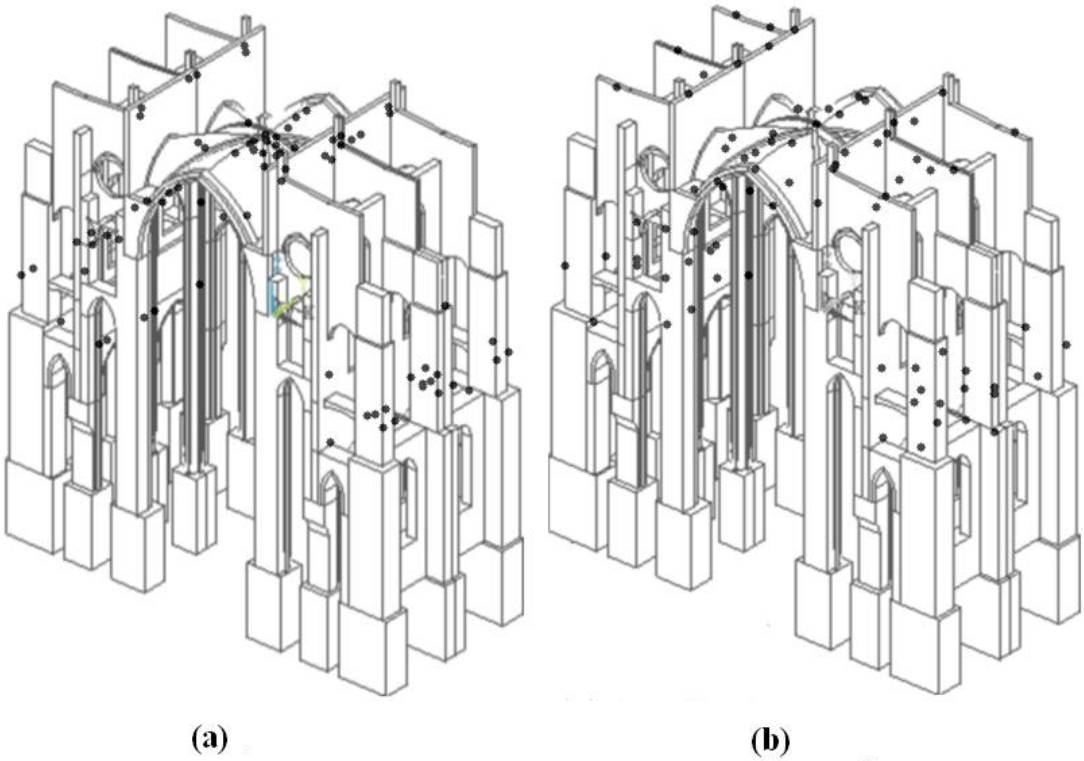

Figure 10: Optimal sensor locations for triaxial sensors on the full bay (a) without DBC, (b) with DBC of 3 meters.

6 DISCUSSIONS

The choice of sensor locations on a functioning monumental structure is governed by many factors (e.g. accessibility, maintaining the aesthetics), in which some of the actual optimal locations are eliminated by default. Therefore, the problem becomes that of selecting the optimal locations out of the feasible candidate locations. In this selection, several important factors must be properly evaluated, such as the threshold value used for the distance based criteria and the

robustness of the findings to the uncertainty in model predictions. In the end of this section, we make inferences regarding the optimal regions for sensor placement in Gothic style structures.

6.1 SENSITIVITY TO MINIMUM DISTANCE CRITERIA

While the DBC may eliminate sensors that are mathematically more optimal (Figure 10), the DBC supplies visual observability, which is particularly useful while comparing the analytical and experimental mode shapes. Figure 11 shows the higher rate of information loss as the threshold distance between sensors is increased. Note the exception where DBC = 0.5m yields more optimal solutions between 45-80 sensors compared to DBC=0.0 m. This can be explained by the inherent sub-optimality due to the iterative nature of EIM.

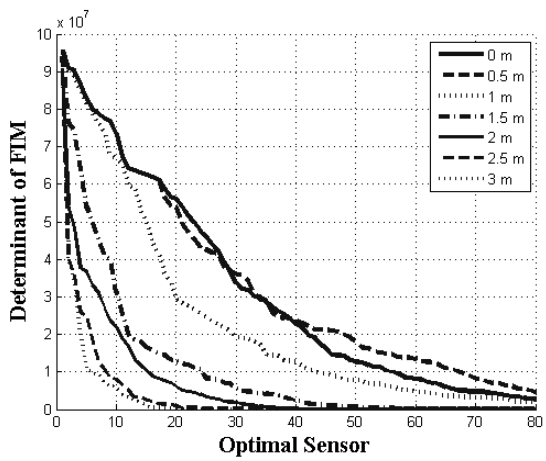

Figure 11: Behavior of the Fisher information matrix determinant for different DBC.

6.2 ROBUSTNESS TO MODELING ERROR

The model used in this study is correlated with experimental measurements as well as with on site inspections. However, slight uncertainties remain in the model predictions. Therefore, it is of value to ensure that such uncertainty does not interfere with the main findings obtained through EIM.

To demonstrate the robustness of the method, assuming a 5% error in the model parameters, six FE models are generated: one reference model with material properties given in Table 2 and the other five, each with a 5% reduction in the elastic modulus of one of the five materials given in Table 2. First, the optimal locations for the six models are plotted without employing a DBC (Figure 12). As seen, the sensor locations are all localized in a few regions on the model, while sensors in some regions are consistently eliminated by the EIM for all five cases. This observation shows that if one considers the regions within the structure and not individual candidate DOFs, the EIM selections are consistent and are robust to errors in model parameters.

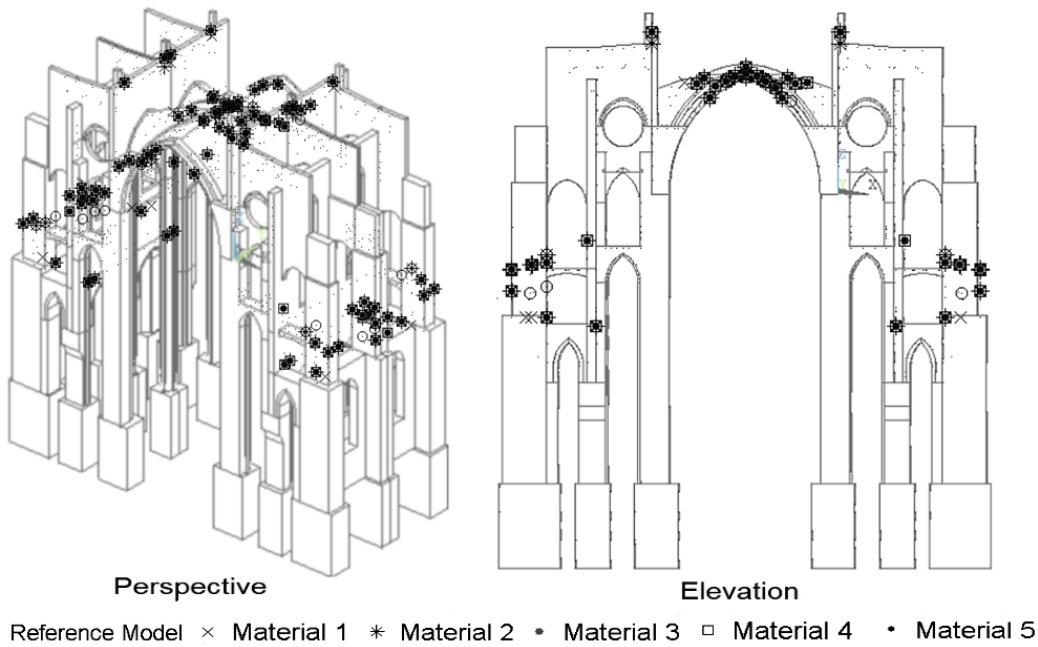

Figure 12: Optimal sensor locations after 5% reduction in the Elastic modulus of each of five materials without a DBC.

The EIM is more sensitive to modeling errors in the presence of a threshold distance between sensors as it is without one. Figure 13 shows the sensor configurations for various DBC from 0 meters up to 3 meters. As the distance is increased, the robustness of the EIM diminishes. In an effort to achieve a compromise between the retention of information about the mode shapes, the

visual observability of the mode shapes and the robustness of the method to change in input parameters, a DBC of 1.5 meters is deemed suitable.

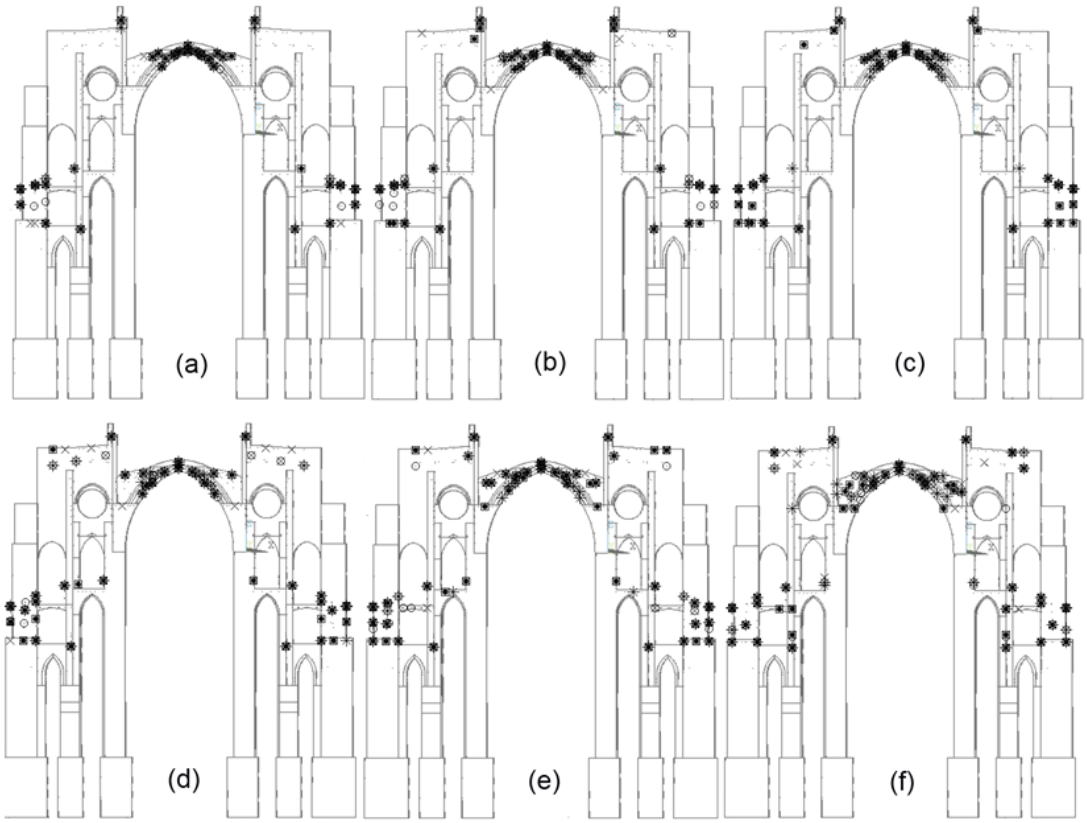

Figure 13: The optimal sensor locations for the 6 models with DBC of (a) 0m (or no DBC); (b) 1m; (c) 1.5m; (d) 2m; (e) 2.5m; (f) 3m.

To reduce the variability of sensor locations due to changes in material properties, the error theory is applied wherein the sensors that cause the net information matrix to remain positive definite are retained. Figure 14 shows the sensor locations on the six models generated with varying material properties where a DBC of 1.5m is applied to each. There is more than one sensor that is retained by the EIM at every iteration after applying the error theory. Hence, there maybe a few sensors in the final configuration that are spaced less than 1.5m apart.

6.3 OPTIMAL SENSOR LOCATIONS FOR GOTHIC CHURCHES

In Figure 14, the optimal sensor locations are consistently concentrated around (i) ribs on the vaults, (ii) vault webbing around the crown, (iii) top of the nave walls, (iv) buttresses above the vaults and (v) outer edges of the buttresses at level of the first crosswalk.

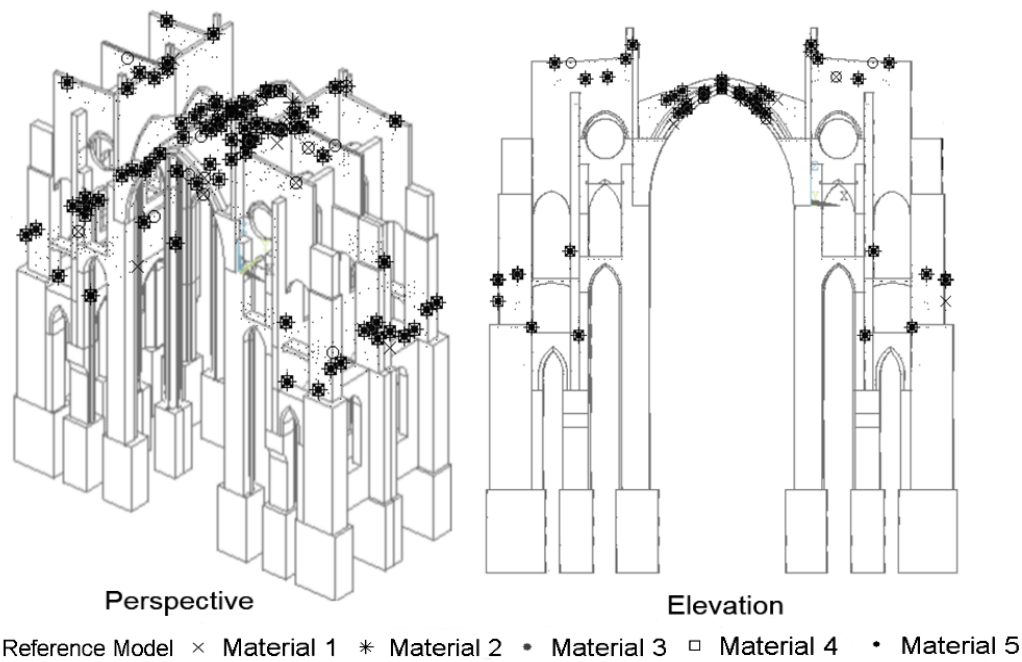

Figure 14: Optimal sensor locations in the six FE models using a DBC of 1.5m and applying the error theory.

While testing large scale Gothic style churches, placing the sensors at the abovementioned locations are most advantageous from the viewpoint of system identification. The mode shapes derived from these locations ensure maximum independence of the mode shape matrix considering the nine global modes discussed before. Although demonstrated using 80 sensor locations, if the user possesses a lesser number of sensors, it will be most valuable to place them at these general regions. For applications where visualization of the mode shapes is of more importance, the DBC can be increased acknowledging the fact that the linear independence of the mode shapes is sacrificed in the process.

7 CONCLUSIONS

In this paper, the application of an existing analytical procedure, the Effective Independence Method, is discussed and demonstrated to maximize the information gained during *in-situ* modal analysis of a Gothic style masonry Cathedral. Herein, this existing established method is modified by the addition of a distance based criteria, which assures that the sensors are placed with sufficient distance from each other to better explore the structure. To reduce the effects of modeling error on the sensor placement, the error theory is applied that acts as a constraint on the elimination of critical sensors that are important for the identification of the real modes. Ultimately, through the application of the modified EIM, we recommend selected regions for sensor placement to expedite the process of and reduce the resources necessary for the full-scale modal testing of Gothic Cathedrals, such as the Cathedral of St. John the Divine, the subject of this study.

In this study, a vibration test on the easily accessible vaulted section of SJD is first performed using previously recommended sensor locations (Atamturktur et al. 2009). A partial FE model is constructed and calibrated against the experimentally-obtained mode shapes and natural frequencies. At this phase, the boundary conditions mimicking the structural components excluded from the model are adjusted and the material properties are fine-tuned. Next, this partial model is extended to a full bay model by adding the missing components such as the aisles, buttresses, piers and walls. This full FE model is tested against the visual observations during the site survey. The high tensile stress regions from a static analysis under self-weight are compared against visually-observed crack locations in the structure. As a result of the satisfactory agreement, the model is accepted as a useful tool for determining the optimal sensor locations.

The possible candidate sensor locations are determined from a site reconnaissance survey. The mode shape matrix is generated with all of the candidate locations from the FE model and the target modes are chosen. Finally, the candidate locations are reduced to a required number of sensor locations using the EIM modified with the DBC. While the DBC causes a loss in information about the mode shape vectors, it distributes the sensors so that the final optimal set of sensors are not clustered and thus results in better visualization of the mode shapes.

The robustness of the method to uncertainties in FE model parameters is also studied and it is seen that the optimal locations chosen by the EIM localize in specific regions within the geometry even when the material properties are varied. However, the robustness of the method is compromised in the presence of too high a distance criterion, which for SJD is found to be equal or higher than 2m.

Although demonstrated on the Cathedral of St. John the Divine, a historic masonry structure, the concepts presented herein are applicable to many structural systems. The variable introduced by the DBC of the modified EIM, the minimum distance between sensors, requires a measure of engineering judgment that, of course, varies with the objective of the test campaign.

ACKNOWLEDGMENTS

This work is performed under the auspices of the PTT Grants program of National Center for Preservation Technology and Training (NCPTT) of Department of Interior: the Grant Agreement Number MT-2210-10-NC-01. Many thanks to Dr. Daniel C. Kammer (Professor of University of Wisconsin- Madison) for his valuable comments on the methodology employed in the paper. We

also wish to thank Godfrey Kimball of Clemson University for his editorial assistance. We also thank Andrew Phifer, a Creative Inquiry student, for his meticulous and thorough search of the archival document of SJD.

CONCLUSIONS

The three manuscripts attempt to address two of the major problems associated with deploying SHM on historic masonry structures.

The first study deals with the selection and assimilation of **optimal response features** for damage detection using an FE model of an arch as well as a scaled laboratory model. Features are found to show varying damage sensitivities based on the damage severity as well as location. The noise sensitivity of the structure is also shown to increase with the increase in the level of damage. There is not one particular feature that is robust to the type, location and severity of damage and to the inherent noise. By normalizing the damage indicating features to make them unitless quantities, one can assimilate a number of features to get a better damage indicator that reduces the uncertainties caused due to extraneous noise and the non-linear sensitivities of the features to the damage severity.

In the third study, force and acceleration time series data is collected through modal tests performed on the damaged and undamaged vaults of the Beverly Minster, UK. Auto-Regressive Support Vector Machine (AR-SVM) models of the raw data are found to be successful in differentiating the damaged and undamaged state of the vaults. The analysis in the frequency domain indicates that the damaged vaults have higher amplitude vibrations compared to the undamaged vaults which points to the loss in dynamic stiffness of the damaged vaults. The analysis of the natural frequencies and mode shapes is ineffective, as there is insignificant change observed on comparison of damaged and undamaged vaults.

In the third study, guidelines for the **optimal sensor placement** on historic masonry monuments are presented using a modified version of the Effective Independence method. A distance based criteria is enforced that allows the sensors to better explore the structural geometry

in order to allow visualization of mode shapes, an important aspect from the testing engineers standpoint. The method uses numerical FE models of the Cathedral of St. John the Divine which is developed in two stages. First, a substructure of the building is modeled and calibrated to the experimental results and then, the entire model of one of the nave bays is created and validated with the on-site inspection of existing cracks. Following the application of a modified Effective independence method, optimal sensor locations are suggested, which are applicable to many Gothic style Cathedral built, which poses typical structural configurations.

Although this report is focused on historic structures, professionals involved in testing any structural form can follow the methodologies presented for an efficient deployment of SHM.

REFERENCES

Adamson, J., (1917), Letter to James Grant dated January 25th 1917, Saint John the Divine Cathedral archives.

Akaike, H., (1969),"Power Spectrum Estimation through Autoregressive Model Fitting," Ann. Inst. Statist. Math., Vol. 21, 1969, pp. 407-419.

Alampalli, S., Fu, G. and Dillon, E. W., (1997), "Signal Versus Noise In Damage Detection By Experimental Modal Analysis," Journal of Structural Engineering, Vol. 123, No. 2, pp. 237–245.

Allemang, R.J., (1980), "Investigation of Some Multiple Input/Ouput Frequency Response Function Experimental Modal Analysis Techniques," Ph.D. Thesis, University of Cincinnati, USA.

ANSYS (2005). "Ansys Elements Reference." ANSYS v 12.0, Swanson Analysis System, U.S.

Antonacci, E., (2001), "Retrofitting Effects on The Dynamic Behaviour of Basilica S. Maria Di Collemaggio," Computational Methods and Experimental Measurements, Vol. 10, pp. 479–88.

Antonacci, E., Beolchini, G., Di Fabio, F., and Gattulli, V., (2001), "Retrofitting Effects on the Dynamic Behavior of S. Maria di Collemaggio", Tenth International Conference on Computational Methods and Experimental Measurements, Alicante, Spain.

Aoki, T., Sabia, D., Rivella, D., Muto, H., (2005), "Dynamic Identification and Model Updating of the Howa Brick Chimney, Tokoname, Japan," Structural Studies, Repairs and Maintenance of Heritage Architecture, IX, Vol. 83, pp. 265- 275.

Armstrong, D. M., Sibbald, A., Fairfield, C. A., Forde, M. C., (1995), “Modal Analysis for Masonry Arch Bridge Spandrel Wall Separation Identification,” NDT&E International, vol. 28, no. 6, pp. 377–86.

Atamturktur, S., Hemez, F., Laman, J., (in review), “Verification and Validation Applied to Finite Element Models of Historic Masonry Monuments," Journal of Probabilistic Mechanics.

Atamturktur, S. and Boothby, T., (2007), “Finite Element Modeling of Guastavino Domes”, Bulletin of Association for Preservation Technology, Vol. 28, No. 4, pp. 21- 29.

Atamturktur, S., (2009), Calibration Under Uncertainty for Finite Element Models Of Masonry Monuments, Ph.D. Thesis, The Pennsylvania State University, PA.

Atamturktur, S., Pavic, A., Reynolds, P. and Boothby, T., (2009), “Full-Scale Modal Testing of Vaulted Gothic Churches: Lessons Learned”, Journal of Experimental Techniques, Vol. 33, No. 4, pp. 65- 74.

Atamturktur, S., Boothby, T., (2010), “Calibration of Finite Element Models of Masonry Vaults”, Journal of Masonry Society, Vol. 28, No. 2, pp. 77-93.

Atamturktur, S., Fanning, P., and Boothby, T., (2010), “Experimental and Operational Modal Testing of A Vaulted Masonry Cathedral”, ICE - Engineering and Computational Mechanics, Volume 163, Issue 3, pp. 213 –223, ISSN: 1755-0777, E-ISSN: 1755-0785.

Atamturktur, S., Bornn, L., and Hemez, F., (November 2010, in review), "Damage Detection in Masonry Vaults by Time-Domain Vibration Measurements," Journal of Engineering Structures.

Atamturktur, S., Laman, J., (2010), "Calibration of Finite Element Models of Masonry Structures: A literature Review", Journal of Structural Design of Tall and Special Buildings, doi: 10.1002/tal.577.

Atamturktur, S. and Sevim, B., (accepted 2011, in print), "Seismic Performance Assessment of Masonry Tile Domes through Non-linear Finite Element Analysis", ASCE Journal of Performance of Constructed Facilities.

Atamturktur, S. and Laman, J. A., (2011), "Finite Element Model Correlation and Calibration of Historic Masonry Monuments: Review", The Structural Design of Tall and Special Buildings, 20: n/a. doi: 10.1002/tal.577

Balanda, K.P. and MacGillivray, H.L., (1988), "Kurtosis: A Critical Review," The American Statistician, Vol. 42, No. 2, pp. 111-119.

Barnwell, P. S., (2007), Director of Studies in the Historic Environment & Fellow of Kellogg College, Presentation at the Craftsmen of Beverley Minster program, March 17, 2007.

Bayraktar, A., Sevim, B., Altunişik, A. C., and Türker, T., (2009), "Analytical and Operational Modal Analyses of Turkish Style Reinforced Concrete Minarets for Structural Identification." Experimental Techniques, Vol. 33 No. 2, pp. 65-75.

Bayraktar, A., Altunisik, A.C., Sevim, B. and Türker, T., (2011), "Seismic Response of a Historical Masonry Minaret using a Finite Element Model Updated with Operational Modal Analysis," J. of Vibration and Control, Vol. 17, No. 1, pp. 129-149.

Begg, R.D., Mackenzie, A.C., Dodds, C.J. and Loland, O., (1976), "Structural Integrity Monitoring Using Digital Processing of Vibration Signals," in Proceedings of 8th Annual Offshore Technology Conference, Houston, TX, pp. 305-311.

Bensalem A., Fairfield C. A. Sibbald A., (1995), “NDT for Condition Based Maintenance of Arch Bridges,” Proc. 8th Int. Conf. Condition Monitoring, 2, Kingston, Canada 1995, pp. 503–509.

Bensalem, A., Fairfield, C. A., Sibbald, A., (1997), “Non-destructive Evaluation of The Dynamic Response of A Brickwork Arch,” Proceedings of the Institution of Civil Engineers, Structures and Buildings, Vol. 122, No. 1, pp. 69–82.

Bensalem, A., Ali-Ahmed, H., Fairfield, C. A., Sibbald, A., (1999), “Non-destructive Testing to Detect Voids Hidden Behind The Extrados of An Arch Bridge,” NDT and E International, Vol. 32, No. 6, Sep, pp. 343–53.

Bhatia, R., (2007), “Positive Definite Matrices, Princeton Series in Applied Mathematics”, Princeton University Press, Princeton, NJ.

Binda, L., Gatti, G., Mangano, G., Poggi, C., and Landriani, G. S. (1992). "Collapse of the Civic Tower of Pavia: A Survey of the Materials and Structure." Masonry International, 6(1), 11-20.

Binda, L., Baronio, G., Gavarini, C., De Benedictis, R., and Tringali, S. (1999). "Investigation on materials and structures for the reconstruction of the partially collapsed Cathedral of Noto (Sicily)." International conference structural studies, repairs and maintenance of historical buildings, 323-332.

Boothby, T. E., Atamturkur, H. S., and Hanagan, L. M., (2006), "Modal Analysis Methods for Validation of Vaulted Stone Masonry Models", Proceedings of the 2006 Architectural Engineering National Conference; Omaha, Nebraska, USA, doi:10.1061/40798(190)66

Bornn, L., Farrar, C., Park, G., Farinholt, T. (2009), “Structural Health Monitoring with Autoregressive Support Vector Machines.” Journal of Vibration and Acoustics. Vol. 131, No. 2, pp. 021004.

Carden, E. P., Fanning, P., (2004), “Vibration Based Condition Monitoring: A Review,” Structural Health Monitoring, vol. 3, no. 4, pp. 355- 377.

Chang, P.C., Flatau, A. and Liu, S.C., (2003), “Review Paper: Health Monitoring of Civil Infrastructure,” Structural Health Monitoring, Vol. 2, No. 3, pp. 257-267.

Colla, C., Lausch R., (2002), “Influence of Source Frequency on Impact-Echo Data Quality for Testing Concrete Structures”, NDT&E International, Vol. 36, pp. 203- 13.

De Sortis, A., Antonacci, E., and Vestroni, F., (2005), “Dynamic Identification Of A Masonry Building Using Forced Vibration Tests.” Engineering Structures, 27(2), 155-165.

De Stefano, A., (2007), “Structural Identification and Health Monitoring on the Historical Architectural Heritage”, Key Engineering Materials, Vol. 347, pp. 37-54.

De Stefano, A., Ceravolo, R., (2007), “Assessing the Health State of Ancient Structures: The Role of Vibration Tests,” Journal of Intelligent Material Systems and Structures, Vol. 1, No. 15, pp. 1- 15.

Doebling S. W., Farrar, C.R., Prime, M. B., Shevitz, D.W., (1996), “Damage Identification and Health Monitoring of Structural and Mechanical Systems from Changes in their Vibration Characteristics: A Literature Review,: Research Rep. No LA-13070-MS, ESA-EA, Los Alamos National Laboratory, Los Alamos, N.M.

Doebling, S., Farrar, C. R., Prime, M. B., (1998), “A Summary Review of Vibration-Based Damage Identification Methods,” Shock and Vibration Digest, Vol. 30, No. 91, pp. 91- 105.

Dong, C., Zhang, P.Q., Feng, W.Q., Huang, T.C., (1994), “The Sensitivity Study of the Modal Parameters of a Cracked Beam,” in Proceedings of the 12th International Modal Analysis Conference, pp. 98-104.

Durukal, E., Cimilli, S., Erdik, M., (2003). Dynamic response of two historical monuments in Istanbul deduced from the recordings of Kocaeli and Duzce earthquakes, Bulletin of Seismological Society of America, 93 (2): 694- 712.

Duggan, D.M., Wallace, E.R., and Caldwell, S.R., (1980), “Measured and Predicted Vibrational Behavior of Gulf of Mexico Platforms,” in Proceedings of 12th Annual Offshore Technical Conference, pp. 92- 100.

Ewins D.J., Ho, Y.K., (2000), “On the Structural Damage Identification with Mode Shapes,” in Proceedings of the Conference held in E.T.S.I. Aeronauticos, Universidad Politecnica de Madrid, Spain, June 2000, pp. 677- 683.

Ellis, B., (1998), "Non-Destructive Dynamic Testing of Stone Pinnacles on the Palace of Westminster", Proceedings of the Institution of Civil Engineers. Structures and Buildings, Vol. 128, No. 3, pp. 300-307.

Erdogmus, E., (2004), “Structural Appraisal of the Florentine Gothic Construction System”, PhD Thesis, The Pennsylvania State University, State College, PA.

Erdogmus, E., Boothby, T.E., and Smith, E.B., (2007), “Structural Appraisal of the Florentine Gothic Construction System”, Journal of Architectural Engineering, Vol. 13, pp. 9-17.

Erdogmus, E., (2008), “Timbrel Domes Of Guastavino: Nondestructive Assessments on a Half-Scale Model”, International Journal of Architectural Heritage, Vol. 2, No. 4, pp. 330-352.

Ewins, D. J., (2000), “Modal Testing: Theory, Practice and Application”, Research Studies Press, Ltd., Hertfordshire.

Farrar, C.R.,Worden, K., (1992), “An introduction to structural health monitoring,” Phil. Trans. R. Soc., Fox, C.H.J., “The Location of Defects in Structures: A Comparison of the use of Natural Frequency and Mode Shape Data,” in Proceedings of the 10th International Modal Analysis Conference, pp. 522- 528.

Farrar, C.R., Baker, W.E., Bell, T.M., Cone, K.M., Darling, T.W., Duffey, T.A., Eklund, A. and Migliori, A., (2007), “Dynamic Characterization and Damage Detection in the I-40 Bridge Over the Rio Grande,” Los Alamos National Laboratory report LA-12767-MS, Vol. 365, No. 1851, pp. 303- 315.

Farrar, C. R., Worden, K., Todd, M. D., Park, G., Nichols, J., Adams, D. E., Bement, M. T. and Farinholt, K., (2007), “Nonlinear System Identification for Damage Detection,” Los Alamos National Laboratory Report, LA-14353, 2007.

Farrar, C.R., and Worden, K., (2007), “An Introduction to Structural Health Monitoring”, Philosophical Transactions of the Royal Society A: Mathematical, Physical and Engineering Sciences, Vol. 365, No. 1851, pp.303-315.

Fritzen, C.P., Seibold, S. and Buchen, D., (1995), “Application of filter Techniques for Damage Identification in Linear and Nonlinear Mechanical Structures,” in Proceedings of the 13th International Modal Analysis Conference, pp. 1874- 1881.

Gantert Engineering Studio (1993) “Technical opinion about the collapse of the Bell Tower of St. Maria Magdalena in Goch (Germany).”

Garaygordóbil, J.C.A., (2003), “Dynamics Assessment of Structural Building Components,” Ph.D. Thesis, Universitat Politècnica de Catalynya, Barcelona, Spain.

Gentile, C., Saisi, A., (2007), “Ambient Vibration Testing of Historic Masonry Tower for Structural Identification and Damage Assessment,” Construction and Building Materials, Vol. 21, No. 6, pp. 1311- 1321.

Gere, J. and Timoshenko S., (1997), “Mechanics of Materials 4th ed.”, PWS Publishing Co., Boston.

Glassburn, R. S., (1994), "Evaluation of Sensor Placement Algorithms for On-orbit Identification of Space Platforms", PhD Thesis, Department of Mechanical Engineering, University of Kentucky, USA.

Ignoul S., Van Gemert D., (2006). “Bell Tower of Church of St. Willibrordus”, D00466, Triconsult NV, internal report, in Dutch.

Ignoul S., Van Gemert D., (2007). “Maagdentoren at Zichem”, D00394, Triconsult NV, internal report, in Dutch.

Hall, E.H., (1920), “A Guide to the Cathedral Church of St. John the Divine in the City of New York”, The Laymen’s Club of The Cathedral Church of St. John the Divine, New York.

Hemez, F. M., and Farhat, C., (1994), "An Energy Based Optimum Sensor Placement Criterion and its Application to the Structural Damage Detection", 12th International Modal Analysis Conference (IMAC), Honolulu, HI, pp.1568-1575.

Heo, G., Wang, M., and Satpathi, D., (1997), "Optimal Transducer Placement for Health Monitoring of Long Span Bridge", Soil Dynamics and Earthquake Engineering, Vol. 16(7-8), 495-502.

Heylen, W. and Lammens, S., (1996), “FRAC: A Consistent Way of Comparing Frequency Response Functions,” in Proceedings of International Conference on Identification in Engineering, Swansea, UK, pp.48- 57.

Heyman J., (1966), “The Stone Skeleton,” International Journal of Solids and Structures, 2nd Edition, pp. 249- 79.

Heyman, J., (1995), The Stone Skeleton, Cambridge University Press, UK.

Heyman, J., (1997), “The Stone Skeleton: Structural Engineering of Masonry Architecture,” Cambridge University Press.

Horrox, R., (2000), Beverley Minster: An Illustrated History, University Press, Cambridge.

Ju, F. and Mimovich, M., (1986), “Modal Frequency Method in Diagnosis of Fracture Damage in Structures,”in Proceedings of the 4th Internatinal Modal Analysis Conference, pp. 1168-1174.

Kammer, D. C., (1991), "Sensor Placement for On-orbit Modal Identification and Correlation of Large Space Structures", Journal of Guidance, Control and Dynamics, Vol. 14, pp. 251-259.

Kammer, D. C., (1992), "Effect of model error on sensor placement for on-orbit modal identification of large space structures", Journal of Guidance, Control, and Dynamics, Vol. 15, pp. 334-341.

Kammer, D. C., (1996), "Optimal Sensor Placement for Modal Identification Using System-Realization Methods”, Journal of Guidance, Control, and Dynamics, Vol. 19, No. 3, 729-731.

Lawler, J.S.,(1979), “Modal Coherent Equivalents Derived from an RMS Coherency Measure,” Ph.D. Thesis, Michigan State University, USA.

Lieven, N.A.J., Ewins, D.J., (1988), “Spatial Correlation of Mode Shapes, the Coordinate Modal Assurance Criterion (COMAC),” in Proceedings of 6th International Modal Analysis Conference, pp. 690- 695.

Maeck, J., (2003), “Damage Assessment of Civil Engineering Structures by Vibration Monitoring,” Ph.D Thesis, Katholieke University, Leuven, Belgium.

Mark, R., and Hutchinson, P., (1986), "On the Structure of the Roman Pantheon", The Art Bulletin, Vol. 68, No. 1, pp.24-34.

Meneghetti, U., Maggiore, A., (1994), "Crack Detection by Sensitivity Analysis," in Proceedings of the 12th International Modal Analysis Conference, pp. 1292- 1298.

Meo, M., and Zumpano, G., (2005), "On the Optimal Sensor Placement Techniques for a Bridge Structure", Engineering Structures, Vol. 27, No. 10, pp. 1488-1497.

Özen, G.Ö., (2006), “Comparison of Elastic and Inelastic Behavior of Historic Masonry Structures at Low Load Levels”, Master’s thesis, Middle East Technical University, Ankara, Turkey.

Panday, A.K., Biswas, M., Samman, M.M., (1991), “Damage detection from changes in curvature modes shapes,” J. of Sound and Vibration, Vol. 145, No. 2, pp. 221- 332.

Price & Meyers Consulting Engineers, Beverley Minster: Report on Recent Movement in the Nave Vaults, July 2004, ref: 1273.

Ramos, L. F., Lourenço, P. B., Costa, A. C., (2005), “Operational Modal Analysis for Damage Detection of A Masonry Construction,” Proceedings of the 1st Int. Operational Modal Analysis Conference, Copenhagen, Denmark, pp. 495- 502.

Ramos, L.F., (2007), “Damage Identification on Masonry Structures Based on Vibration Signatures,” Ph.D. Thesis, University of Minho, Portugal.

Ramos, L.F., De Roeck, G., Lourenço, P.B., and Campos-Costa, A., (2010), “Damage Identification on Arched Masonry Structures using Ambient and Random Impact Vibrations”, Engineering Structures, Vol. 32, No. 1, pp. 146-162.

Reynolds, P., Pavic, A., (2000), “Quality Assurance Procedures for the Modal Testing of Building Floor Structures,” Experimental Techniques, Vol. 24, No. 4, pp.36- 41.

Ricart-Nouel, A., (1991), "Report on the Structure of the Cathedral of Santo Domingo", Structural Repair and Maintenance of Historical Buildings II, Vol. 1, pp. 37-52.

Rossell, J., (1995), “Rafael Guastavino I Moreno Inventiveness in 19th Century Architecture”, Guastavino C., Col-legi ‘Arquitectes de Catalunya, Barcelona.

Ruotolo, R., Surace, C., (1997), “Damage Assessment of Multiple Cracked Beams: Numerical Results and Experimental Validation,” J. of Sound and Vibration, Vol. 206, No. 4, pp. 567-588.

Rytter, A., (1993), “Vibration Based Inspection of Civil Engineering Structures,” Ph.D. Thesis, Dept. of Bldg Tech. and Struct. Eng., Aalborg Univ., Denmark.

Rytter, A., and Kirkegaard, P. (1997) “Vibration Based Inspection Using Neural Networks,” Structural Damage Assessment Using Advanced Signal Processing Procedures, Proceedings of DAMAS ‘97, University of Sheffield, UK, pp. 97- 108.

Rizos, P., Aspragathos, N., Dimarogonas, A., (1990), “Identification of Crack Location and Magnitude in a Cantilever Beam from the Vibration Modes,” J. of Sound and Vibration, Vol. 138, No. 3, pp. 381- 388.

Safak, E. (2008), Structural Health Monitoring:Needs For Data Archiving, Exchange, And Analysis, First Euro-Mediterranean meeting on Accelerometric Data Exchange and Archiving - Grenoble, 10- 11.

Saliklis, E., Kurtz, S., and Furnbach, S., (2003), "Finite Element Modeling of Guastavino Tiled Arches", Proceedings of the Eighth International Conference on Structural Studies, Repairs and Maintenance of Heritage Architecture, Halkidiki, Greece, pp. 257-266.

Sansalone, M., (1997), "Impact-Echo: The Complete Story", ACI Structural Journal, Vol. 94, No. 6, pp. 777- 86.

Scholkopf, B., Sung, K.K., Burges, CJC, Girosi, F., Niyogi, P., Poggio, T. and Vapnik, V. (1997) "Comparing support vector machines with Gaussian kernels to radial basis function classifiers." IEEE Transactions on Signal Processing. Vol. 45, pp. 2758- 2765.

Schubert F., Wiggenhauser H., Lausch R., (2004) "On the accuracy of thickness measurements in impact-echo testing of finite concrete specimens—numerical and experimental results," Ultrasonics, Vol. 42 pp. 897- 901.

Sohn, H., Farrar, C. R., Hemez, F. M., Shunk, D. D., Stinemates, D. W., Nadler, B. R. and Czarnecki, J. J., (2004), "A Review of Structural Health Monitoring Literature: 1996-2001," Los Alamos National Laboratory Report, LA-13976-MS.

Statistics Toolbox Users Guide, (2003), The Mathworks, Natick, MA.

Theodossopoulos, D., (2004), "Structural Scheme of the Cathedral of Burgos", Proceedings of the 4th International Conference Structure Analysis of Historical Constructions, Padua, Italy, pp. 10–13.

Turek, M., Ventura, C. E., Placencia, P., (2002), “Dynamic Characteristics of a 17th Century Church in Quito,” Proceedings of the International Society of Optical Engineering, Vol. 4753, No. 2, pp. 1259- 1264.

Udwadia, F. E., (1994), "Methodology for Optimum Sensor Locations for Parameter Identification in Dynamic Systems", Journal of Engineering Mechanics, Vol. 102, pp. 368–390.

URL-1 http://www.dur.ac.uk/~des0www4/cal/dams/geol/mod.htm <accessed 6/30/2011>.

Vestroni F., Beolchini G. C., Antonacci E., Modena C., (1996), “Identification of Dynamic Characteristics of Masonry Buildings from Forced Vibration Tests,” Proceedings of the 11th World Conference on Earthquake Engineering, Acapulco, México.

Verstrynge, E., Schueremans, L., Van Gemert, D., and Hendriks, M.A.N. (2011). “Modeling and analysis of time-dependent behavior of historical masonry under high stress levels.” Engineering Structures, 33(1), 210-217.

Wickersham, G. W., and Cathedral Church of St. John the Divine. New York, NY., (1998), “The Cathedral Church of Saint John the Divine: A House of Prayer for All Nations”, Cathedral Church of Saint John the Divine.

Williams, R., Crowley, J. and Vold, H., (1985), “The Multivariate Mode Indicator Function in Modal Analysis,” in Proceedings of Third International Modal Analysis Conference.

Yang, S. M., Lee, G. S., (1999), “Effects of Modeling Error on Structure Damage Diagnosis by Two-Stage Optimization,” Structural health Monitoring 2000, Stanford University, Palo Alto, California, pp. 871- 880.

Zembaty, Z., Kowalski, M., (2000), “Dynamic Identification of a Brick Masonry Building,” Archives of Civil Engineering, Vol. 46, No. 1, pp. 106- 136.

Zonta, D., (2000), "Structural Damage Detection and Localization by Using Vibrational Measurements", PhD thesis, University of Bologna, DISTART. Bologna, 2000.